PLUME FLOWFIELD ANALYSIS OF THE SHUTTLE PRIMARY REACTION CONTROL SYSTEM (RCS) ROCKET ENGINE

J. E. HUESER and F. J. BROCK

Research Professors, Physics

OLD DOMINION UNIVERSITY RESEARCH FOUNDATION

Norfolk Virginia

January 1990

Final Report for Cooperative Agreement NCC 1-94
with
NASA Langley Research Center
Hampton, Virginia

PLUME FLOWFIELD ANALYSIS OF THE SHUTTLE PRIMARY REACTION CONTROL SYSTEM (RCS) ROCKET ENGINE

J. E. HUESER and F. J. BROCK

Research Professors, Physics

OLD DOMINION UNIVERSITY RESEARCH FOUNDATION

Norfolk Virginia

January 1990

Final Report for Cooperative Agreement NCC 1-94
with
NASA Langley Research Center
Hampton, Virginia

!

ABSTRACT

A solution has been generated for the physical properties of the Shuttle RCS 4000 N (900 lb) rocket engine exhaust plume flowfield. The modeled exhaust gas consists of the 5 most abundant molecular species H_2, N_2, H_2O, CO, and CO_2. The solution is for a bare RCS engine firing into a vacuum; the only additional hardware surface in the flowfield is a cylinder (=engine mount) which coincides with the nozzle lip outer corner at X = 0, extends to the flowfield outer boundary at X = −137 m and is coaxial with the negative symmetry axis. Continuum gas dynamic methods and the Direct Simulation Monte Carlo (DSMC) method were combined in an iterative procedure to produce a selfconsistent solution. Continuum methods were used in the RCS nozzle and in the plume as far as the P = 0.03 breakdown contour; the DSMC method was used downstream of this continuum flow boundary. The DSMC flowfield extends beyond 100 m from the nozzle exit and thus the solution includes the farfield flow properties, but substantial information is developed on lip flow dynamics and thus results are also presented for the flow properties in the vicinity of the nozzle lip.

Enrichment of the plume gas flowing along the positive symmetry axis by heavy molecular species is observed as well as enrichment of the flow along the negative symmetry axis by light molecular species. Departure from translational equilibrium is observed in the breakdown parameter range 0.03 to 0.05 and substantial variation is observed between translational and internal 'temperatures' as well as between species 'temperatures' beginning a few millimeters downstream of the P = 0.03 breakdown contour. Variation of flow speed and flow angle with species is observed (especially in the vicinity of the lip). The mean molecular weight of the plume gas mixture is observed to vary from about 23 along the positive symmetry axis to just over 2 as the flow angle approaches π and all molecular species in the RCS exhaust at the nozzle exit plane are observed everywhere in the flowfield. The molecular flux density incident on the engine mounting cylinder includes all species except CO_2 and the observed incident flux density decrease with distance from the nozzle exit fits well (in the least square sense) a set of exponential functions.

TABLE OF CONTENTS

TABLE and FIGURES

INTRODUCTION

This paper deals with a new solution for rocket plume flow and the results should contribute substantially to the further understanding of rocket plume dynamics; the paper presents the exhaust plume flow properties of the Shuttle RCS 4000 N (900 lb) thruster with particular attention given to the flow properties in the farfield, to 100 m or so, from the nozzle exit (exit radius = 0.12 m). This rocket was selected for study since it has the stable and reproducible performance characteristics expected of quality controlled flight hardware, is currently in use routinely, and is anticipated to remain in use well into the future. Further the possibility exists of acquiring measured plume properties data in the future which may be used to validate the solution presented here. This work continues the investigations begun in previous studies[1,2] in which the composite method was developed, by now applying those procedures to the farfield plume analysis of the Shuttle RCS engine as well as developing refinements to lip flow analysis. Since the farfield is everywhere beyond the translational equilibrium limit of continuum flow, the rocket engine entire thruput (=mass flux) passes thru the plume flow solution space, a very demanding boundary condition believed to have been applied for the 1st time.

To exclude from the plume flowfield all nonessential complexities and to avoid many troublesome ambiguities, this work deals with the bare RCS

engine: the engine is mounted in the end of a long cylinder, the radius of which is the same as the outer radius of the nozzle lip; the mounting cylinder is the only additional hardware surface in the flowfield; there is no freestream gas external to the flowfield; vacuum conditions are applied at the outer boundary of the flowfield and the exit Mach number is very much greater than 1.0 everywhere along the outer boundary. A solution which incorporates the interaction of the freestream (atmosphere at orbit) at the flowfield outer boundary is contemplated for the future.

Rocket plume flows extend across all flow regimes (continuum, transition and 'collisionless' flow). No single method has yet been developed which can adequately deal with all flow regimes; continuum methods encounter validity problems with very large gradients and rarefied flow (low collision frequency); and gas dynamic molecular modeling methods encounter storage (memory) problems in large flows and computation time problems at high density.

The plume flow solution presented here was generated by a composite method, a synthesis of continuum methods and a molecular (discrete particle) modeling method, and which relies heavily on the strengths of each method while avoiding the limitations attached to each. This composite method increases the computational complexity but yields a far more reliable (=physically sound) solution. The nozzle coreflow solution was generated by a Reacting And Multi Phase (RAMP) code, essentially a Method of

Characteristics code with ancillary routines, and the boundary layer solution was generated by a Boundary Layer Integral Matrix Procedure (BLIMP) code. The plume solution was generated using the Direct Simulation Monte Carlo Method[3] (DSMC). These methods were combined in an iterative procedure which assured that the continuum methods were confined to their domain of validity and that the flow at the intermediate boundary (Monte Carlo input boundary) was in equilibrium and that the flow conditions were selfconsistent along the input boundary. A strict axisymmetric flow assumption has been invoked in all the computational procedures.

Continuum methods were used for the nozzle internal flow and the high density part of the plume flow up to the breakdown boundary[4] and the DSMC method was used in the rarefied regime downstream of the breakdown boundary. Description of the plume properties in the farfield requires locating the exit boundary of the flowfield well downstream (say 100 m or so) of the point at which the breakdown boundary intersects the symmetry axis (about 10.7 m), thus the entire mass flux of the RCS engine flows thru the Monte Carlo flowfield. The mass flux of the engine is 1.26 kg/s and the density at the exit plane is approximately $0.5*10^{24}$ m^{-3} corresponding to an exit plane pressure of 7800 Pa (about 0.08 atmospheres).

The flowfield is made up of a large number of physically contiguous (no voids, no overlaps), 4 sided regions as viewed in the (X,R) plane (in 3D

space they are of course toroids). Each region is subdivided into computational cells to limit the separation between molecular pairs randomly nominated as potential collision partners and to provide a geometrical reference point (cell centroid) to which sampled flow properties may be assigned. In the DSMC method the regions function as solution subspaces in each of which the scaling relation between the physical space and the model space (region) are independent of all other regions. The solution of large flows (geometry or thruput) is indebted to this procedure of dividing the physical flowfield into many subspaces in the model. It is usually also necessary in large flows to run the clocks at different rates in different regions to minimize computation time. If these procedures are performed independently, as is frequently necessary in plume flows, time dependent solutions are inaccessible. In constructing the flowfield, attention is focused on the local mean free path λ as a device (reference guide) to assure that the local flow gradients are not smoothed, deformed, or blurred due to excessively large cells. While both collision partners are chosen from the same cell, values of a flow parameter carried by molecules at one side of a cell may collisionally mix with values carried by molecules at the opposite side. If the cell is large compared with λ and the local gradients vary rapidly (2nd derivative large), the computed flow properties may be displaced and the gradients distorted.

A straightforward application of the DSMC method to the RCS plume flow (including the farfield) leads immediately to a very large data storage (memory) requirement. Invoking the conventional criterion that the cell size should be small compared to the local mean free path requires a very large number of cells in the high density region adjacent to the Monte Carlo input boundary in the vicinity of the nozzle lip where the mean free path is of the order of $4*10^{-6}$ m. In the farfield the need for adequate spatial resolution (cells much smaller than the mean free path) adds substantially to the total cell requirement. The storage requirement is even further increased since the cell mean occupation number (number of modeled molecules in the cell) must be adequate to model each of the 5 molecular species in the exhaust gas, which even along the Monte Carlo input boundary have relative abundance ratios as large as 20, and substantially larger further downstream.

A less restrictive but probably adequate cell size reference length may be constructed based on the local mean free time between collisions τ and the local flow speed C_0. For a stationary observer (=a computational cell) molecules move down stream a mean distance $C_0*\tau$ between consecutive collisions. In the flow direction then, the reference length may be taken as $\lambda + C_0*\tau$ which is substantially larger than λ along most of the input boundary where the flow speed is moderately large. Previous numerical experiments dealing with the influence of cell size on the value of flow parameters yielded

the conclusion that contour curves of most of the flow properties were not substantially displaced unless the cell size was much greater than the local mean free path or the gradients were rapidly changing. The more relaxed criterion was found necessary to honor the objective of including both the nearfield and farfield in the solution space; even so, the running program required about 9 megabytes of direct address space (memory).

The usual assumption was made that the chemical reactions reached completion somewhere in the nozzle, upstream of the exit plane; and that the gas experienced no further change in composition due to chemical reactions downstream of this point (including the plume flow). Thus all variation in gas composition downstream of the exit plane is associated with gas dynamics, not chemistry.

During normal steady operation, small rocket engines commonly eject some fraction of their total mass flux (usually less than 8%, but not precisely known) in the particulate phase (droplet size = few micrometers and smaller). The particulate phase has not been included in any of the methods used in generating the RCS plume solution.

Combustion chamber resonances ('chugging', similar to Helmholtz resonance) are observed in many small rocket engines which surely lead to a variation in fuel to oxidizer ratio on a small time scale (perhaps 100 ms or

less). These variations are commonly thought to have a negligible effect on the mean value of the fuel to oxidizer ratio and therefore have been neglected in all the models used.

It may be observed from some of the results presented below that the translational 'temperature' on the symmetry axis drops to about 30 K at 100 m downstream of the exit plane and as low as 15 K at a flow angle of 60° near the outer boundary of the flowfield. Under these conditions several species in the plume gas mixture may experience some condensation, yielding an unknown number density of molecular clusters of unknown molecular weight. In rarefied plume flow, molecular interactions which yield gas phase condensation are regarded as rare and therefore have not been included in the DSMC routines used for the RCS plume solution.

METHODS AND BOUNDARY CONDITIONS

The flow conditions at the nozzle exit were obtained by combining a nozzle flow solution which was generated by a RAMP (Method of Characteristics) code for the nozzle core flow and a boundary layer solution near the nozzle wall which was generated by a BLIMP code. These solutions are approximately coextensive in the axial direction but overlap slightly in the radial direction. In the exit plane the overlapping solutions were smoothed to yield a set of startline conditions for a MOC 1st approximation to a plume solution[1,2].

The flow parameter distributions from this 1st plume solution were used to define the input boundary conditions for a DSMC flowfield surrounding (containing) the nozzle lip. A Monte Carlo solution was generated for the flow properties in the vicinity of the nozzle lip. Since this flowfield extends back upstream several hundred mean free paths into the nozzle, this solution is expected to surmount the approximations in the 1st startline and yield flow parameters which are selfconsistent (except perhaps for 1 or 2 cells immediately adjacent to the input boundary, these cells are of order 10^{-5} m).

A 2nd startline (displaced downstream slightly) was defined by replacing the flow conditions from the 1st MOC plume solution with the results from the DSMC lip flow solution where the solution spaces overlapped. From this

combined data startline, a 2nd (refined) MOC plume solution was generated. The location of the P = 0.03 breakdown[4,5] contour was extracted from this 2nd plume solution. Fig(1) showns the breakdown contour (dotted), the Monte Carlo input boundary (rightmost curve), and region and cell distributions near the lip. Evidence of translational equilibrium breakdown has been observed in similar flows[1,2,4] in the breakdown parameter range 0.03 to 0.05; in this work breakdown was conservatively assumed to begin near P = 0.03.

The input boundary of the DSMC flowfield was constructed parallel to this breakdown contour but displaced upstream slightly (=on the continuum side). Fig(2) shows the entire input boundary for the Monte Carlo flowfield and the P = 0.03 contour (dotted) and displays more of the region geometry (with cells suppressed). The flow conditions along the input boundary were taken from the 2nd MOC plume solution. As shown in Figs(1) and (2) the Monte Carlo flowfield input boundary begins at the nozzle wall and follows (approximately) along the high density side of the P = 0.03 breakdown contour which expands to R = 3.35 m at X = 7.5 m and then curves back to the symmetry axis at X = 10.7 m downstream of the exit. Along this input boundary the flow is in translational equilibrium. Downstream of this contour the flow rapidly departs from translational equilibrium; within the flowfield boundaries there is no evidence in the DSMC plume solution that the flow returns to equilibrium (nor would it be expected, since in the downstream direction the collision frequency continues to decrease such that the collision process which

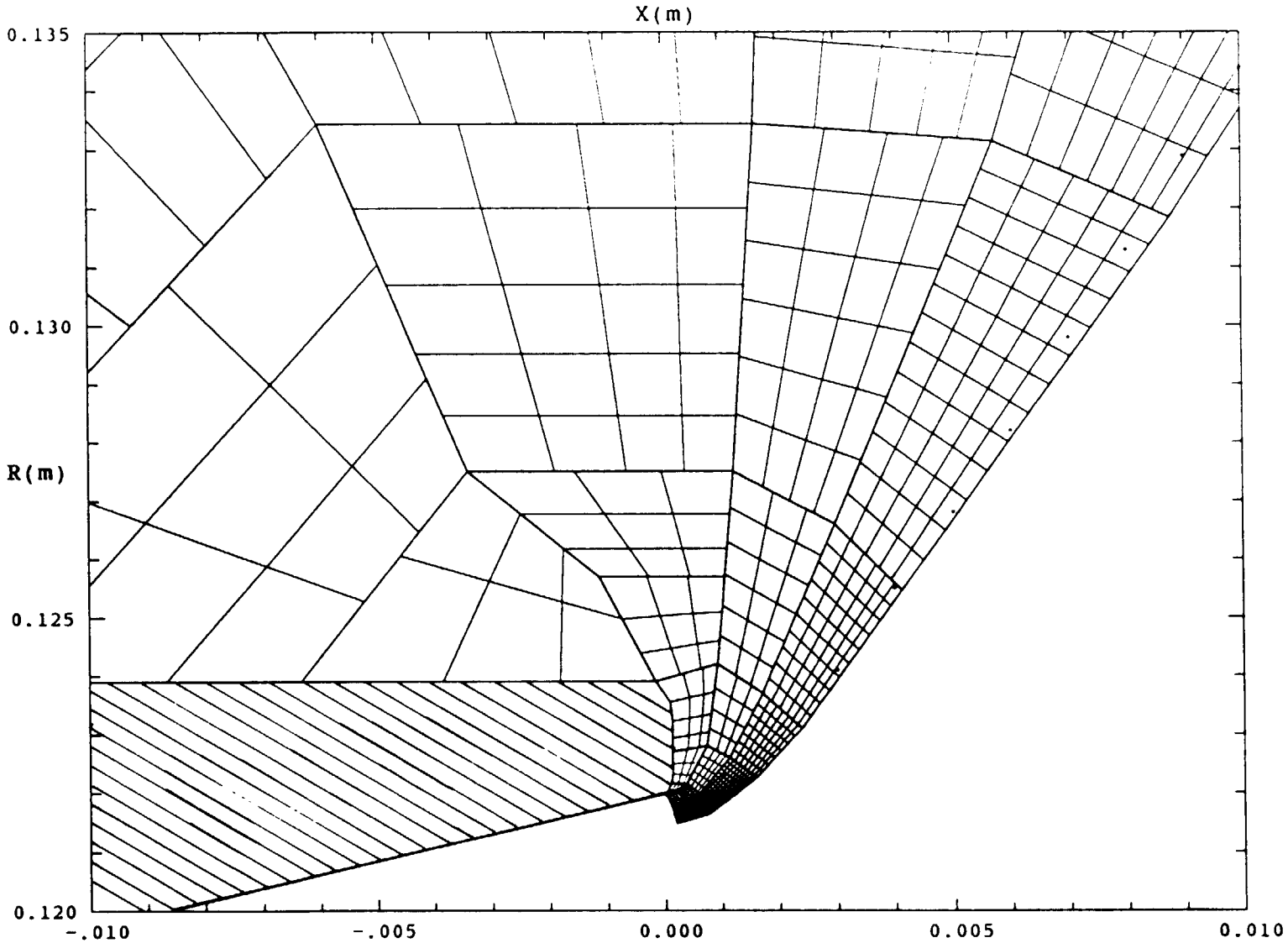

Fig(1) Magnified display of the RCS nozzle lip(hatched), the P = 0.03 breakdown contour(dotted), DSMC input boundary(rightmost curve), and some typical region and cell distributions.

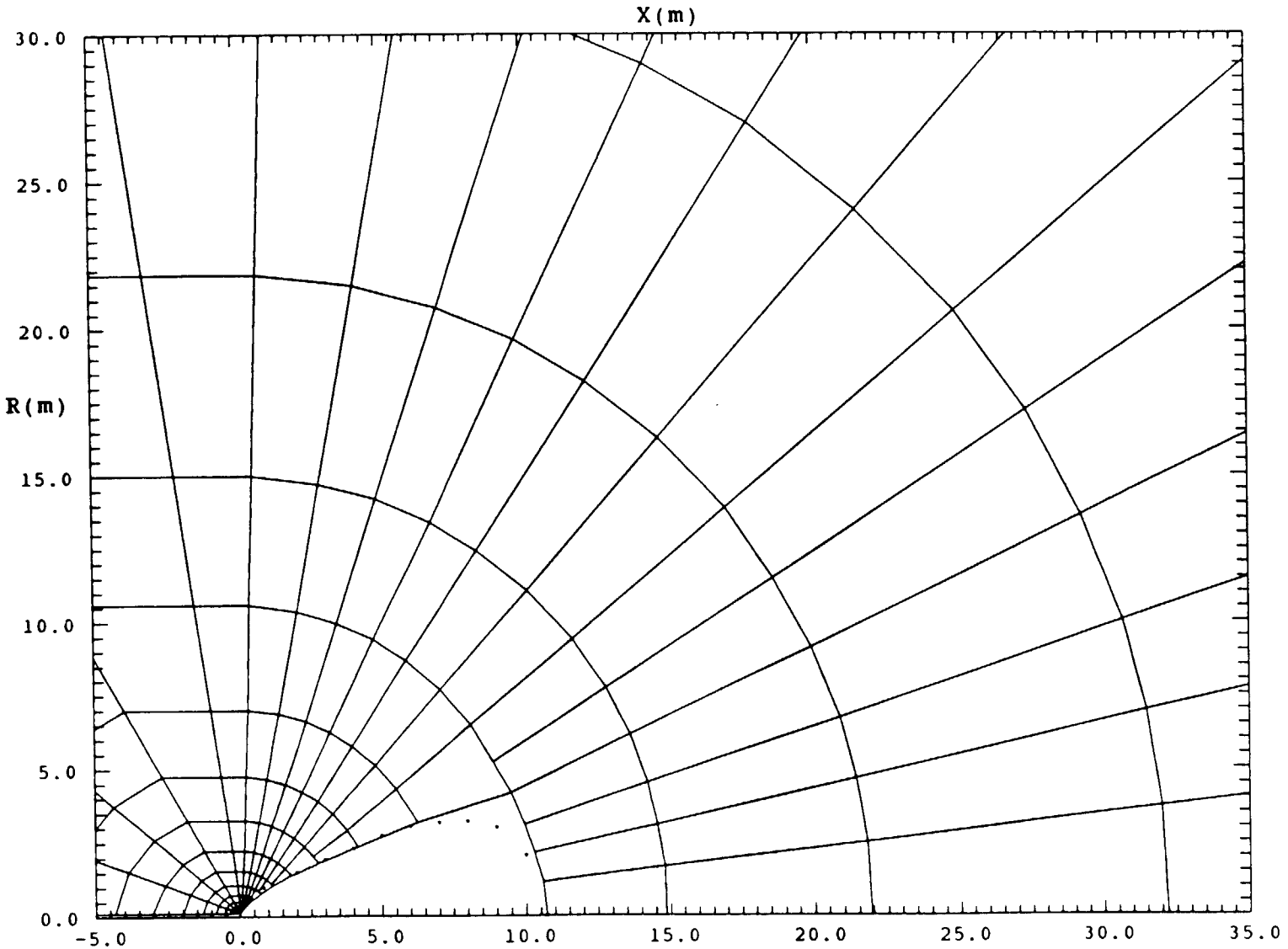

Fig(2) Monte Carlo flowfield input boundary(solid), P = 0.03 breakdown contour(dotted), and typical region distribution.

produces equilibration, never catches up with the motion process). (Return to equilibrium commonly occurs in compressive flows.)

While the data from the 2nd MOC plume solution beyond the P = 0.03 contour was not regarded as physically valid it was used to provide an initial estimate of the number density distribution and from this the mean free path distribution, which was used to construct initial estimates of cell size and distribution and region boundary locations. This density distribution was also used to make initial estimates (for each region) of the DSMC scaling parameter: Fn = n(physical)/n(model), the ratio of physical number density to model number density. This is the only scaling parameter in the DSMC method and thus the only adjustable (=free) parameter in the model (all other DSMC parameters have a direct physical interpretation). The derived cell size and the local flow speed taken from the 2nd MOC plume solution were used to make the initial estimates of the DSMC computational time step Δt for each region. In rapidly expanding flows, especially large flowfields dealing with rocket plumes it is not practicable (however desireable) to maintain the ratio $Fn/\Delta t$ constant for the entire flowfield. (Nor was it necessary in this work since only a steadyflow solution was contemplated.) But the introduction of this additional degree of freedom brings about considerable unavoidable statistical noise. Within the flowfield Fn varied from $0.75*10^{13}$ to $0.3*10^{21}$, the computational time step Δt varied from $0.15*10^{-8}$ s to $0.14*10^{-2}$ s and the

ratio $Fn/\Delta t$ varied from $0.28*10^{20}$ to $0.82*10^{24}$. Limiting the magnitude of the change (step) in the ratio of $Fn/\Delta t$ for adjacent regions is a particularly difficult task and was given considerable attention during evolution of the flowfield geometry.

In constructing the flowfield geometry the cell size criterion mentioned above (drifting gas mean free path) was applied to the high density regions using numerical data from the 2nd MOC plume solution. Preliminary DSMC results were then used to reevaluate the mean free path distribution which was in turn used to refine the flowfield geometry (region boundary locations, number of cells, cell size, computational time step, etc). Several iterations of this procedure were necessary to obtain an adequate flowfield geometry.

Fig(3) shows the flowfield overall geometry and region distribution (cell distribution is suppressed for clarity). There are 248 regions, divided into 5121 computational cells. The nozzle exit plane is at X = 0, the symmetry axis is R = 0 and the rocket exhaust flux exits the nozzle in the +X direction. The mean free path along the DSMC input boundary varies from about $4.0*10^{-6}$ m at the exit plane adjacent to the nozzle wall to about $1.0*10^{-2}$ m on the symmetry axis at X = 10.7 m downstream of the exit plane (based on input conditions taken from the 2nd MOC plume solution). From the DSMC solution, the mean free path along the flowfield outer boundary varies from 0.6 m on the symmetry axis at X = 100 m downstream of the nozzle exit, to 400 m in the

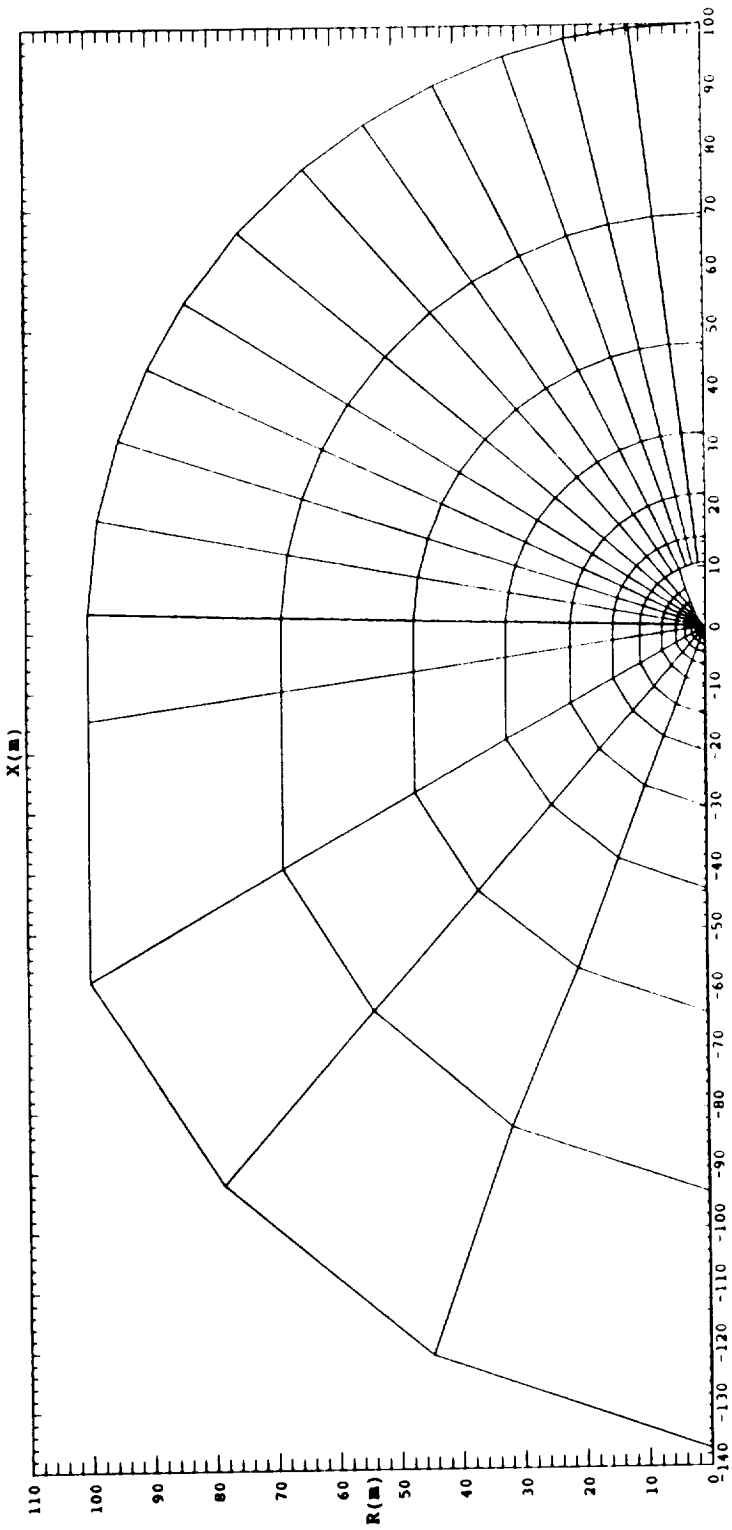

Fig(3) Fullscale Monte Carlo flowfield and region distribution geometry.

plane X = 0 at R = 100 m above the exit, and finally to $4.0*10^{4}$ m on the symmetry axis at X = −140 m, the most distant point in the rarefied ('backflow') region. The ratio of cell size to drifting gas mean free path ($\lambda+C_0*\tau$) varies from about 4 (in the flow direction) at the input boundary near the lip to about $4.0*10^{-4}$ at X = −140 m near the symmetry axis. For something over 80% of the flowfield volume the cell size is smaller than the local mean free path (conventional).

The Variable Hard Sphere (VHS) molecular model[6] (essentially: relative velocity dependent collision cross sections but isotropic scattering in the center of mass frame) was used in the collision routine of the DSMC code. This model requires a molecular diameter for each species at a prescribed reference temperature (the same for all species); it also requires a single (same value for all species in the mixture), constant (temperature independent) exponent for the temperature dependent term in the expression for viscosity $\eta \propto T^{(\omega+1/2)}$ where $(\omega+1/2)$ is the measured (laboratory) value of the temperature exponent (usually found to be temperature dependent). Thus ω is replaced with a constant that best represents the measured (indirectly) variation of collision cross sections with relative velocity of collision pairs for all species in the mixture. The collision routine uses the Larsen–Borgnakke[7] statistical model to distribute the collision energy among the translational and internal degrees of freedom for a prescribed fraction of the collision pairs, the remaining fraction are treated as elastic collisions. The Larsen–Borgnakke

model also requires a fixed value of ω which must be the same for all species in the mixture.

In the DSMC solution for the RCS rocket plume flow the reference temperature for molecular collision diameters was fixed at 300 K and ω (as defined in 6) was set at 0.25 for all species (thus the temperature exponent of the coefficient of viscosity = 0.75); the probability of rotational energy transfer was set at 0.2 for all species and the probability of vibrational energy exchange[8] was set to 0.02 (see relaxation numbers in 8). The remaining parameters required to define the RCS exhaust gas are given in Table 1. The gas composition varies continuously along the input boundary of the Monte Carlo flowfield; the composition at the nozzle wall near the exit plane (given by the 1st relative abundance line in Table 1) yields a mean molecular weight of 18.21 and the composition at the downstream end of the input boundary (given by the 2nd line) yields a mean molecular weight of 23.12.

TABLE 1 RCS Exhaust Gas Parameters

Species	H2	N2	H2O	CO	CO2
Molecular weight	2	28	18	28	44
Diameter(nm) at 300K	0.2948	0.3934	0.4951	0.3960	0.4760
Degrees of freedom:					
rotational	2	2	3	2	3
vibrational	1	1	1	1	1
T(vb) K	6159	3390	2292	3103	960
Relative abundance:					
nozzle wall	0.3034	0.2883	0.2280	0.1568	0.0236
symmetry axis	0.0732	0.3438	0.4142	0.0932	0.0746

RESULTS and DISCUSSION

The DSMC steadyflow solution for the RCS exhaust plume is presented graphically below; the results displayed in many of the figures are directly interpretable, however since not everyone who uses or needs to understand the results is a rocket plume specialist, the meaning, interpretation and implications of the data are discussed where appropriate.

Farfield Results and Discussion

The number density distribution for the RCS plume gas mixture summed over the 5 species: H_2, N_2, H_2O, CO, and CO_2 is given in Fig(4). The ratio of contour values for adjacent curves is $10^{1/5}$ (=1.585) and curves with integer exponent (base 10) contour values are dark. The noise on segments of some of the contour curves (in this and subsequent figures) is a computational artifact and has no substantial effect on the location of the smoothed (mean) contour curve. Along the symmetry axis (R = 0), downstream of the Monte Carlo input boundary (X > 10.7 m) the density decreases as X^{-2} ; in the radial plane containing the nozzle exit (X = 0), the density decreases as $R^{-1.92}$ for R > 0.25 m; and in the rarefied ('backflow') region adjacent to the symmetry axis the density decreases as $(-X)^{-1.94}$. Since there are 5 species in the gas mixture with molecular weights ranging from 2 to 44 with the mixture mean molecular weight varying from 23+ to nearly 2 it is improbable that there is a simple physical explanation for the exact value of these

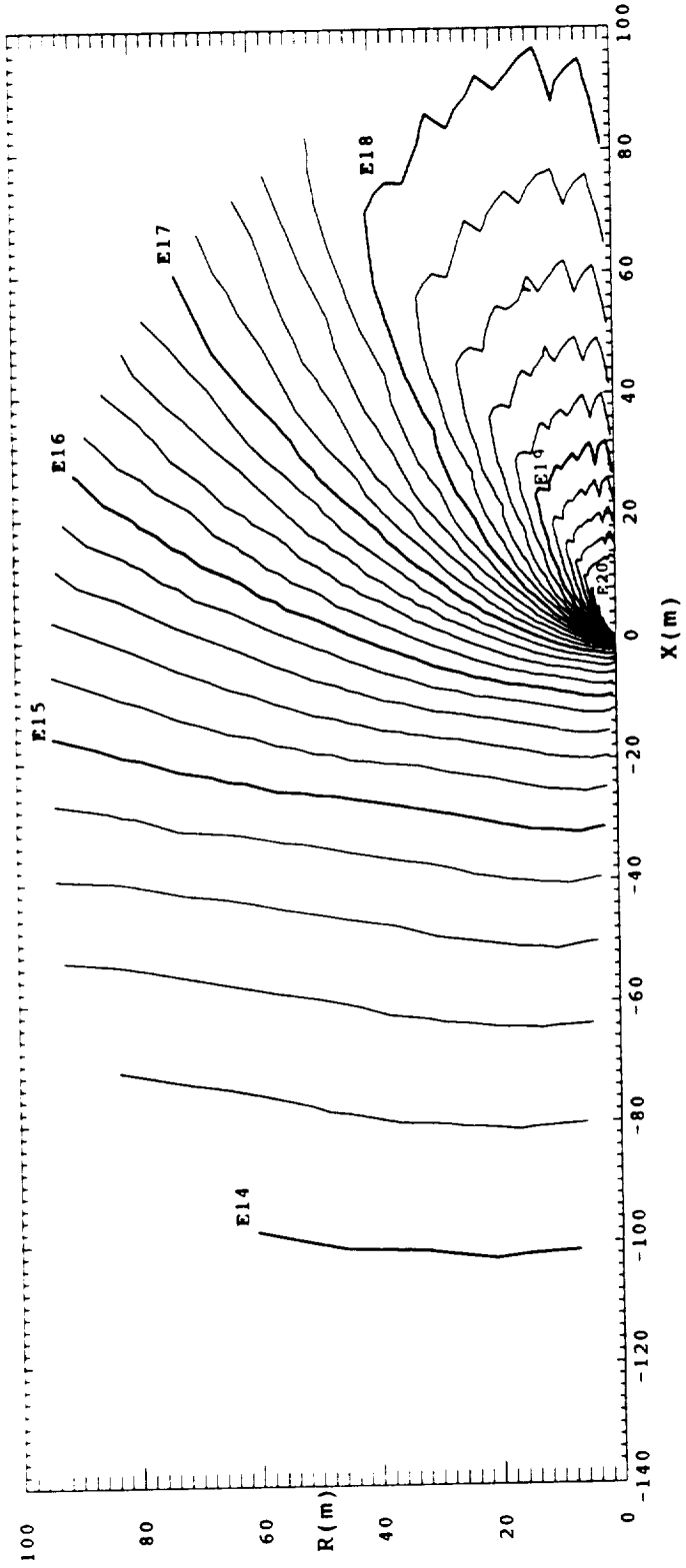

Fig(4) The plume gas mixture mean number density distribution (m^{-3}).

exponents, but the analytical statements may be used for limited, approximate extrapolation of the farfield density beyond the flowfield boundary.

The flow angle distribution for the plume gas mixture is given in Fig(5) and the flow speed distribution is given in Fig(6). The flow angle contours which on this scale appear to originate at the origin, lie very close to straight lines at a geometrical angle (with respect to +X) that is equal to the contour value. Thus locations in the flowfield may be conveniently referenced simply by identifying the local flow angle. From the symmetry axis up to a flow angle of 0.85(48°) and extending from the input boundary near X = 10.5 m to the flowfield outer boundary (exit) at X = 100 m, the surface representing the flow speed as a function of X and R is quite flat; the ripples in this part of the surface lie between 3510 and 3600 m/s. From the flow angle 0.85 the flow speed monotonically decreases with increasing flow angle until it reaches the bottom of a trough located at the flow angle value 2.2(124°) where the minimum speed is slightly less than 2200 m/s. As the flow angle increases past 2.2 the flow speed steadily increases to a value slightly larger than 2500 m/s at flow angles greater than 2.96(170°). The shape of the flow speed surface for the mixture is strongly influenced by the mixture composition. As the flow angle increases the mean molecular weight of the mixture steadily decreases (the relative abundance of the lightest species increases and the heavier species decrease) and the flow speed of the heavier species lags the flow speed of the lighter species. Thus the heavier species dominate the

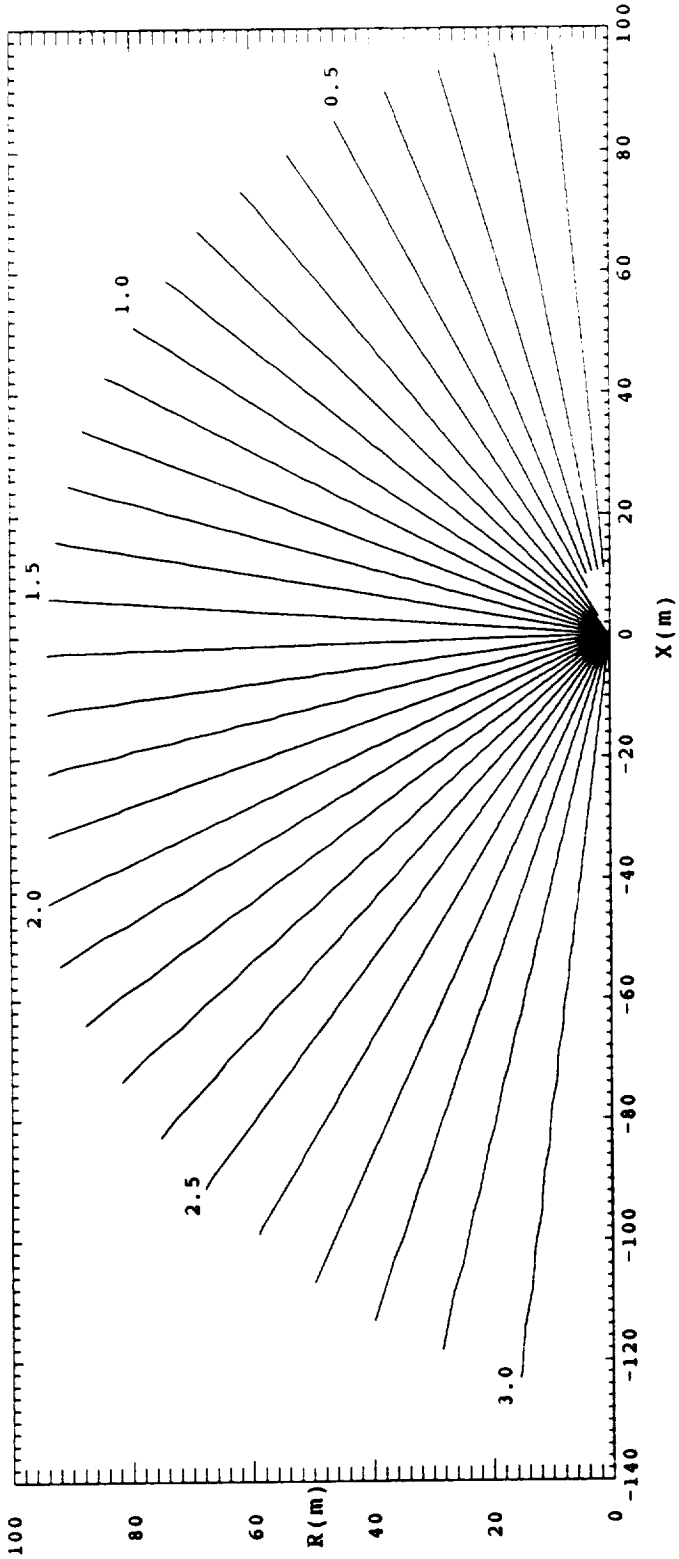

Fig(5) The plume gas mixture mean flow angle distribution (radian).

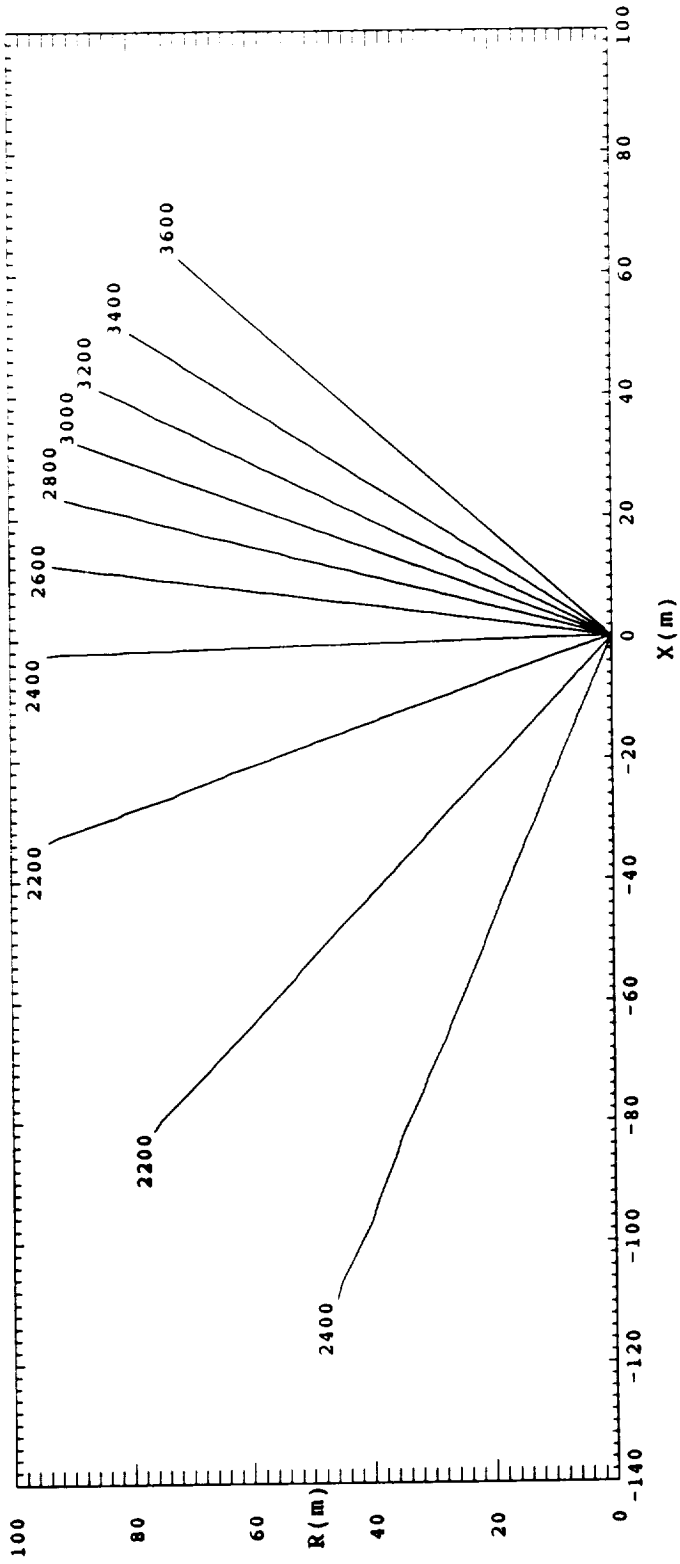

Fig(6) The plume gas mixture mean flow speed distribution (m/s).

mixture flow speed up to some flow angle at which their relative abundance and mass fraction is negligible compared to the lightest species, beyond this flow angle (about 2.2(126°)) the relative abundance and mass fraction of the light species begins to dominate the flow speed. Since the flow speed of the lighter species consistently leads the flow speed of the heavier species, the lighter species begin to dominate the flow speed of the mixture and thus the mixture flow speed continues to increase beyond this flow angle, 2.2(126°).

In the following paragraph (and scattered thru the text) the term 'temperature' is frequently used in a restricted sense: shorthand for a much more involved phrase which implies statistical means of various energy elements or components of the mixture but expressed in the customary and familiar language of temperature. The plume gas mixture is in equilibrium at the Monte Carlo input boundary, but immediately downstream (perhaps a fraction of a millimeter for some boundary elements) the gas begins to depart very rapidly from equilibrium. This intermediate boundary location was carefully selected to be just at the edge of the equilibrium domain (to unburden the DSMC from high density computations in favor of a continuum method which is computationally more efficient). Therefore on the downstream side of this boundary (and extending to the exit boundary of the flowfield) the term 'temperature' usually refers to a value computed from energy components of the mixture using standard formulas, which yield temperature like results but do not imply a single unique value applicable to the entire gas

(all species, all degrees of freedom) at a geometrical point (where, for the RCS plume gas mixture there may be 20 or more such 'temperatures').

The plume gas total 'temperature' (averaged over all species and all degrees of freedom) is shown in Fig(7). The total 'temperature' drops slightly below 30 K at a flow angle of 0.82(47°) near the outer boundary. At large distances from the nozzle exit the 'temperature' increases as the flow angle increases in the rarefied ('backflow') region. This is principally due to the low value of collision frequency in this region, which is insufficient to transfer energy from internal degrees of freedom to translational degrees of freedom at a rate required to maintain equilibrium (the transfer process is intrinsically relatively inefficient).

The limit attached to collisional transfer rate is clearly observable in Figs(8) and (9) which give the translational 'temperature' (averaged over all translational degrees of freedom for all species) and the internal 'temperature' (averaged over all internal degrees of freedom for all species). Fig(8) implies that nearly all the thermal energy has been converted to mass motion translational energy. At a flow angle of 0.8(46°) near the flowfield outer boundary the translational 'temperature' drops slightly below 15 K and even in the rarefied region the translational 'temperature' does not exceed 80 K. In contrast, Fig(9) shows that beyond a flow angle of 0.8(46°) the internal

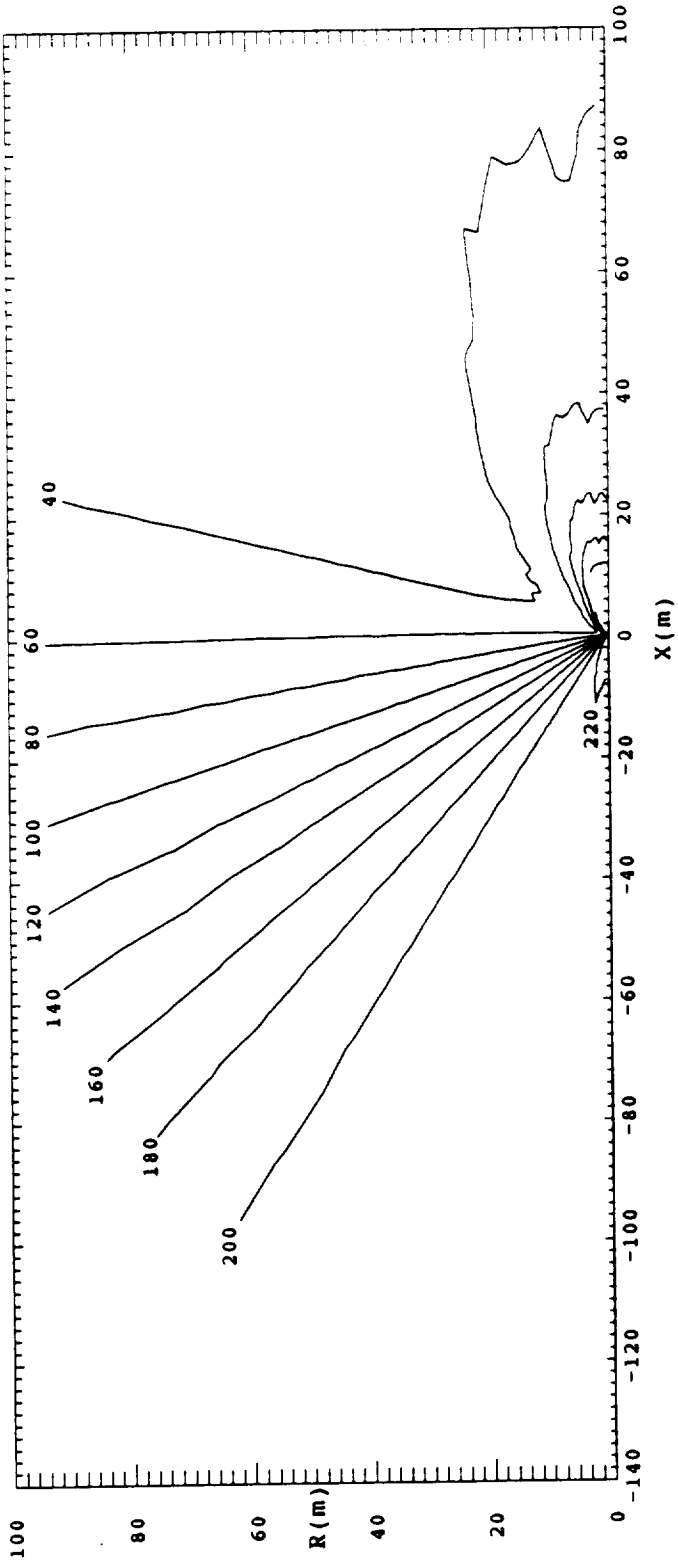

Fig(7) The plume gas mixture mean total 'temperature' distribution (K).

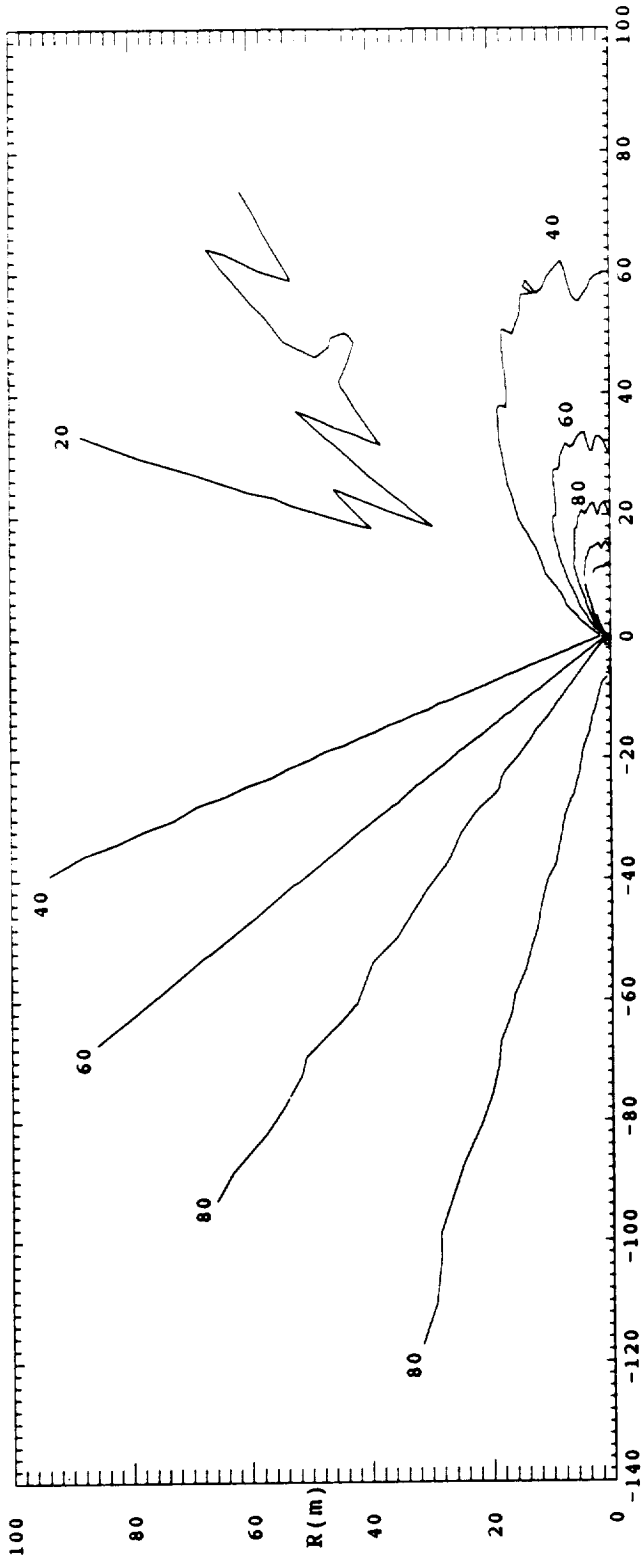

Fig(8) The plume gas mixture mean translational 'temperature' distribution (K).

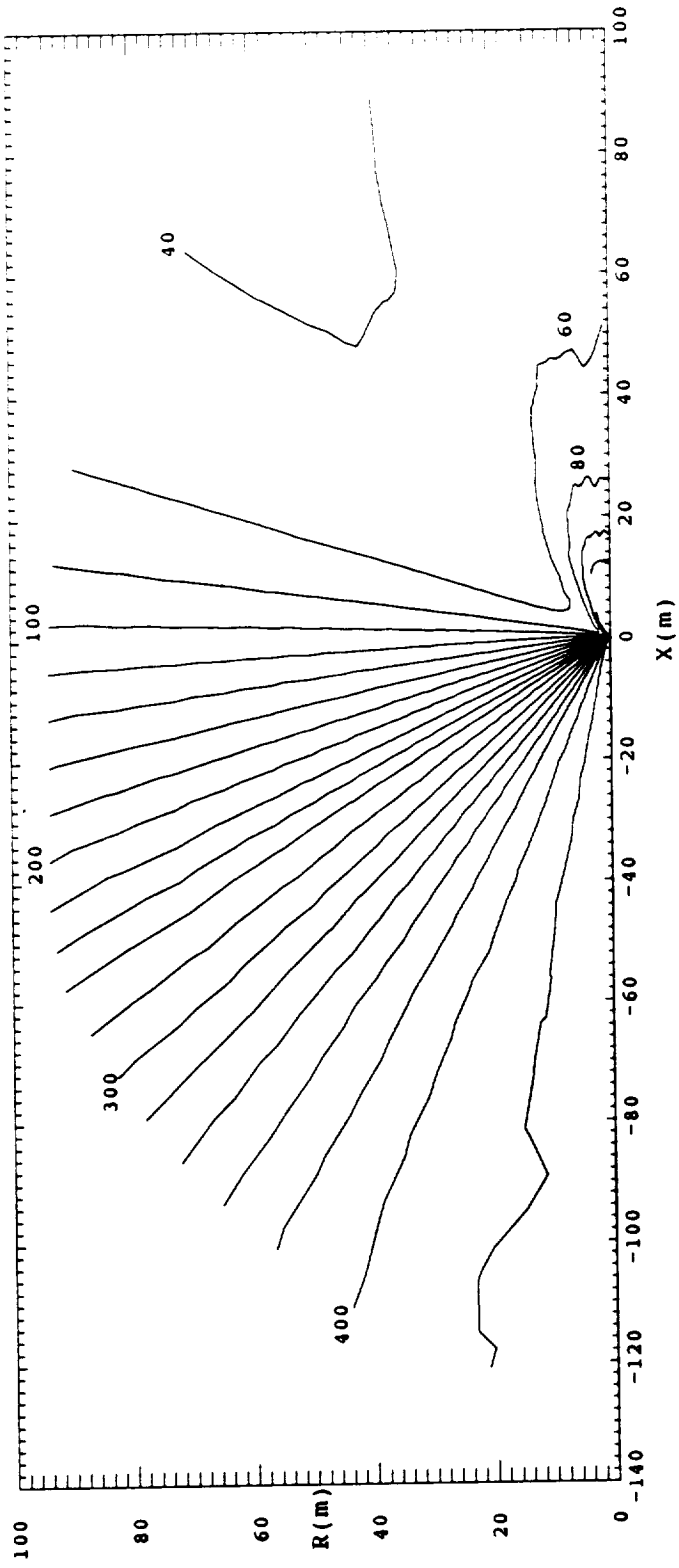

Fig(9) The plume gas mixture mean internal 'temperature' distribution (K).

'temperature' steadily increases with increasing flow angle, a direct effect of the reduction in collision frequency with increasing flow angle, see Fig(28) on page 53.

Near the nozzle lip the Mach number surface, displayed by the contours in Fig(10), has a prominent ridge (cusp) beginning at a flow angle of 1.2(69°) low in the flowfield, and bends toward the symmetry axis further downstream, and passes thru the flowfield outer boundary at a flow angle of 0.7(43°) where the Mach number is slightly larger than 28. This cusp is principally a temperature effect (thru the speed of sound) as may be seen by referring to the flow speed surface in Fig(6) and the temperature in Fig(7). Fig(6) shows that the flow speed surface is quite smooth in this region, while the Mach number is increasing from less than 10 to slightly greater than 28, the flow speed remains constant at 3600 m/s (apart from some small ripples in the surface, probably noise). In the same region Fig(7) has a deep depression in the temperature surface, implying a minimum in the sound speed and thus a ridge (cusp) in the Mach number surface.

The mass density distribution of the plume gas mixture is given by the contours in Fig(11), the ratio of contour values for adjacent curves is $10^{1/5}$. It may be observed that for a large part of the flowfield, for flow angles greater than 1.5(86°) the shape of the mass density distribution surface differs substantially from the number density distribution surface, see Fig(4). The

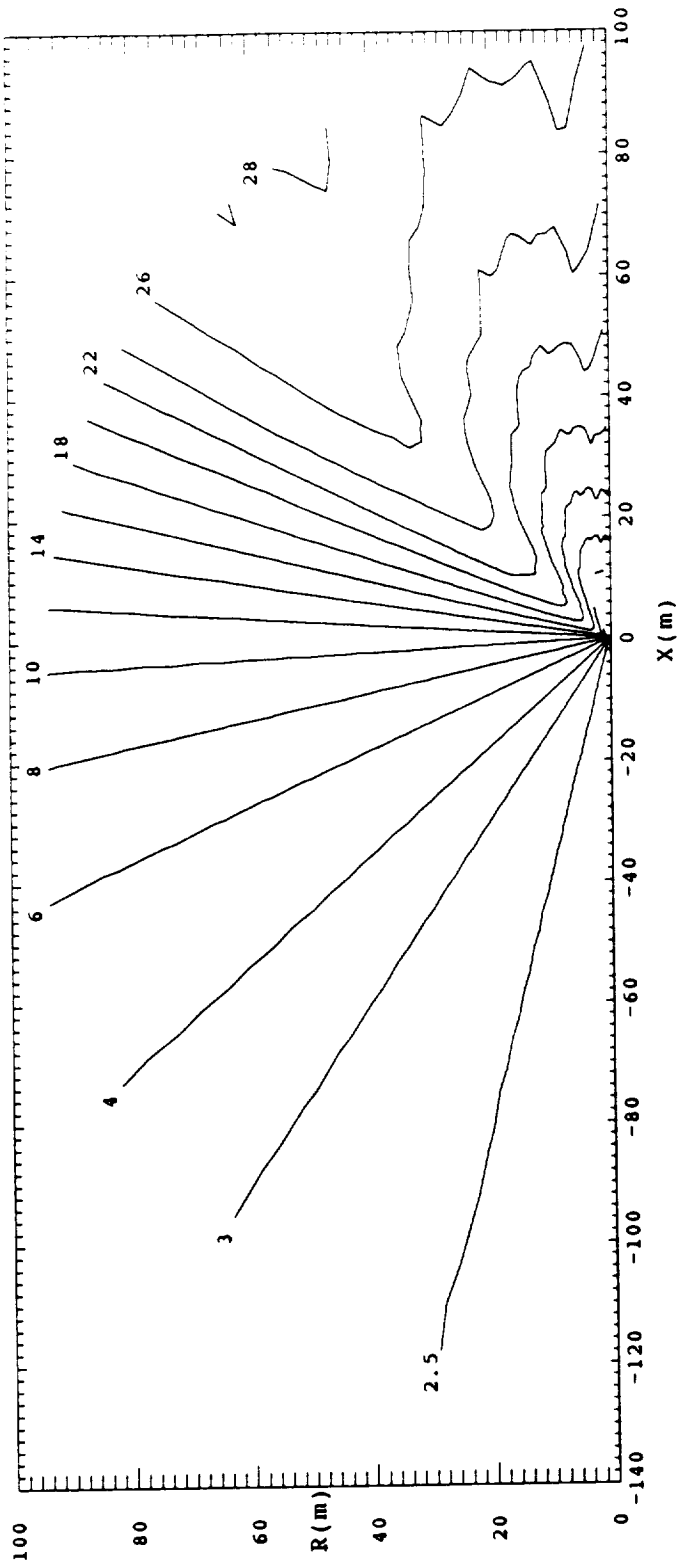

Fig(10) The plume gas mixture mean Mach number distribution.

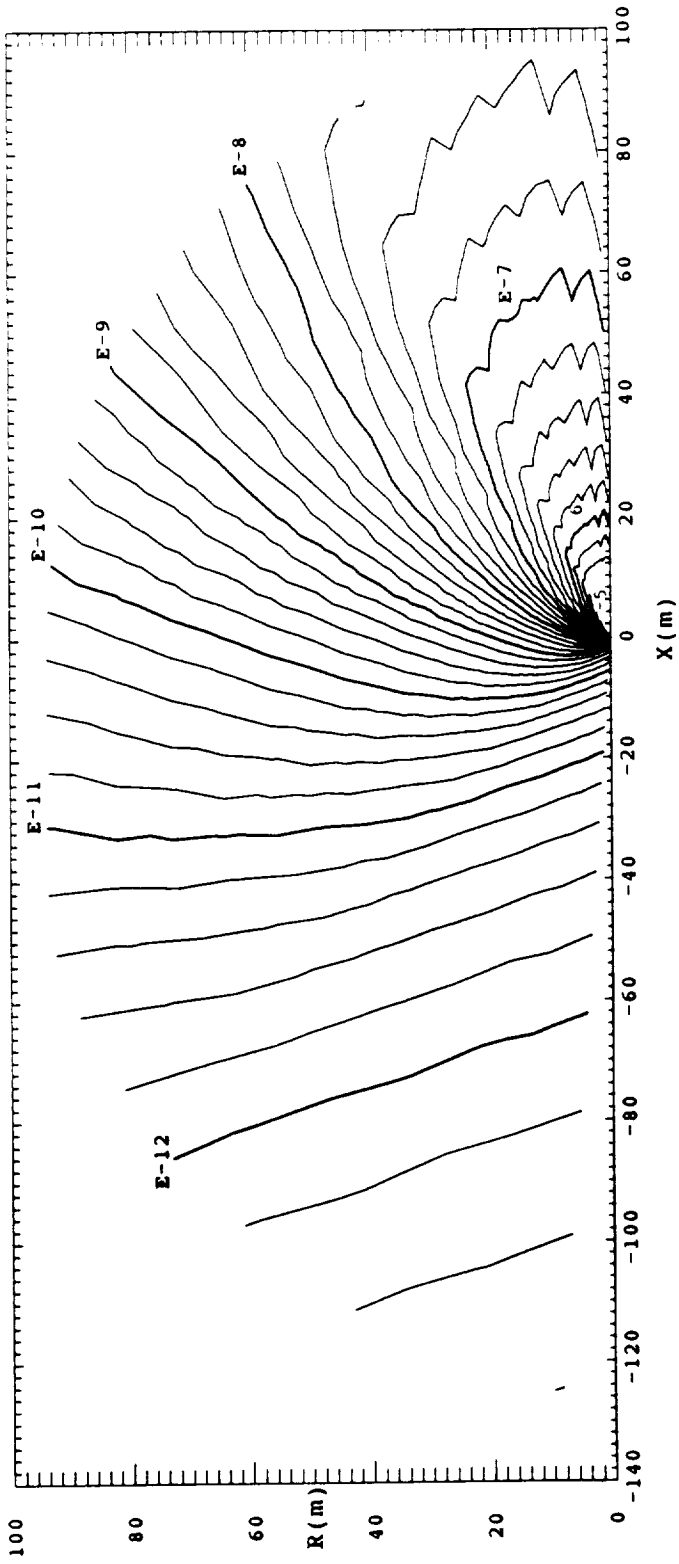

Fig(11) The plume gas mixture mean mass density distribution (kg/m^3).

mass density distribution surface has a large depression at large flow angles, especially approaching the symmetry axis. Taken together, Figs(4) and (11) imply a substantial decrease in mean molecular weight of the mixture as the flow angle increases.

The difference in shapes of the number density surface and the mass density surface is illustrated more graphically in Fig(12) which overlays the number density and mass density contours (for clarity only contour values with integer exponents are shown, the dark curves are mass density). At X = −100 m the number density is nearly independent of radius (as far as the flowfield outer boundary) while the mass density increases by a factor of 1.6 from the axis to the outer boundary. Clearly the number density and mass density are varying independently, implying that the mixture composition and thus the mean molecular weight are changing. There is therefore no elementary functional relation between the number density and mass density as would be anticipated for a simple (1 species) gas or for a gas of fixed composition.

Similarly, the incident number flux density is independent of the incident mass flux density at hardware surfaces, due to gas composition variation, see Figs(34) and (35) on pages 66 and 67.

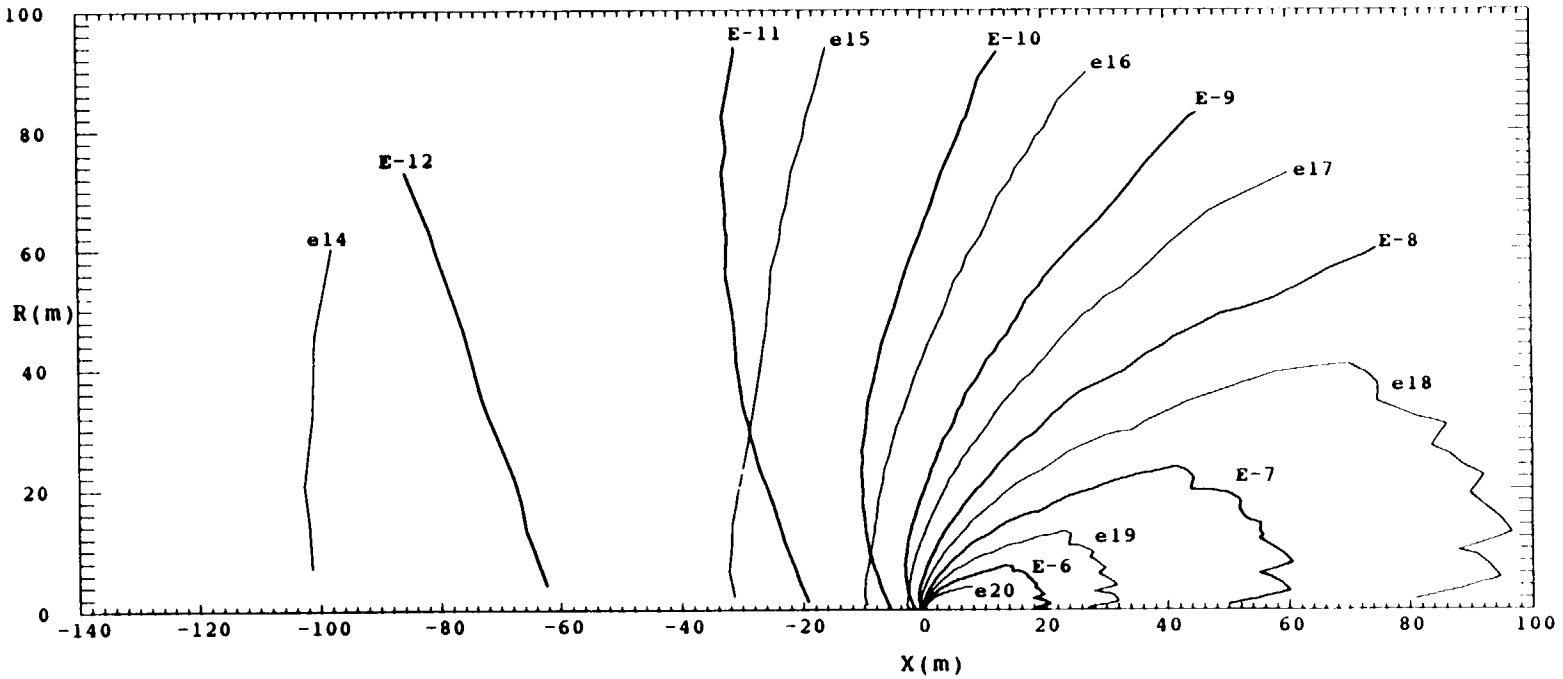

Fig(12) Overplot of the plume gas mixture mean number density(light) and mass density(dark) distributions.

The mass density depression along the symmetry axis in the rarefied region is further illustrated in Fig(13) which presents several vertical cuts thru the mass density surface of Fig(11) at indicated values of X, yielding curves of mass density as a function of radius only.

The mixture mean molecular weight distribution is given in Fig(14). Along the Monte Carlo input boundary the mean molecular weight varies smoothly from about 18 at the nozzle wall to slightly less than 23 at the symmetry axis 10.7 m down stream of the exit plane. Near the symmetry axis far downstream from the nozzle exit the mean molecular weight reaches a value of 23.2 which is larger than the maximum value prescribed along the Monte Carlo input boundary (about 22.5), thus the abundance of the heavier species is slightly increased along the symmetry axis (this effect is commonly observed in molecular beams). Near the symmetry axis in the rarefied region ($X < 0$) the mean molecular weight reaches a value slightly less than 2.5.

The mean molecular weight as a function of flow angle only is given in Fig(15). These data were taken along circular arcs 25 m and 75 m from the origin and imply that at large distances from the nozzle exit the mean molecular weight distribution may be considered a linear function of flow angle only (while not exactly linear the curve departs by no more than $\pm$ 10% from linearity).

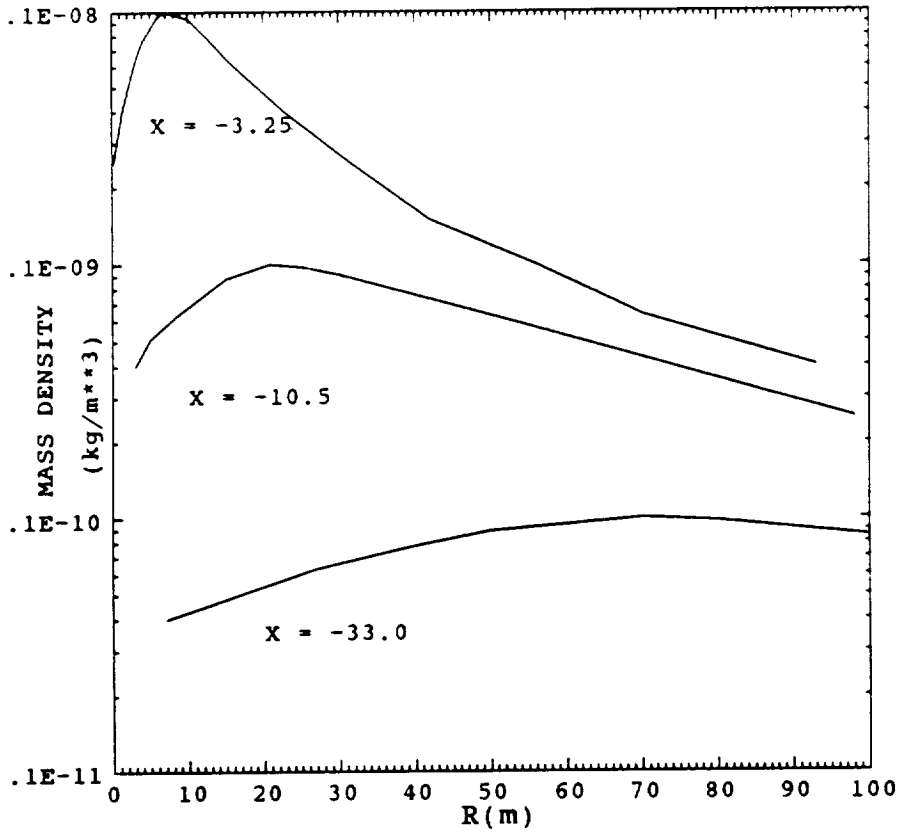

Fig(13) Rarefied region mean mass density at X = (–3.25, –10.5, –33.0) m as a function of radius only.

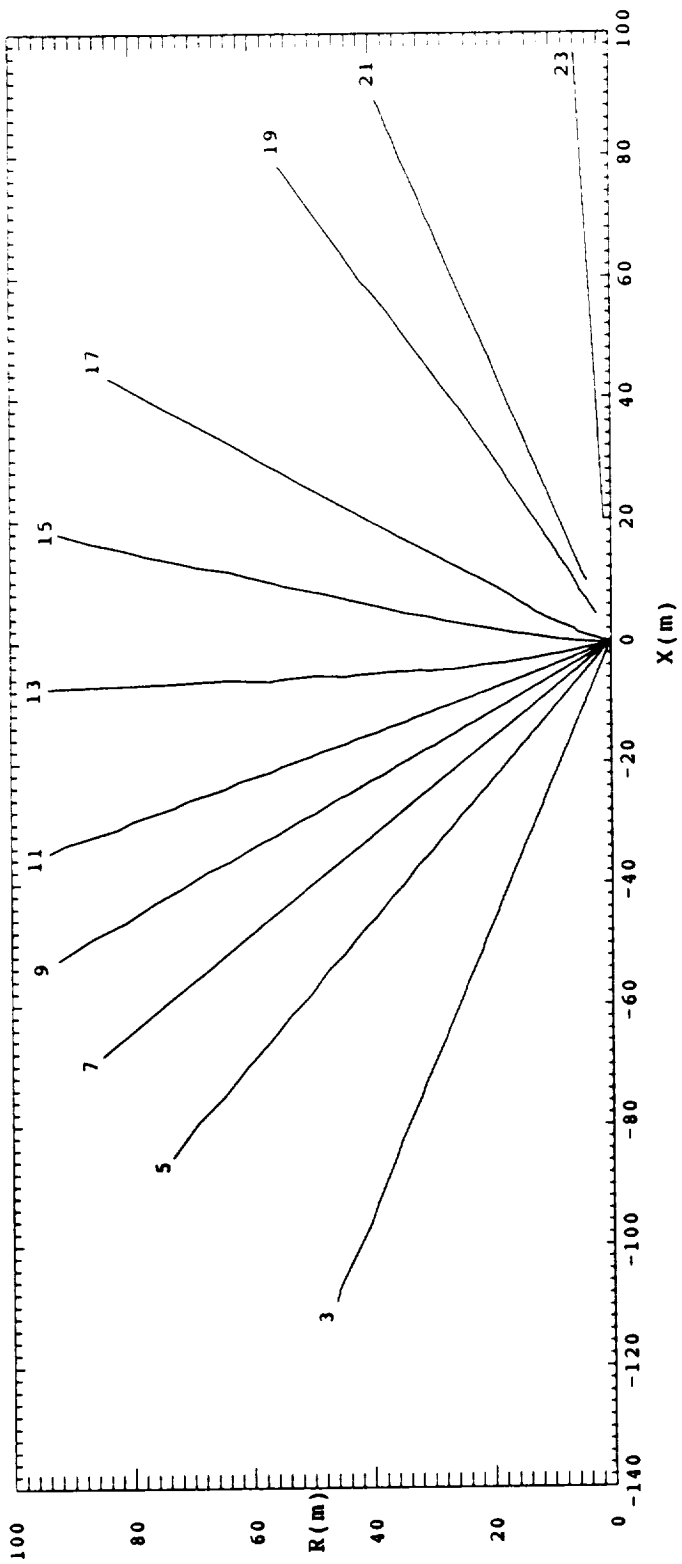

Fig(14) The plume gas mixture mean molecular weight distribution.

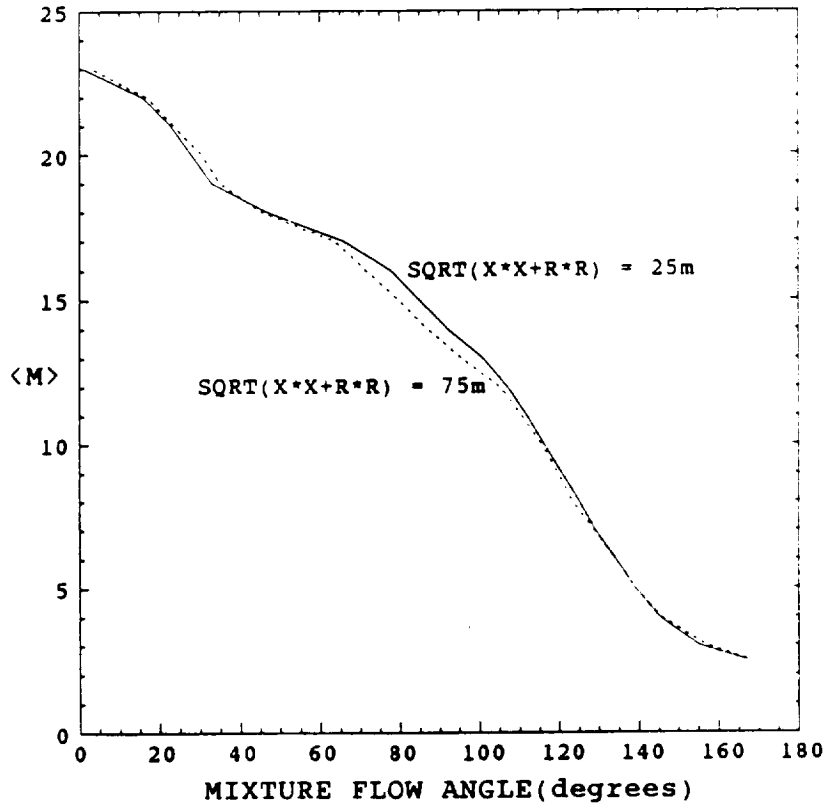

Fig(15) The plume gas mixture local mean molecular weight as a function of mixture local flow angle (°), both measured along the circular arcs 25 m (solid) and 75 m (dotted) from the origin.

The mean molecular weight as a function of arc length along the density contour 10^{18} m^{-3} is shown in Fig(16); for reference several discrete values of flow angle are indicated on the curve. Fig(4) on page 19, shows that S = 0 is on the symmetry axis at about X = 95 m (near the outer boundary) and that the last point on the curve is in the rarefied flow region near R = 0.5 m and X = −1.0 m. Along this contour (constant number density) most of the variation in mean molecular weight occurs beyond a flow angle of 1.75(100°).

It is frequently assumed in approximate treatments of plume flows that the heavier species in the mixture do not flow into the rarefied (backflow) region; but to the contrary the DSMC results show a steady decrease of mean molecular weight with flow angle, see Fig(14). This implies that the lighter species tend to dominate the mixture composition at large flow angles; however the relative abundance contours for each species displayed in Figs(17) thru (21) show that each species makes a measurable contribution to the mixture everywhere in the flowfield. These contour plots define smooth relative abundance surfaces for each species; there are no steps in the surfaces or abrupt changes in slopes.

The number fraction of H_2 is about 0.075 at a flow angle of 0.0 (symmetry axis) and steadily increases to 0.975 at a flow angle of 2.97(170°). The relative abundance of all other species tends to decrease with increasing flow angle; however N_2 decreases slowly for flow angles less than about 1.75(100°) then

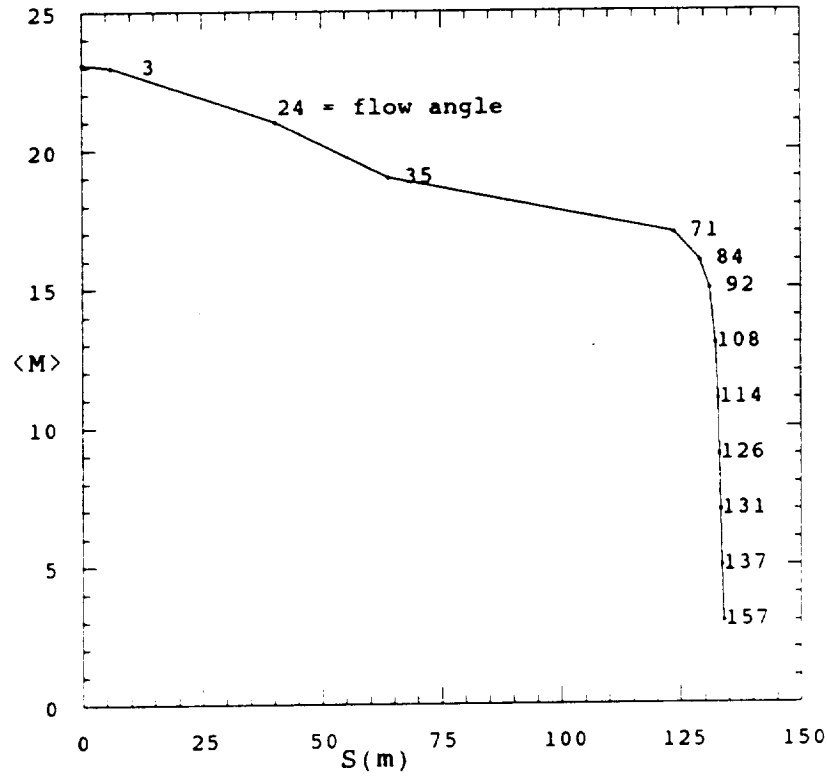

Fig(16) The plume gas mixture mean molecular weight measured along the density contour n = 10^{18} m^{-3}.

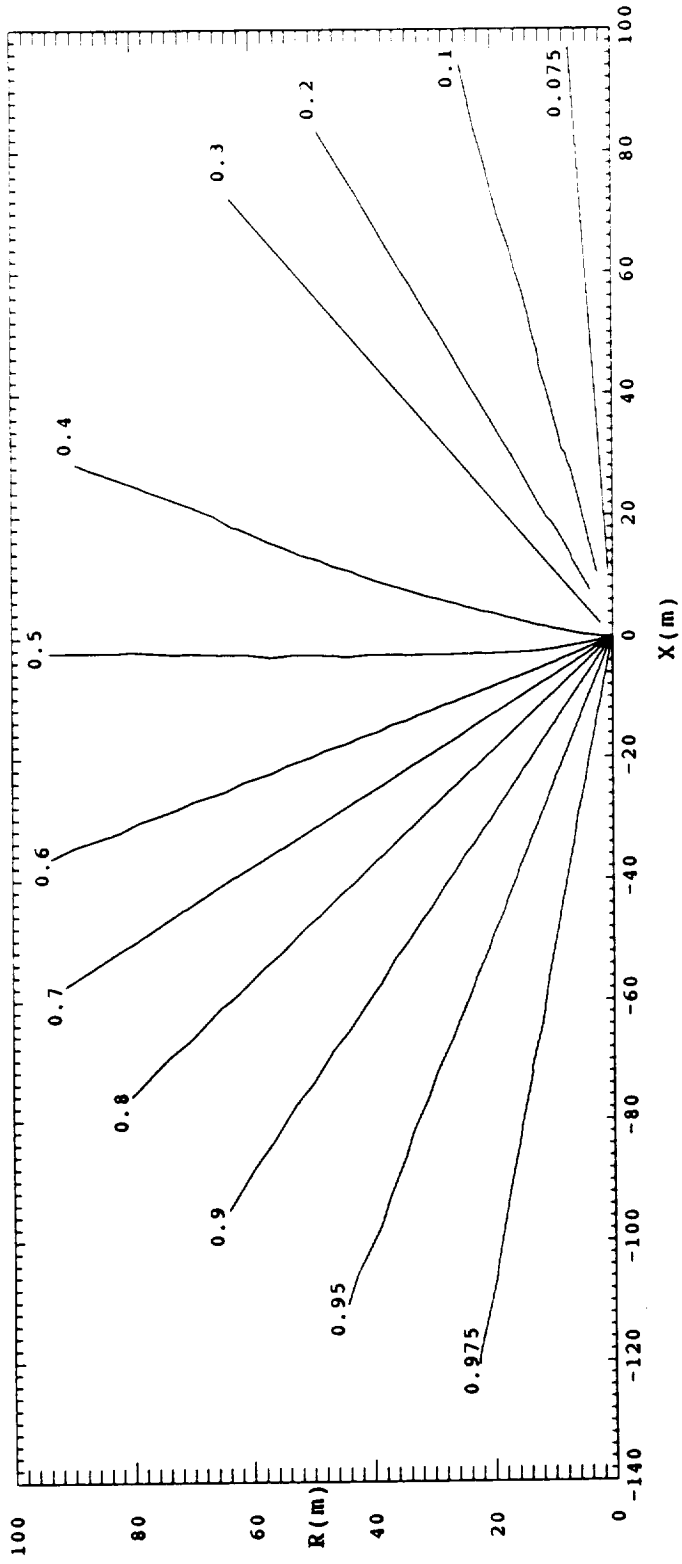

Fig(17) Molecular hydrogen relative abundance(= number fraction) distribution.

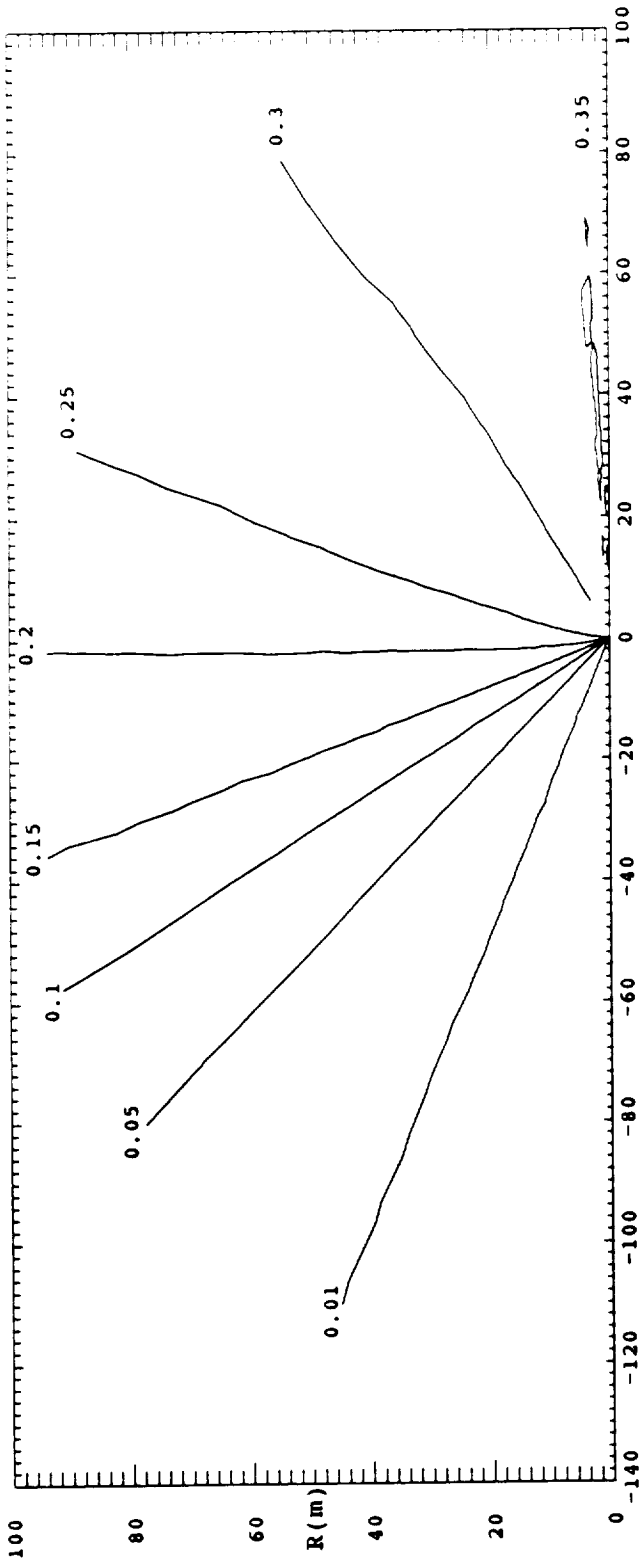

Fig(18) Molecular nitrogen relative abundance distribution.

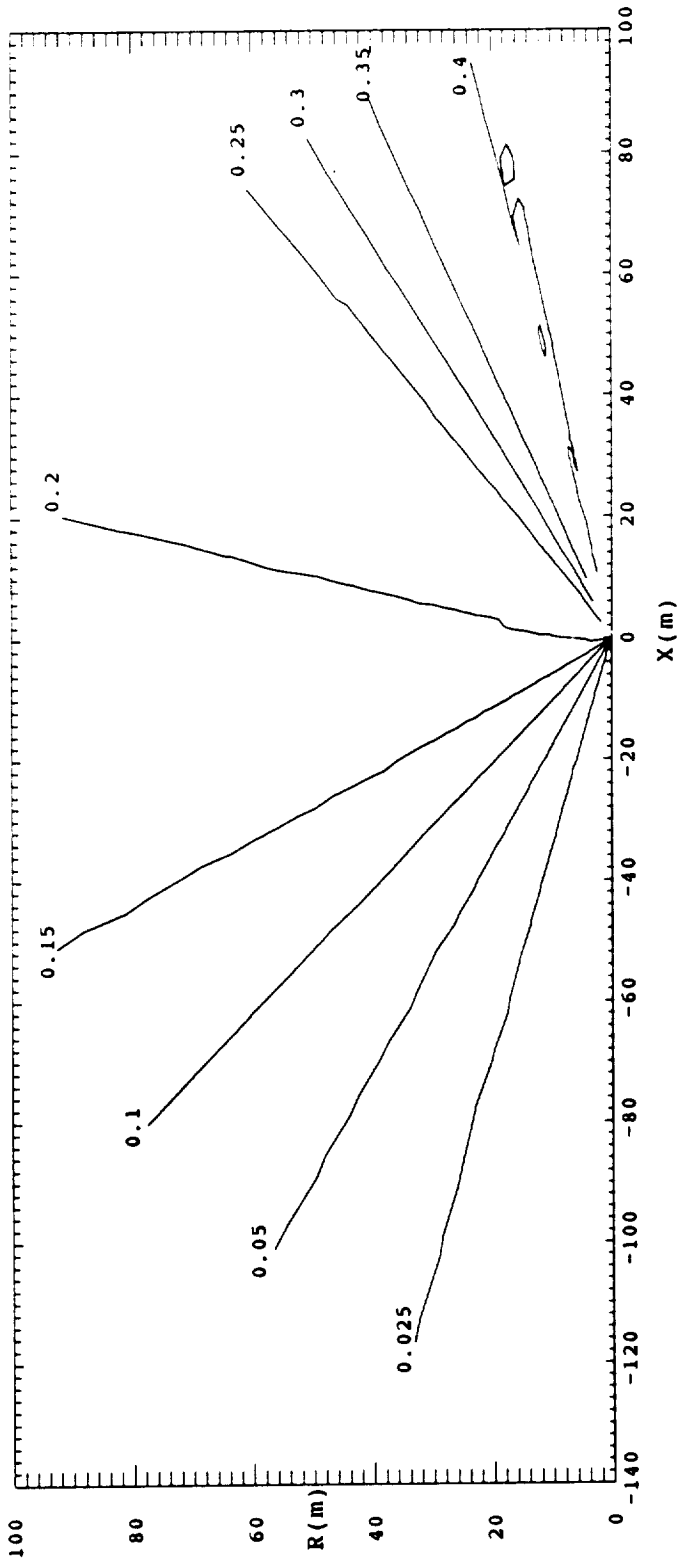

Fig(19) Water relative abundance distribution.

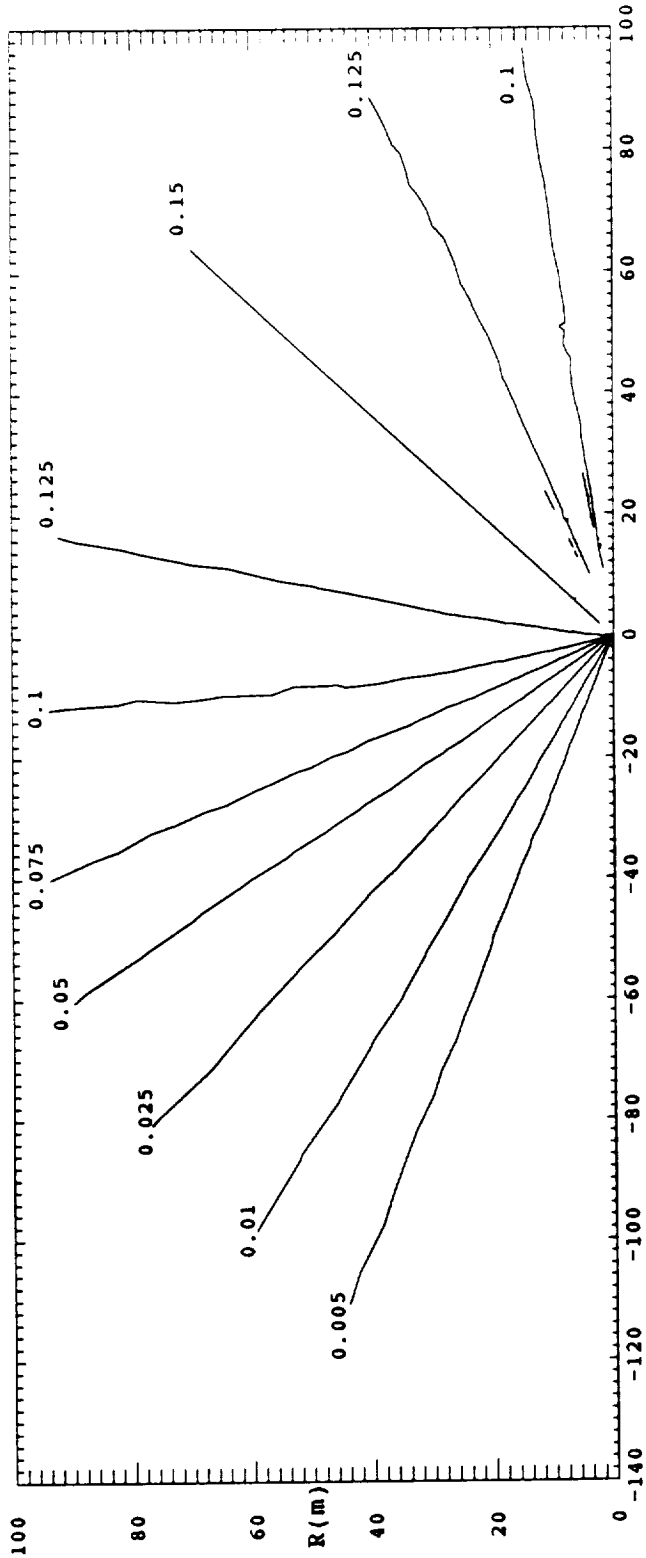

Fig(20) Carbon monoxide relative abundance distribution.

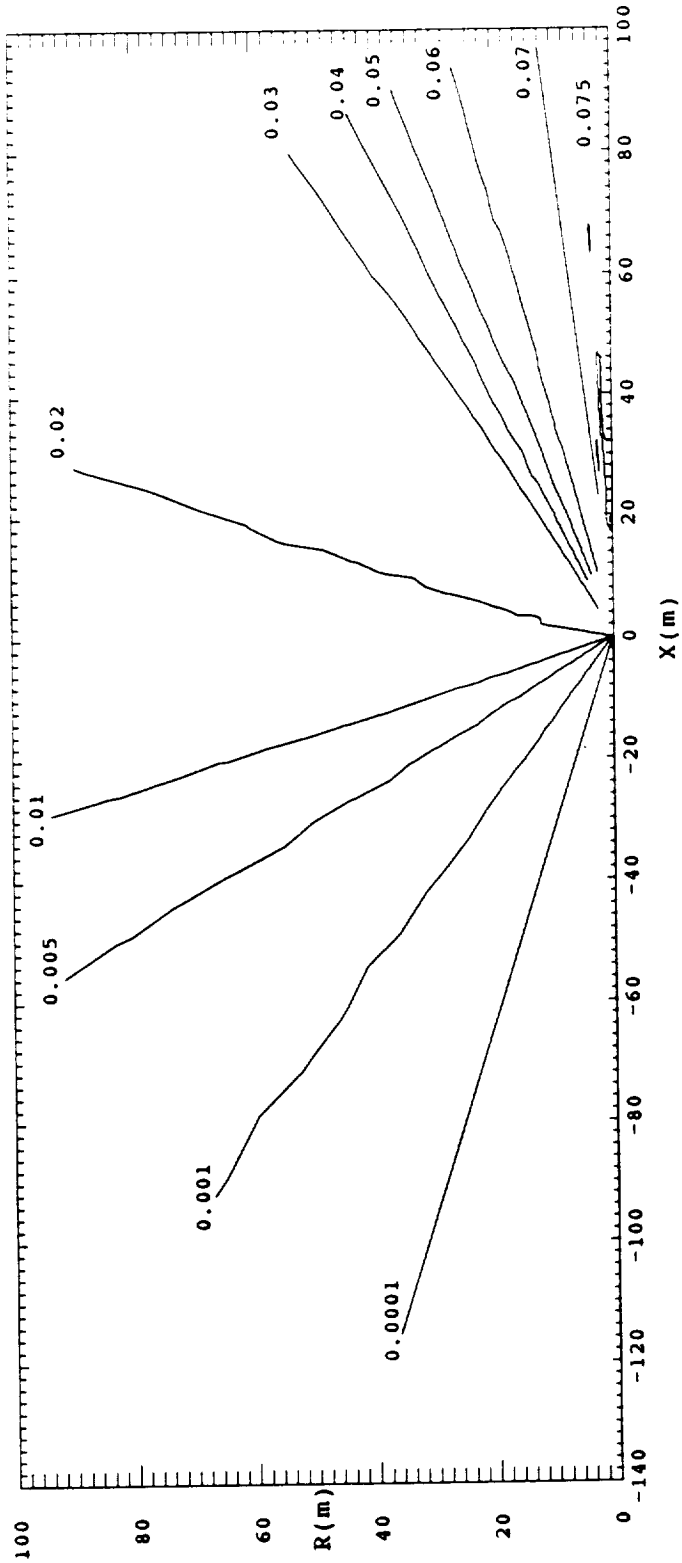

Fig(21) Carbon dioxide relative abundance distribution.

decreases more rapidly, the abundance of H_2O decreases rapidly up to a flow angle of 0.66(38°) and then decreases more slowly, the relative abundance of CO actually increases up to a flow angle of about 0.87(50°) before decreasing rapidly, and the abundance of CO_2 decreases rapidly up to a flow angle of 0.56(32°) and then decreases more slowly. These effects are partly associated with changes in gas composition along the Monte Carlo input boundary and partly associated with species separation according to molecular mass due to variation in flow dynamics between species, see discussion above.

Further information on the dynamics of the plume flow may be obtained by examining the species mass fraction distributions. While the mean molecular weight is a steadily decreasing and relatively smooth function of flow angle, the mass fraction distributions of the components of the mixture are more complex. Figs(22) thru (26) present the plume gas mixture decomposed into mass fraction distributions by species.

These data show that the mass fraction of H_2 in the plume mixture increases from slightly less than 0.005 on the symmetry axis (flow angle = 0.0) to 0.85 at a flow angle of 2.97(170°). Thus the mass fraction of molecular hydrogen in the plume increases by a factor of 170 in the solution space. The hydrogen mass fraction of 0.005 near the symmetry axis far downstream of the exit plane is lower than at any Monte Carlo input boundary segment, again implying mixture enrichment by heavier species near the symmetry axis.

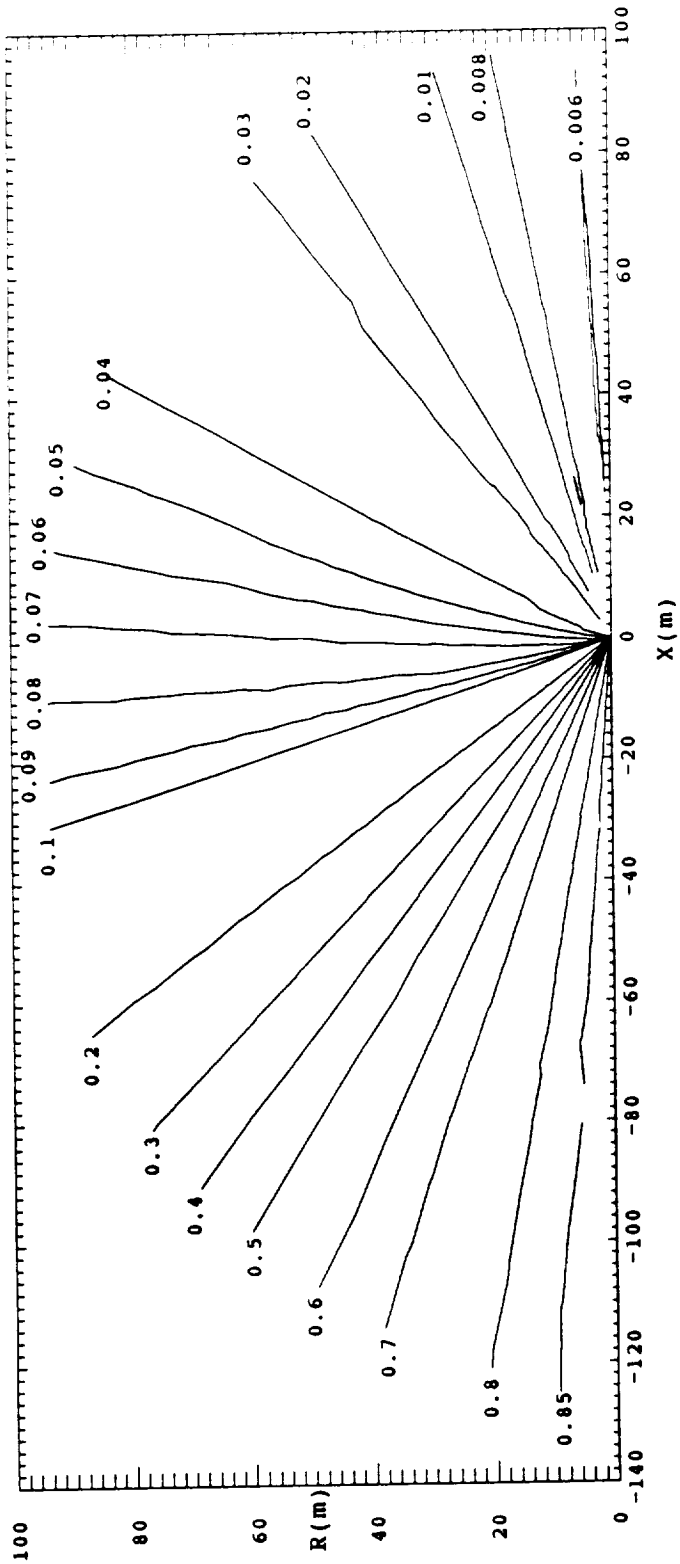

Fig(22) Molecular hydrogen mass fraction distribution.

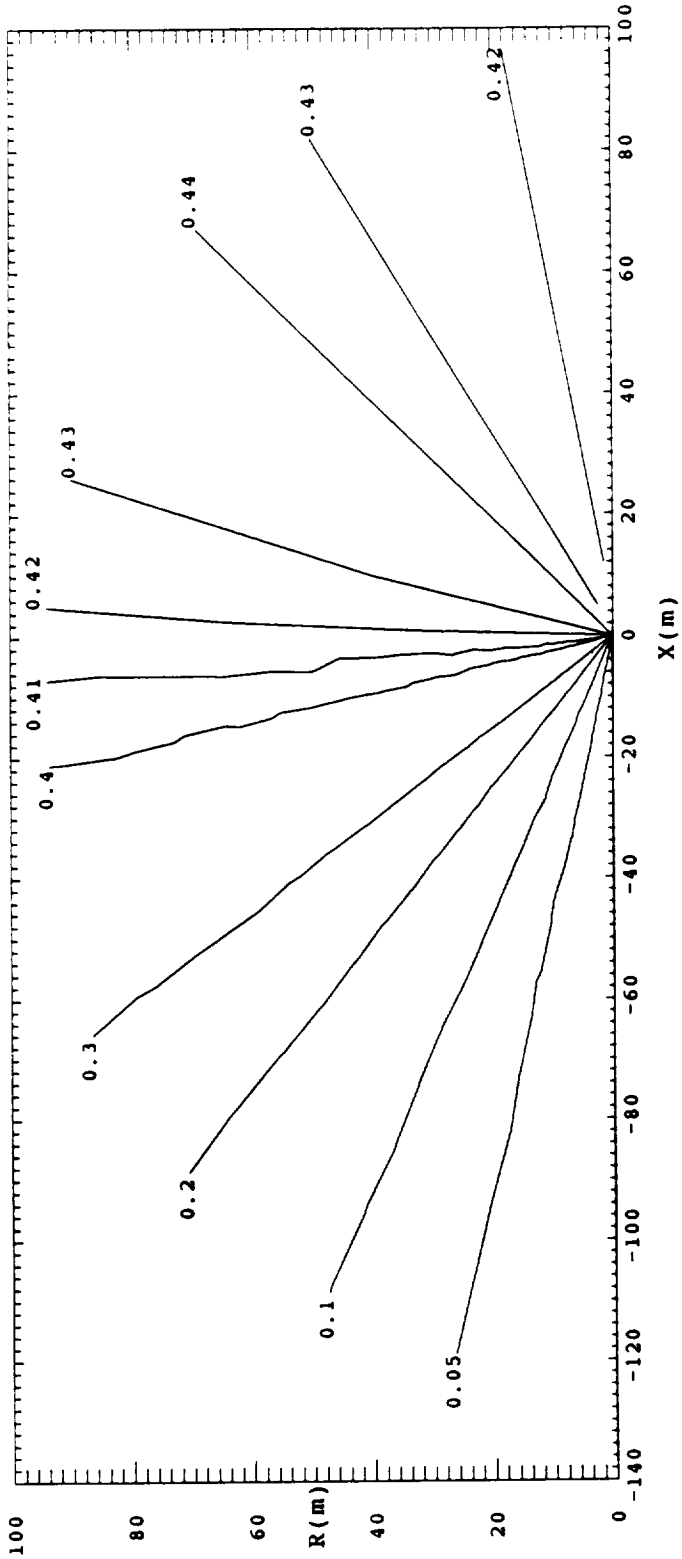

Fig(23) Molecular nitrogen mass fraction distribution.

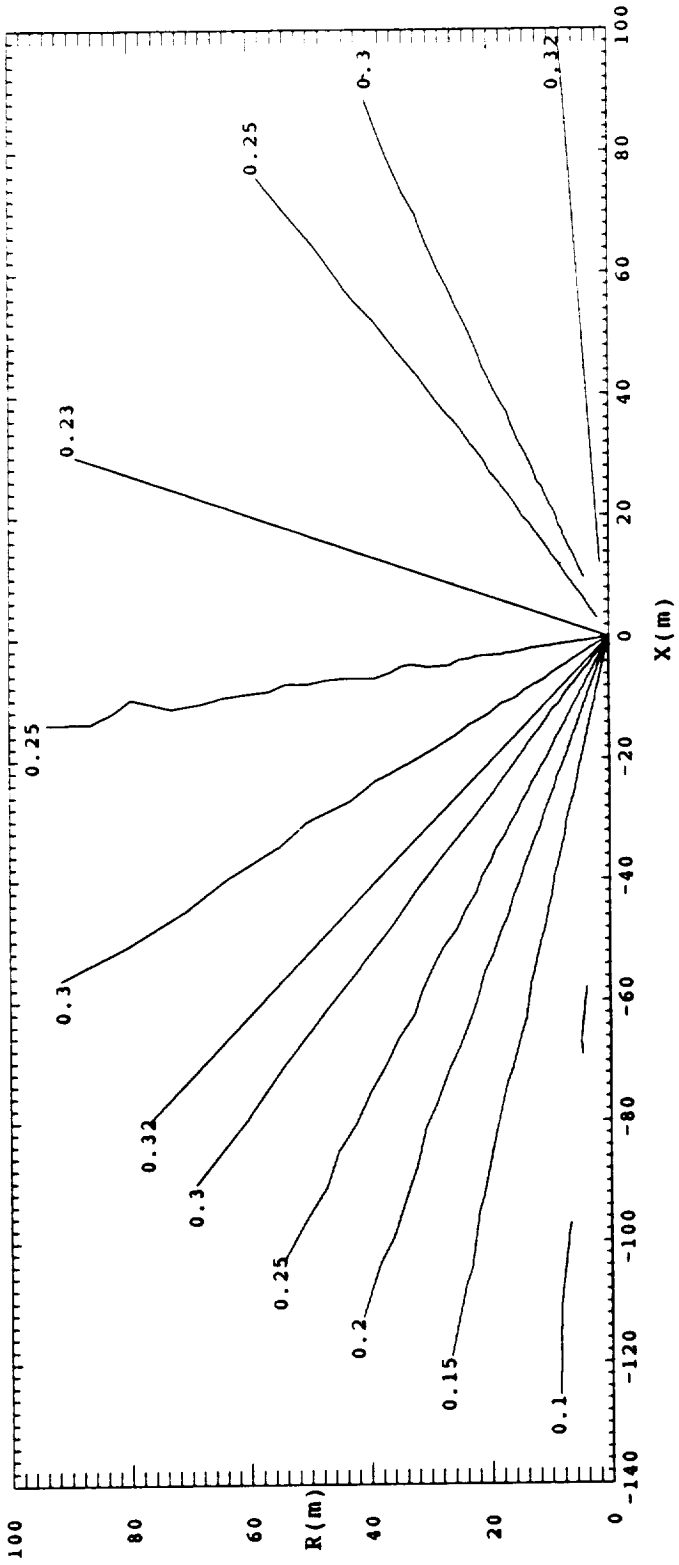

Fig(24) Water mass fraction distribution.

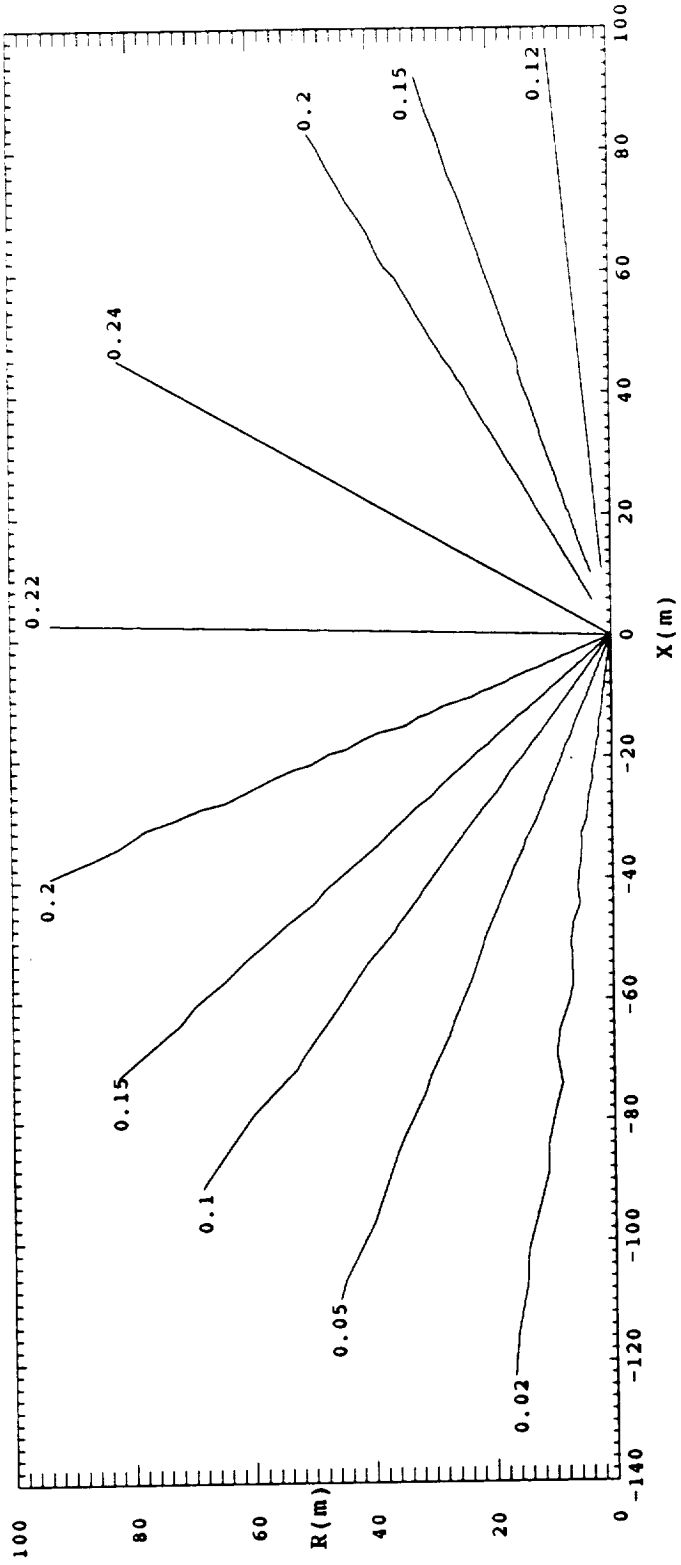

Fig(25) Carbon monoxide mass fraction distribution.

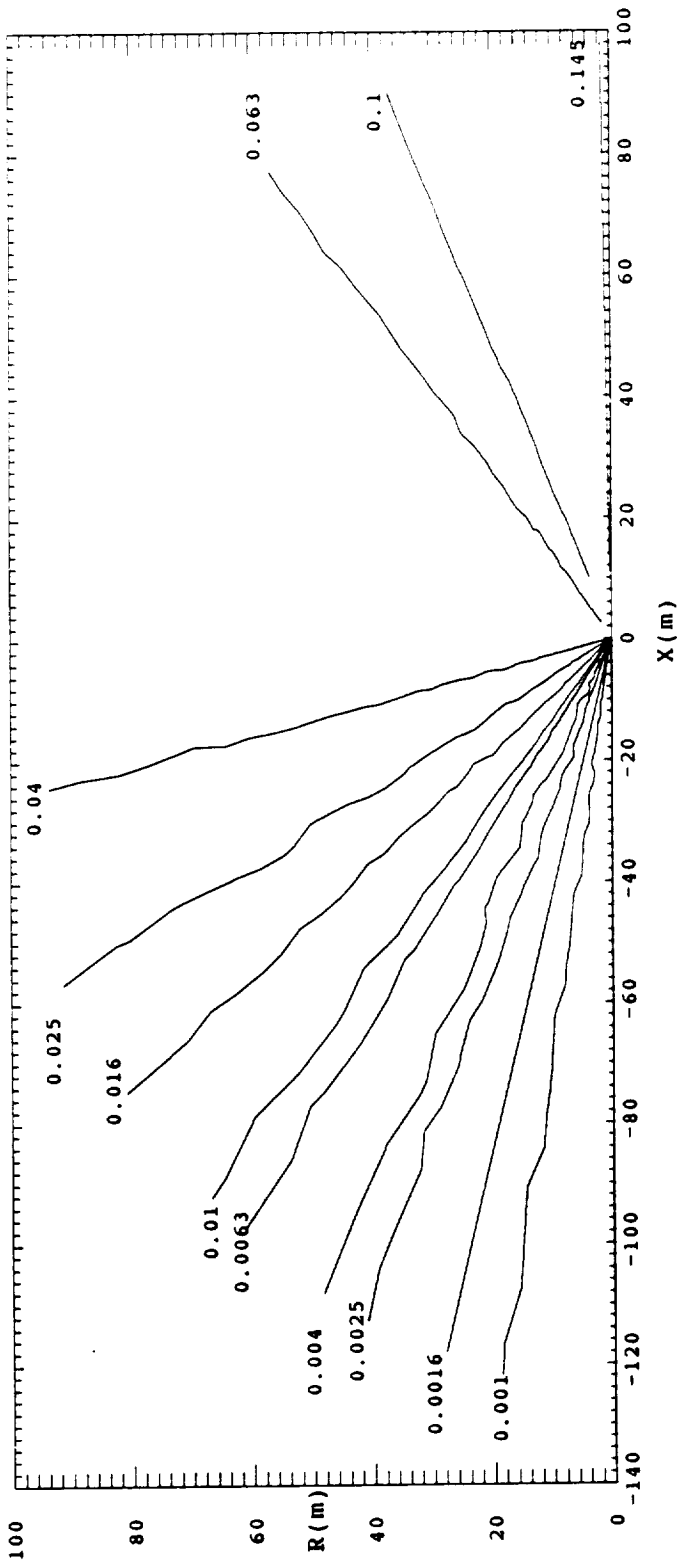

Fig(26) Carbon dioxide mass fraction distribution.

Proceeding away from the symmetry axis the molecular nitrogen (molecular weight 28) actually increases with increasing flow angle up to a flow angle of 0.87(50°) (from 0.42 to 0.44) where it begins to decrease slowly at first then more rapidly. At a relatively low flow angle the mass fraction of H_2O begins to decrease from 0.32 to 0.23 at a flow angle of 1.08(62°), then reverses and increases to 0.32 at a flow angle of 2.37(136°) then reverses again and drops to 0.1 at a flow angle of 3.07(176°). In contrast the mass fraction of carbon monoxide begins immediately to increase from 0.12 near the symmetry axis to 0.24 at 1.06(61°) and then steadily decreases to 0.02 at 3.02(173°). While CO_2 has the largest molecular mass in the mixture, it accounts for only 0.13 of the mixture mass density near the symmetry axis and drops steadily to 0.001 at a flow angle of 3.0(172°).

The dynamic loss of the heavier species with increasing flow angle does not account for all the variations of relative abundance and mass fraction; the variations are partly due to the changing gas composition (and therefore mean molecular weight) along the Monte Carlo input boundary. These variations are illustrated in Fig(27) which displays the mass fractions by species as a function of flow angle along the circular arc 75 m from the origin. The flow angle (abscissa) is of course 0.0 along the symmetry axis. The mean molecular weight along the Monte Carlo input boundary as a function of flow angle (also along the input boundary) is given by the heavy curve (compressed by the exponential ordinate). This curve terminates at a

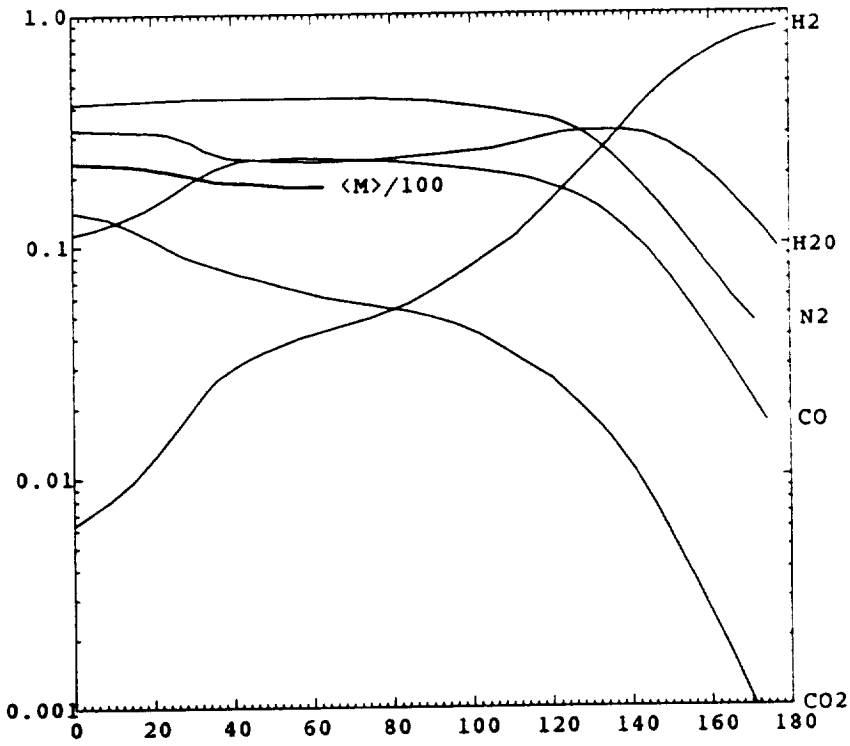

Fig(27) Mass fraction by species as a function of mixture local flow angle (°)measured along the circular arc 75 m from the origin.

flow angle of 1.1(63°) which is the maximum flow angle along the input boundary. The substantial initial increase in the mass fraction of CO is more clearly displayed in this figure.

The mean collision frequency for the plume gas mixture is displayed in Fig(28); the darker curves have integer exponent contour values as indicated and the ratio of any pair of adjacent values is $10^{1/5}$ (= 1.585, approximately). These results indicate that the collision frequency gradient is very large near the Monte Carlo input boundary, especially near the nozzle exit and continuing downstream from the lip into the rarefied region. The gas departs from equilibrium as the collision frequency gradient becomes so large that the incremental reduction in collision frequency yields insufficient collisions in a spatial increment to support collisional transfer of information. Near the nozzle exit plane the collision frequency is of the order of $4*10^8$ s^{-1} and Fig(28) indicates that it has dropped below 0.04 s^{-1} in the rarefied region for X less than −100 m. The collision frequency of the mixture given in Fig(28) was constructed by averaging over all species which sometimes yields a rather misleading numerical value since the collision frequency of the individual components differ substantially in some regions of the solution space yet are nearly equal in other parts of the flowfield, as shown in Fig(29). The H_2 collision frequency is clearly larger than the CO_2 collision frequency everywhere in the flowfield.

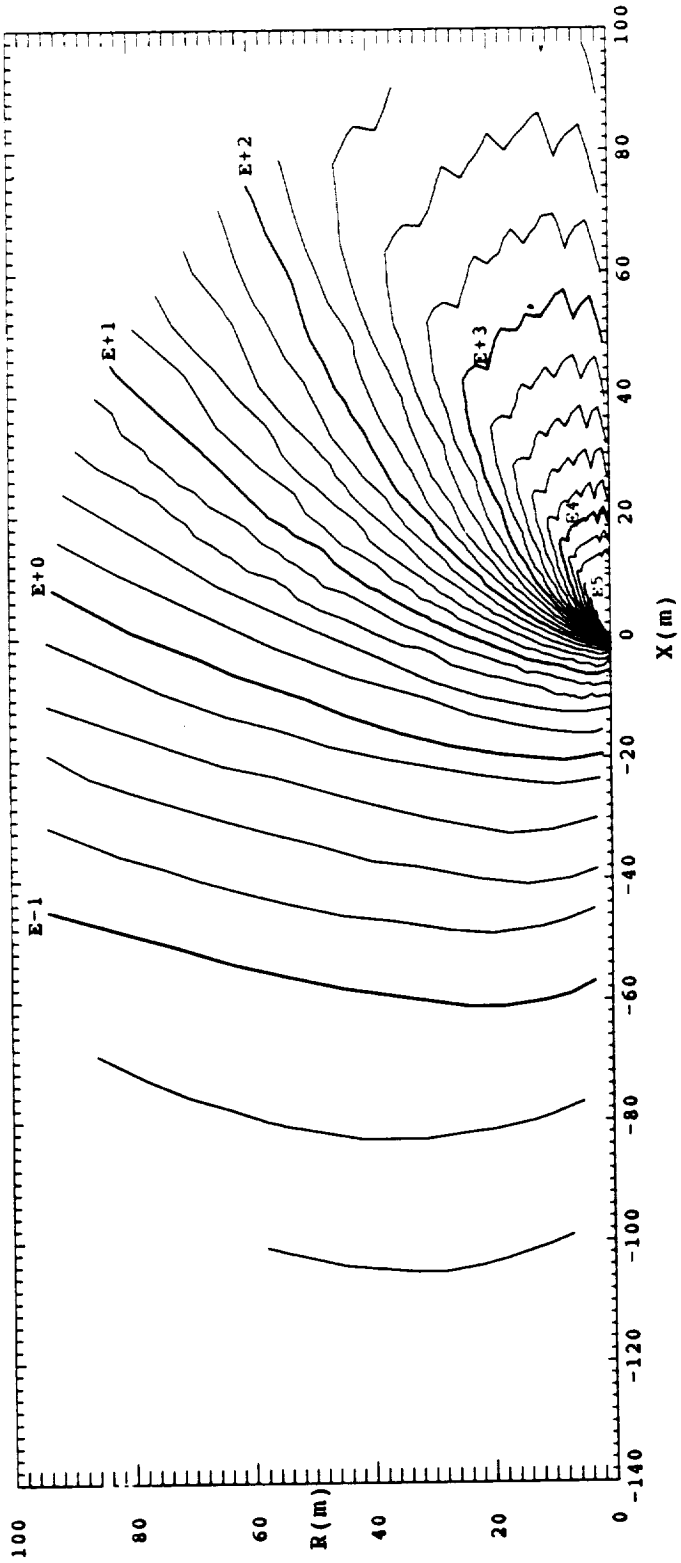

Fig(28) The plume gas mixture mean collision frequency distribution (s^{-1}).

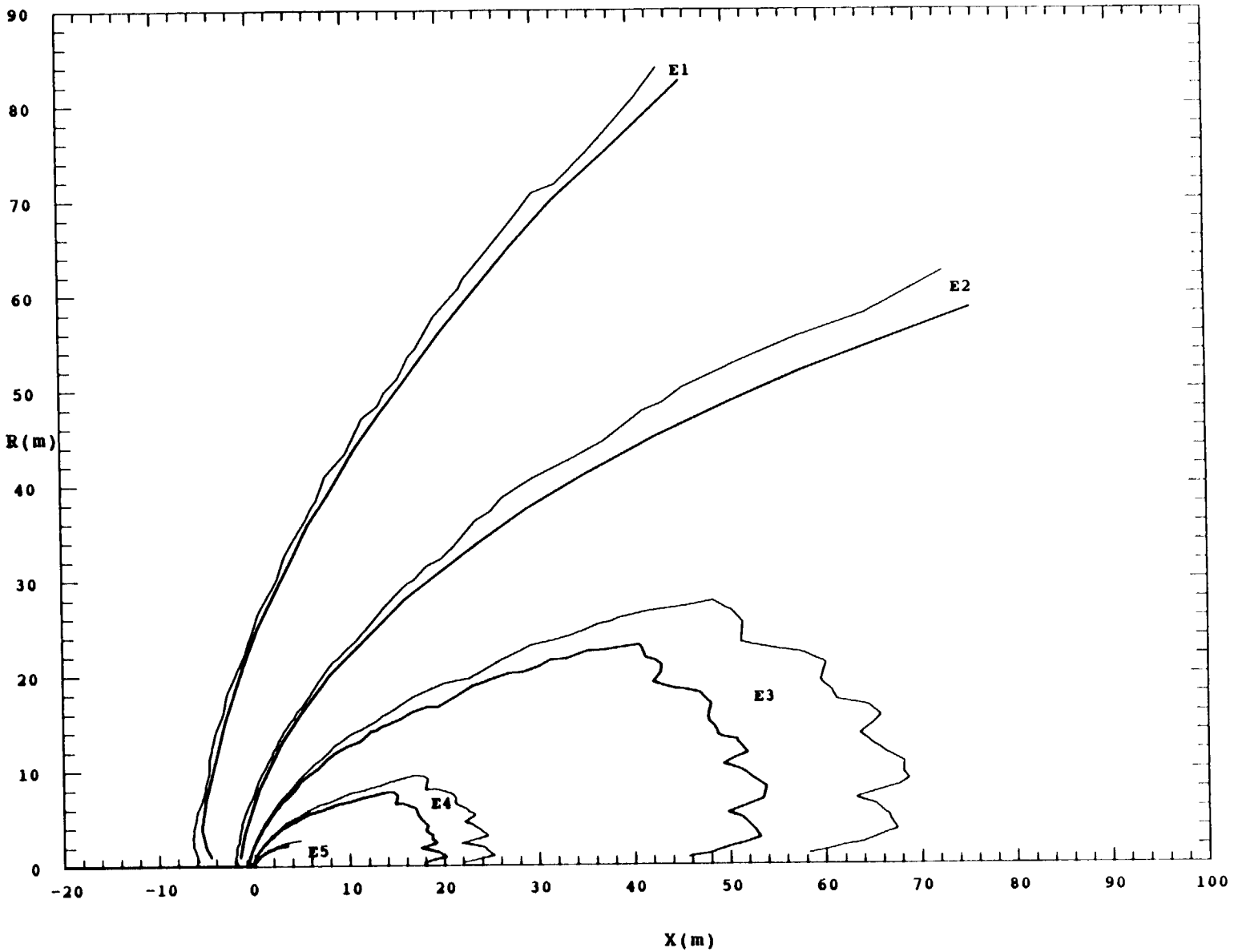

Fig(29) Overplot of H_2 (light) and CO_2 (dark) collision frequency distributions.

Variation of collision frequency by species depends on gas composition, molecular mass, cross section, relative velocity, etc in a complex way. For the pair (H_2,CO_2) shown in Fig(29), giving neither the largest nor smallest variation, contours having the same collision frequency value are separated by as much as 15 m near the symmetry axis. It is clear from Fig(29) that the magnitude of the collision frequency variation with species is a function of geometrical location in the flowfield (thru density). Corresponding to the 100 s^{-1} contour in Fig(28), a collision frequency contour for each species (light curves) along with the mixture mean (dark curve) are shown in Fig(30). For this location in the flow and the extent of these contours, the maximum separation is no more than 6 m and becomes much smaller approaching the origin. Further, Fig(30) clearly illustrates that the collision frequencies for each species is not strictly ordered by molecular mass.

Enrichment of the plume gas mixture with heavy species at small flow angles near the symmetry axis is displayed in Fig(31) in which the number density distribution of both H_2 and CO_2 are overplotted, for integer contour values (light curves give the H_2 number density, e = base 10, and the heavy curves give CO_2 , E = base 10). Fig(31) presents several gas dynamic phenomena rarely observed so clearly: For flow angles less than about 0.57(33°) the H_2 number density slope in the radial direction is positive ($\partial n(H_2)/\partial r > 0$, number density increases with increasing distance from the symmetry axis) while the partial of the CO_2 density with respect to R is

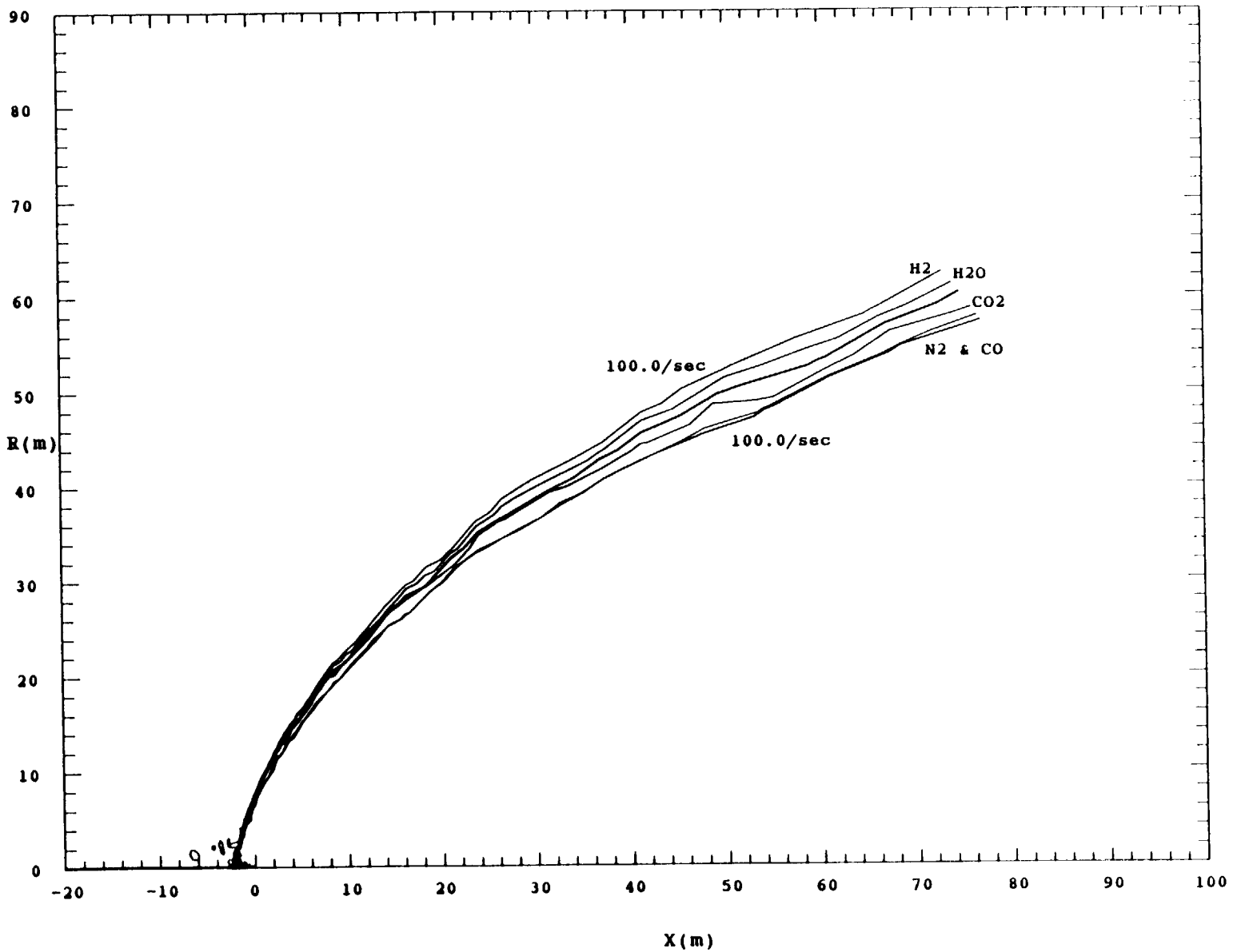

Fig(30) 100s^{-1} collision frequency contours for each species(light) and the mixture(dark).

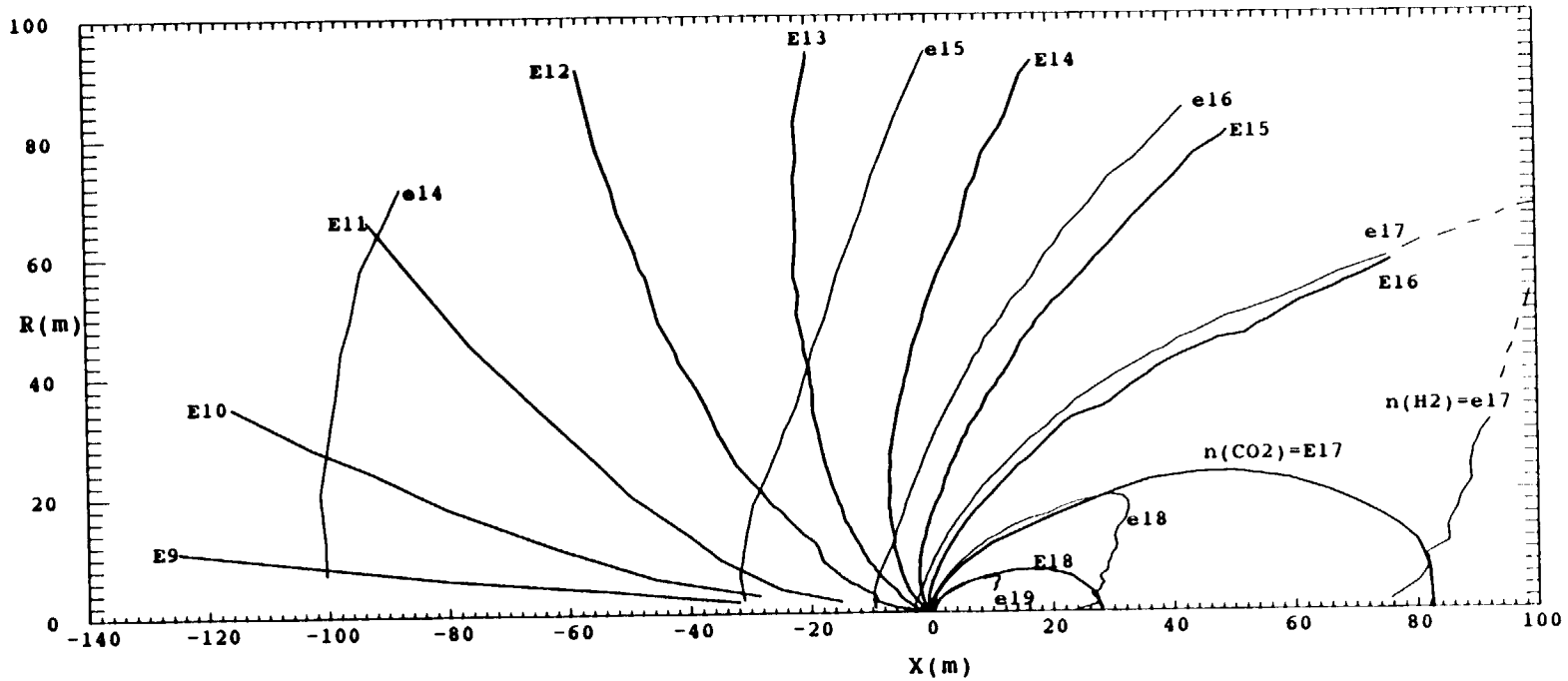

Fig(31) Overplot of H_2 (light) and CO_2 (dark) number density distributions. (The dashed curve indicates the expected shape of the $n(H_2) = 10^{17}$ m^{-3} if the Monte Carlo flowfield had extended to the edge of the frame.)

negative. The higher collision frequency measured in the DSMC model for the lighter species as shown in Fig(29) yields a relatively rapid collisional transfer of kinetic energy from H_2 to CO_2 (in the mean) thus maintaining near equality between the flow velocity components (axial and radial) of both the light and heavy species. But further, the higher collision frequency of the lighter species yields a larger mean deflection of H_2 for (H_2,CO_2) scattering, since the mass ratio of 22 implies that the CO_2 postcollision velocity vector is very near the precollision velocity while the H_2 postcollision velocity vector is only weakly coupled to the precollision velocity[9] (momentum persistence). Therefore, in the mean, the lighter species has a higher probability of accumulating a larger radial deflection as the flow proceds downstream, yielding a substantial difference in the shape of the density distributions for the lighter (H_2) and heavier (CO_2) species, as shown in Fig(31). From another prospective, due to momentum persistence, the mean radial acceleration for the lighter components of the mixture is slightly larger than for the heavier components which tends to deplete the mixture of light species near the symmetry axis while enhancing the heavier species. The collisional energy transfer and scattering process outlined above is the physical foundation for 'seeding' a heavy species molecular beam with a much lighter species to accelerate the heavy species to a higher axial speed while minimizing beam contamination by the seed species which was introduced to enhance the collisional transfer of energy. In the rarefied part of the solution space the CO_2 density slope in the axial direction is much steeper than the H_2 density axial slope

($|\partial n(CO_2)/\partial x| >> |n(H_2)/\partial x|$). At a prescribed value of X deep in the rarefied region, the H_2 density contour surfaces approach radial planes (disks) such that the H_2 density is principally a function of X and depends only weakly on R while the CO_2 contour surfaces approach cones such that the CO_2 density is a strong function of both X and R. This yields a heavy species density cavity adjacent to the negative symmetry axis, while in the same region the density of the lighter species is slightly enhanced (rather opposite of the behavior along the positive symmetry axis).

An estimate of the mean distance molecules move in the flow direction between successive collisions may be constructed from the product of mean free time $\tau = \nu^{-1}$ (ν = measured local collision frequency from the DSMC model) and local flow speed C_0 (provided that the vector velocity and collision frequency are not changing rapidly, which therefore restricts the approximation to the rarefied flow region). Fig(32) shows contours along which the product of local mean free time and flow speed $\tau * C_0$ is constant, the value of which is indicated at the end of each curve. The local vector velocities are indicated by arrows drawn at several points on each contour; the arrows point in the flow direction for the point of origin on the contour and the arrow length indicates the flow speed at that point (see calibration arrow near abscissa). While there are similarities between the conventional mean free path and the logical construct used to generate the contours in Fig(32), severe constraints are attached to the data of Fig(32) and to its interpretation; the product of the

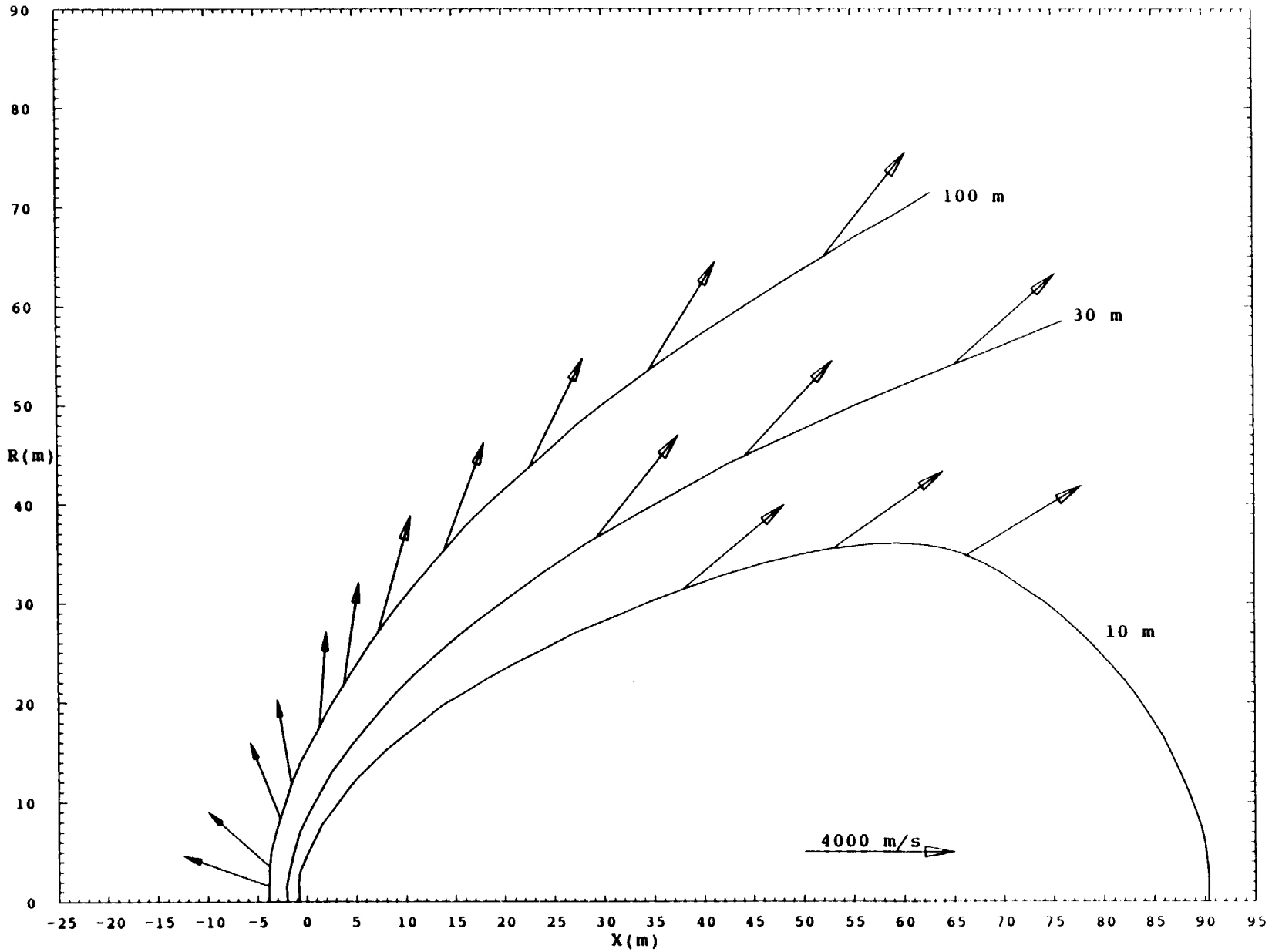

Fig(32) Contours of the product of the plume gas mixture local mean reciprocal collision frequency and the local mean flow speed for the values 10 m, 30 m and 100 m. (The arrows indicate the mixture local mean vector velocity.)

means (individually sampled, accumulated and averaged) is not the same as the mean of the product (product sampled directly (real time), accumulated and then averaged). The mean free path as variously defined by theoretical treatments based directly on kinetic theory has no meaning in the flowfield solution under discussion since the notion of temperature (2nd law) has no unique meaning in this highly nonequilibrium flow (nor is it necessary for the proper generation of a DSMC solution for the plume flow, since the temperature construct is not used in the DSMC method). Even so, a purely statistical but physically realistic mean free motion increment (actual molecular experience) may be defined and measured in the DSMC model without reliance on a kinetic theory derivation. For the RCS plume solution, the model was not setup in advance to make these internal measurements or to accumulate the data samples from which the mean motion increment could be computed, thus after the solution is completed there is no way of making a physically accurate (useful) statement about the mean free path. But deep in the rarefied flow region, the data given in Fig(32) is probably an acceptable approximation.

The molecular flux density passing thru an arbitrary surface element, the normal of which is parallel to the local velocity vector, may be estimated from the product of local density and vector velocity (again, provided that the vector velocity and collision frequency are not changing rapidly, which therefore restricts the approximation to the rarefied flow region). Several

contours for fixed values of the product $n*C_0$ (in m^{-2} s^{-1}) are displayed in Fig(33), contour values are indicated adjacent to each curve. The local vector velocity is indicated at several points along one of the contours (arrow direction indicates flow angle and length gives speed).

In approximate treatments of plume flow it is sometimes assumed that there is an identifiable surface, interface, or intermediate boundary at which the flow becomes collisionless. Fig(28) shows that even for this relatively large solution space and therefore a very large expansion factor, there is an observable collision frequency everywhere in the flowfield. While the above collisionless assumption is, of course, not rigorously correct for finite flow geometries (as in the flowfield under discussion), a surface may be identified beyond which the spatial interval between molecular collisions is sufficiently large that the collisions have a relatively minor direct effect on the local flow properties (at least up to the flowfield exit boundary). The collision frequency contour labeled $10\ s^{-1}$ in Fig(28) may be used to generate a surface of revolution about the symmetry axis. Downstream of this surface the probability is relatively high that molecules exit thru the flowfield outer boundary before experiencing their next collision; based on the local mean flow speed (which exceeds 2000 m/s in the rarefied region), on the local flow angle (which does not change substantially in this part of the flowfield), and on the mean free time at this location (the reciprocal of the mean collision frequency measured in the DSMC model).

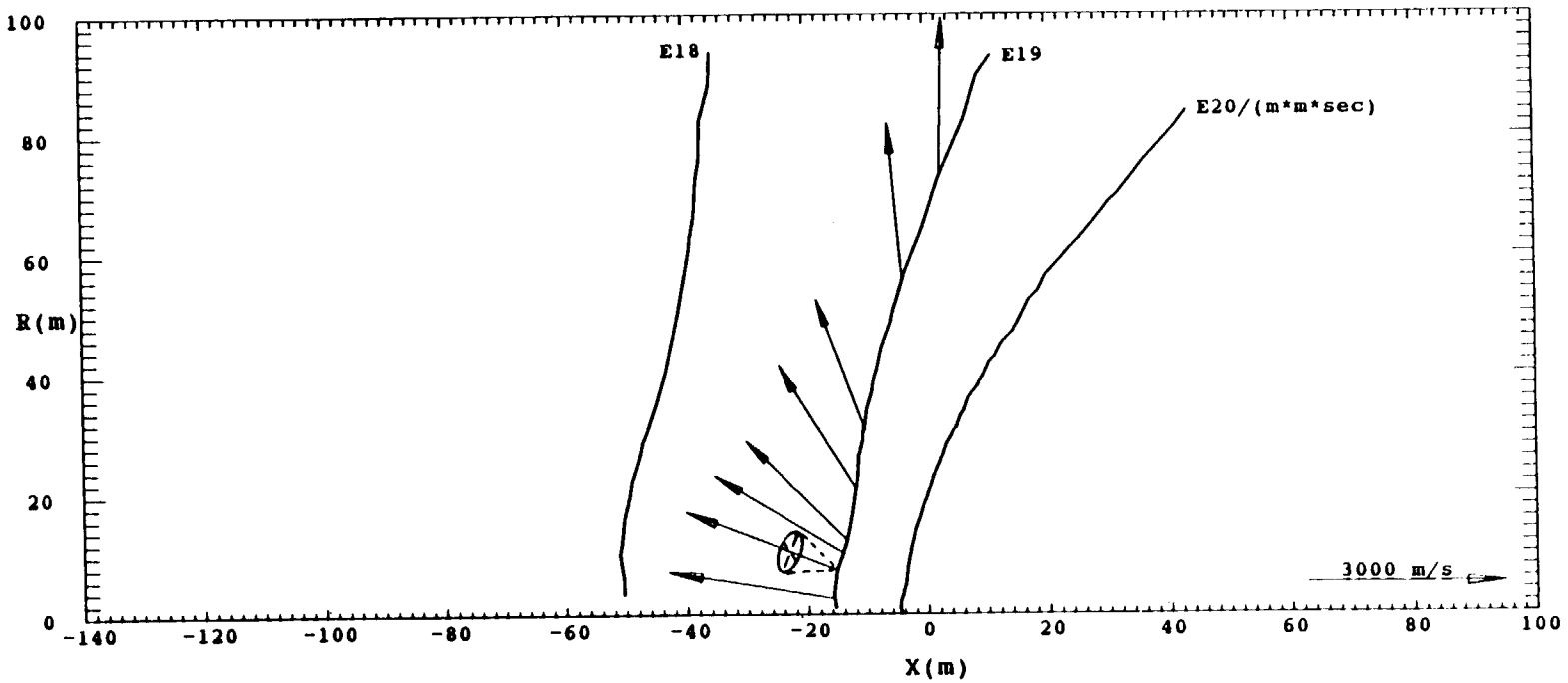

Fig(33) Contours of the product of the plume gas mixture local number density and the local flow speed for the values 10^{18}, 10^{19} and 10^{20} m^{-2} s^{-1} . (The arrows indicate the mixture local mean vector velocity.)

The data in Figs(32) and (33) may be useful in estimating the location of a geometrical surface of revolution beyond which the plume flow may be regarded as nearly collisionless, or for estimating the molecular flux density emitted toward a distant point or object by the plume cloud, or for estimating the force applied to a distant object by the plume molecular flux density incident on the object[10], etc. However, application of these and similar results to resolve ancillary questions call for due regard of their approximate nature: Thus, the arrows indicating flow velocities in Figs(32) and (33) are mean values for the flow properties at a point, but the individual molecular velocities are distributed in an unknown way about this arrow (say, bounded by some conical surface, the apex of which is centered on the arrow as indicated in Fig(33) and the halfangle of which may be approximated by the standard drifting gas formula $\theta_h = \tan^{-1}(S^{-1})$ where S is the speed ratio, and for $S >> 1$ may be taken as $\theta_h = S^{-1}$, about 0.13(7.5°) for the sketch in Fig(33)).

Surface Flux Density

In the plume solution space, the RCS engine is located in the end of a cylinder the axis of which coincides with the negative symmetry axis and the cylinder extends from $X = 0$ to the far downstream flowfield boundary at $X = -137$ m. The cylinder outer radius is equal to the nozzle lip outer radius = 0.1239 m. The cylinder is divided into segments which coincide with adjacent cell sides (these quadrilateral cells have one side which coincides with the hardware). Thus the hardware begins at the 1st surface segment of the lip (lip definition part of the Monte Carlo flowfield boundary) and extends to the downstream (exit) boundary of the flowfield. The surface incident flux density is presented below as a function of the running integral of distance measured along this surface. The surface temperature is fixed for each surface segment and has the value 972 K on the 1st segment (on the wall, inside the nozzle, several hundred mean free paths upstream of the exit plane) and gradually decreases to 300 K at about S(=integrated arc length) = 4 m and is maintained at 300 K to the exit boundary. A mean sample of incident flux density was measured for each species on each surface segment.

The flux density for the plume gas mixture incident on the cylinder surface is shown as a function of integrated arc length along the hardware surface in Fig(34) and for each species in Fig(35). An exponential curve was fitted to the

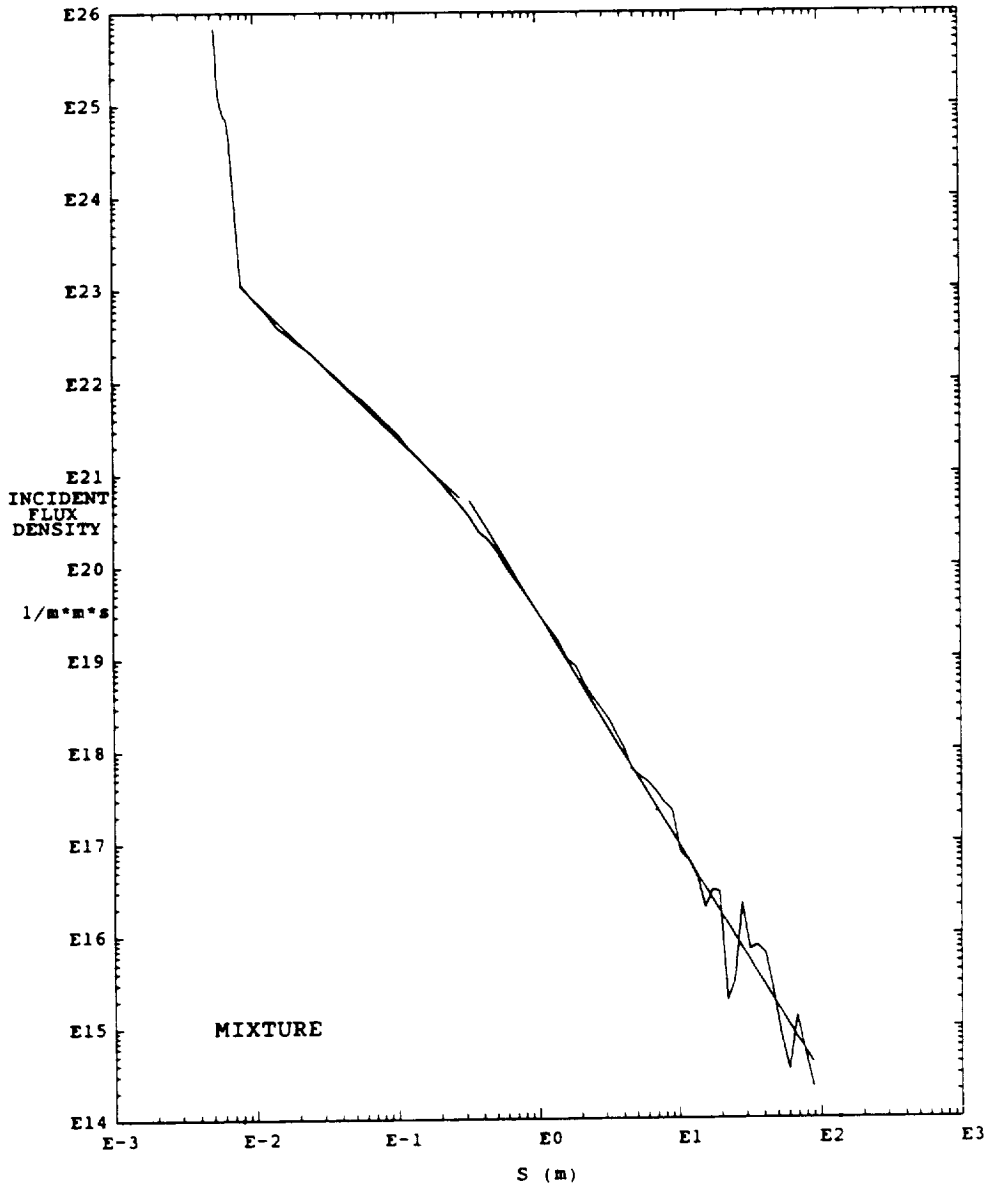

Fig(34) The plume gas mixture mean number flux density incident on the cylindrical surface(extending from the RCS lip outer surface to the flowfield downstream boundary at X = −137 m) as a function of integrated arc length along the surface.

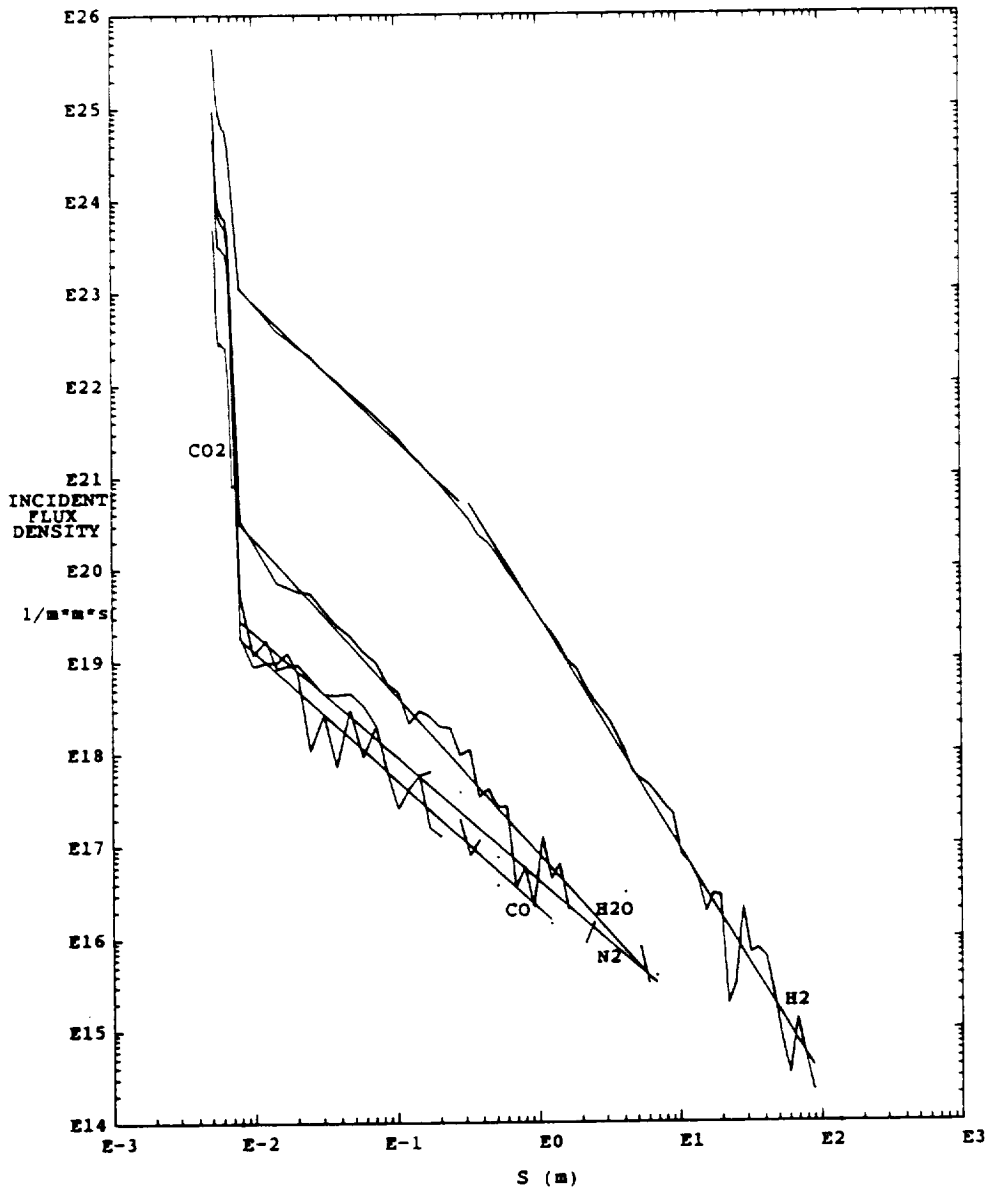

Fig(35) The mean flux density incident on the cylindrical surface by species as a function of integrated arc length along the surface.

measured data along the constant radius part of the cylinder (beginning near S = 8 mm (indicated by a dot on the abscissa) and ending at S = 137 m (also indicated by a dot)) for each species in the mixture using the method of least squares. These curves appear in Fig(34) and (35) as straight lines overlaying the raw data. The values of the correlation coefficients yielded by the fitting algorithm imply that the least square curves fit the data well. It may be observed that the best fit for H_2 was obtained by dividing the data into 2 subsets and computing an exponential fit for each; this was not necessary to obtain a good fit to the N_2, H_2O and CO data. The slope of the most downstream part of the H_2 curve (beginning at about S = 0.2 m) is substantially more negative than the part of the curve near the nozzle lip implying a fundamental change at this location in the process which scatters H_2 toward the surface. None of the slopes for the incident flux density of the individual species are exactly equal, but the slopes for N_2 and CO are quite close. The value of the H_2O slope is between the 2 segment slopes for H_2. The N_2 and CO slopes are not as steep as the 1st segment H_2 slope (implying a slower decrease in flux density with S) but the H_2O slope is steeper than the 1st segment H_2 slope. The 2nd segment H_2 slope is steeper than the slopes of N_2, H_2O and CO implying that at a sufficiently large distance downstream (beyond X = –700 m) the heavier species would make the principal contribution to the incident flux density on the cylinder surface.

No incident flux density for CO_2 was observed on the constant radius part of the cylinder surface (the last data point for CO_2 is near the lip outer corner), but there is a CO_2 component in the mixture flowing nearly parallel to the cylinder surface, see Fig(6) which shows that the axial velocity is greater than 2500 m/s (since the radial velocity is approaching 0.0) and Fig(31) which shows that the CO_2 density is substantially greater than zero in the space adjacent to the cylinder.

The normal pressure on the cylinder outer surface varies from 1.7 Pa at $X = -1$ mm to $4*10^{-9}$ Pa at $X = -88$ m. The pressure distribution may be represented (over short intervals) by the statement $p(X) = K*(-X)^{-q}$ where K and q are constants; but for $X \leq -50$ cm, $K = 1.7*10^{-4}$ and $q = 2.4$. The incident power density (heat flux) varies from 3 kWm^{-2} at $X = -1$ mm to $0.12*10^{-4}$ Wm^{-2} at $X = -88$ m. (Depending on the surface temperature (which was assumed in this solution), some fraction of this power density is carried away by the reflected molecular flux.)

Lip Flow Results and Discussion

Approaching the nozzle exit the flow is principally axial and the gradients are relatively small due to the small rate at which the nozzle radius increases near the exit (the internal expansion is nearly complete). But at the exit the nozzle wall abruptly terminates, radial flow is no longer inhibited, the energy density of the exhaust gas is high, and the number density and mass density are yet high. These conditions lead to a very abrupt increase in the gradients, especially in the radial direction, and the entire expansion process in the vicinity of the lip becomes much more vigorous and dynamic. Since the mixture is made up of a number of species each having different molecular properties (mass, cross section, etc) the individual components of the mixture experience different dynamics (variation in collision frequency, flow angle, flow speed, etc) yielding a continuously varying mixture. The following section presents the detail structure of the flow in the neighborhood of the nozzle lip.

The mean molecular weight distribution in the vicinity of the lip is given in Fig(36), which shows that the plume gas mixture composition is a rapidly changing function of flow angle. In the flow conditions along the Monte Carlo input boundary (dashed curve) the mean molecular weight varies substantially (generally increasing), but along the small segment shown in this display it is nearly constant at the value 18 (approximately). At large flow angles (approaching π) the mean molecular weight approaches, but never actually reaches 2.

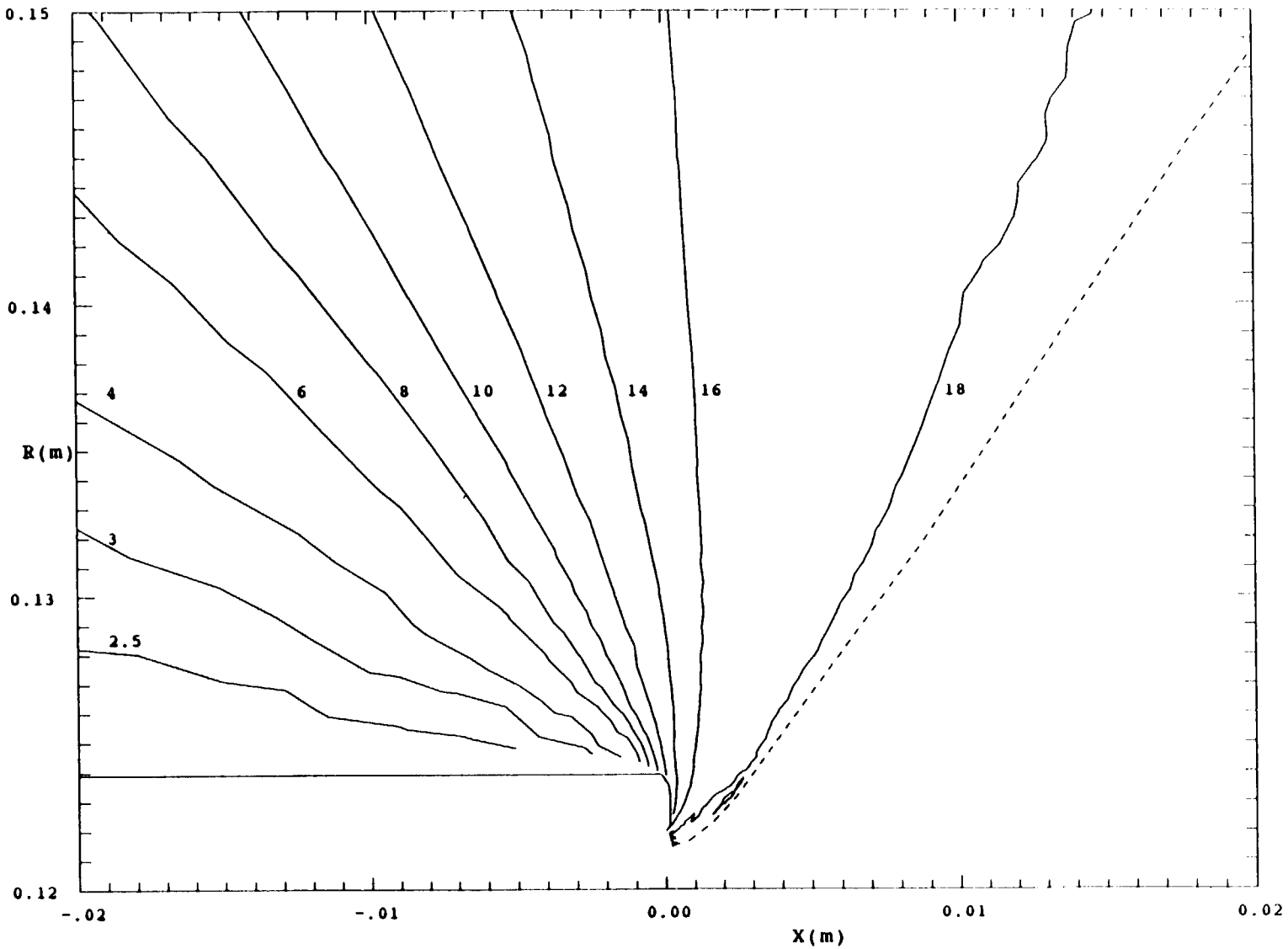

Fig(36) The mean molecular weight distribution. (The dashed curve indicates the Monte Carlo input boundary and the lip hardware is also shown.)

Figs(37) thru (41) display the relative abundance (=number fraction) for each molecular species (from which the mixture mean molecular weight is constructed). Very small relative abundance contours are not displayed since they tend to be very noisy, but all species are observed everywhere in the flowfield. These data imply that the relative abundances of the heavier species decrease with increasing flow angle and that they decrease more rapidly as the species molecular mass increases.

Fig(42) displays the relative abundance of each species in the plume gas mixture as a function of flow angle along the circular arc R = 2.0 cm measured from the outer corner of the lip. At the input boundary, flow angle = 1.08(62°) (see dot on abscissa), both H_2 and H_2O have molecular weights less than or equal to the local mean molecular weight of the mixture, as displayed in Fig(43). Fig(42) shows that the relative abundance of H_2 immediately begins to increase with increasing flow angle, and that the relative abundance of H_2O remains approximately constant up to a flow angle of 1.75(100°) before beginning to decrease, at which point the mixture mean molecular weight has decreased to approximately 16. The relative abundance of the heavier species (heavier than the mean molecular weight of the mixture) immediately begin to decrease with increasing flow angle, and the slope magnitudes increase for the heavier species.

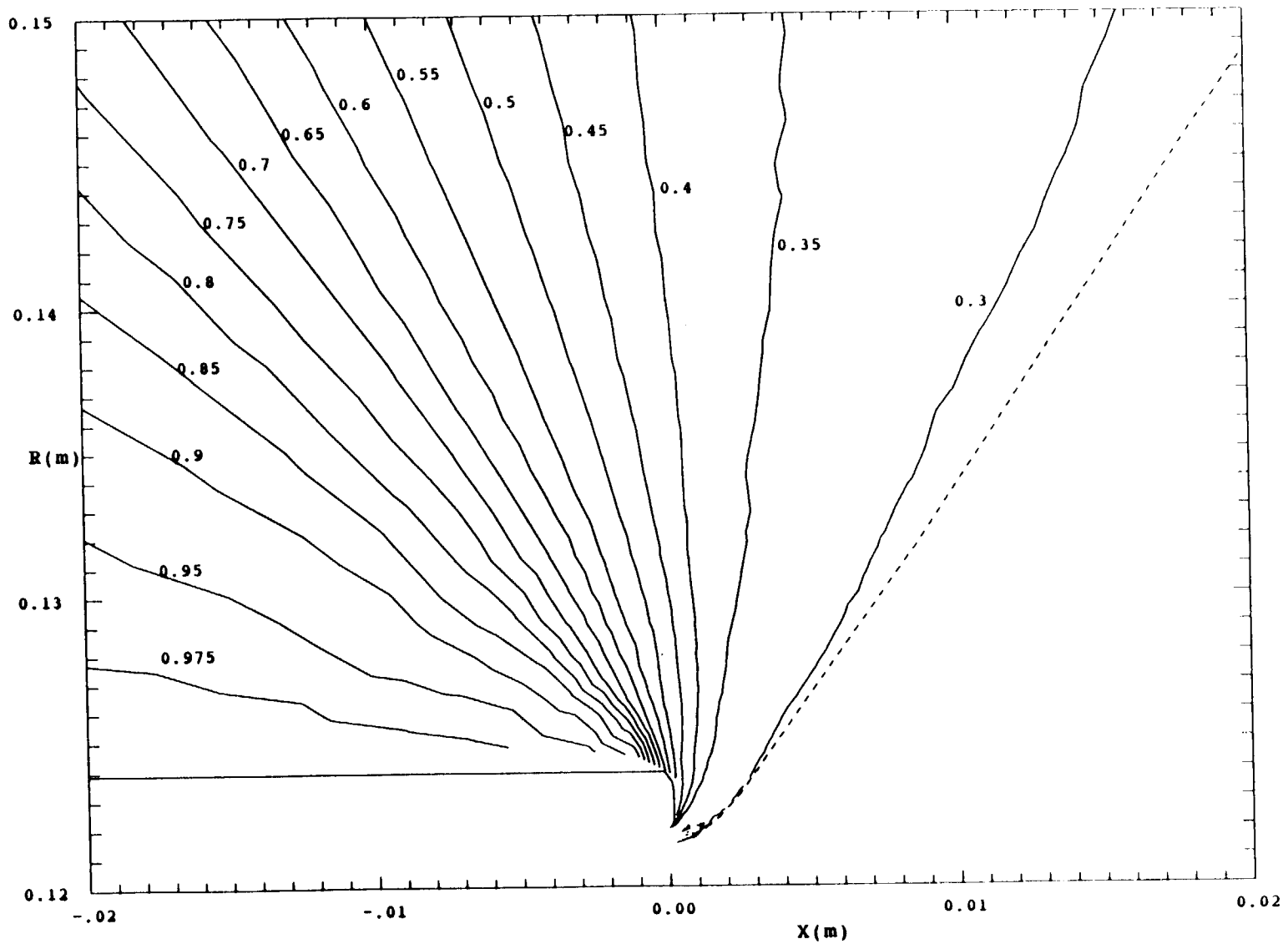

Fig(37) Molecular hydrogen relative abundance(= number fraction) distribution.

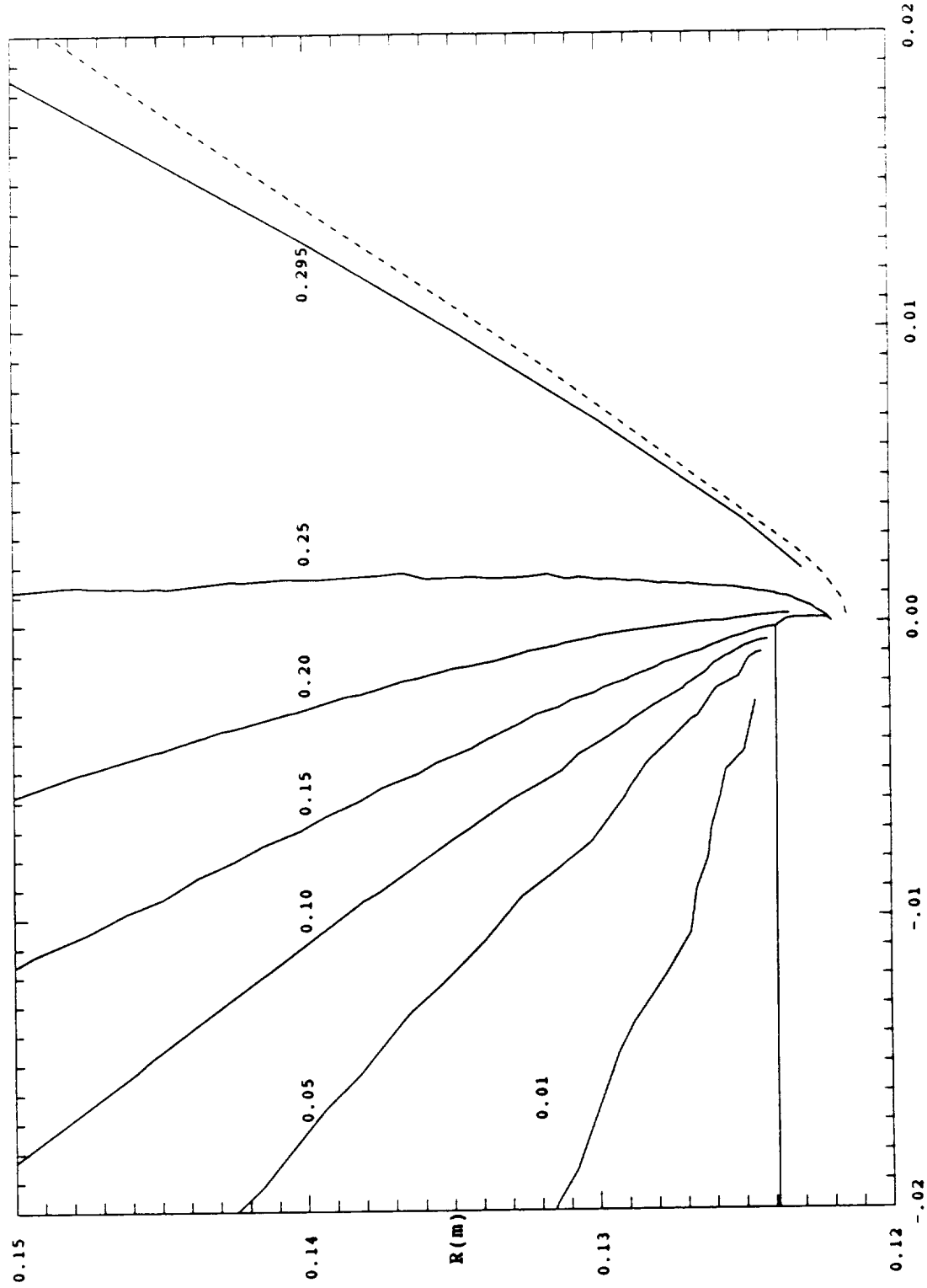

Fig(38) Molecular nitrogen relative abundance distribution.

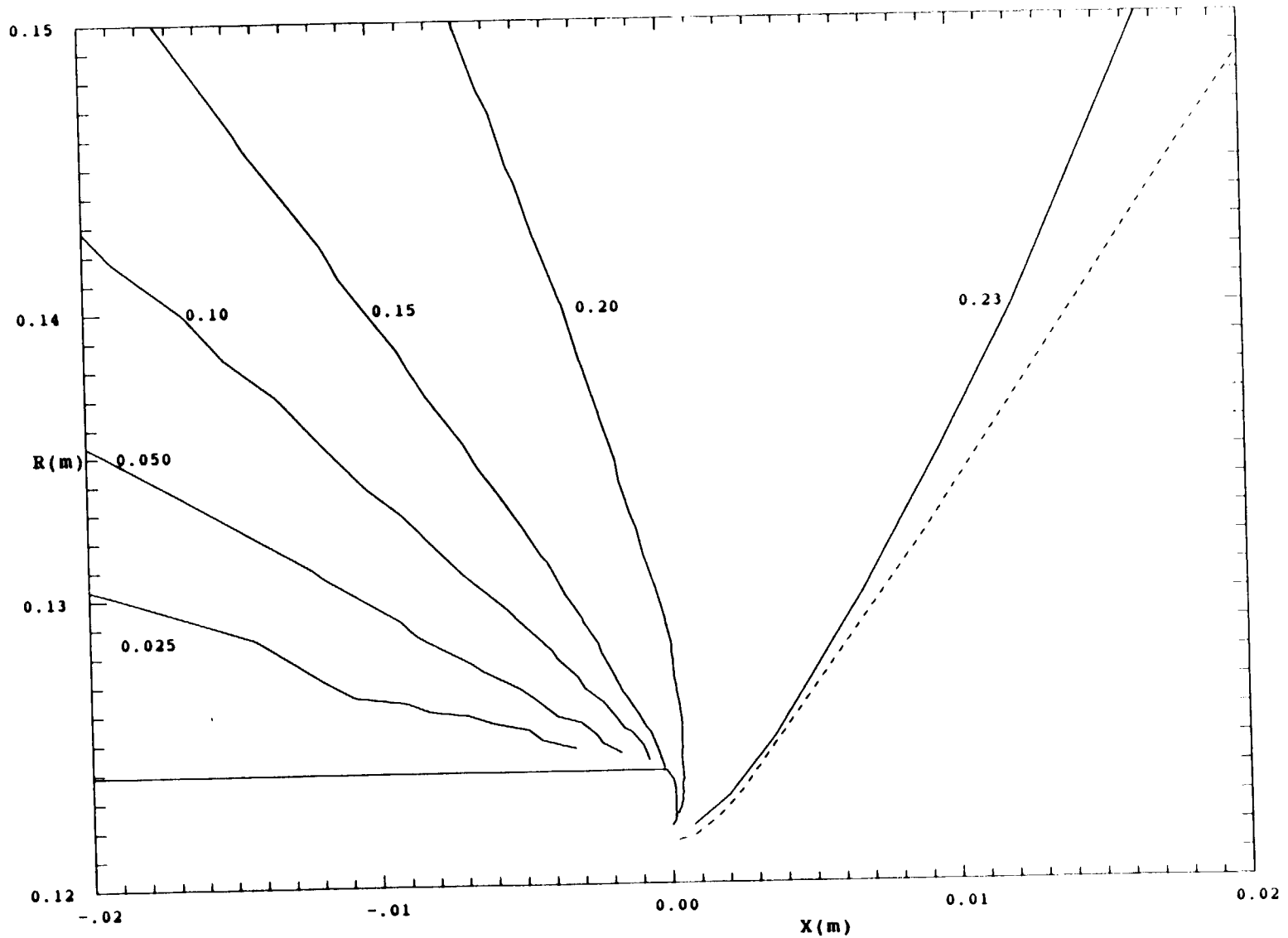

Fig(39) Water relative abundance distribution.

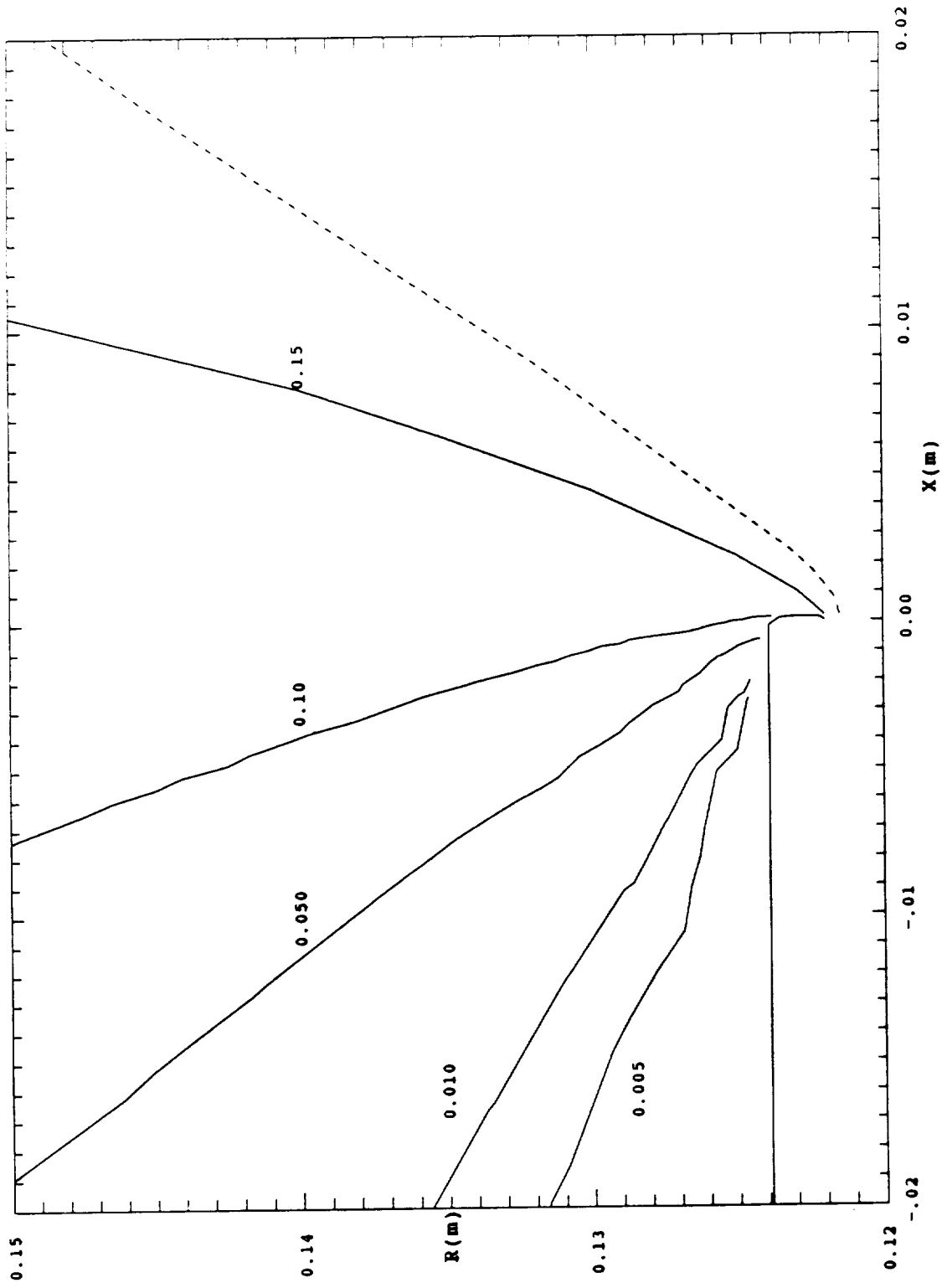

Fig(40) Carbon monoxide relative abundance distribution.

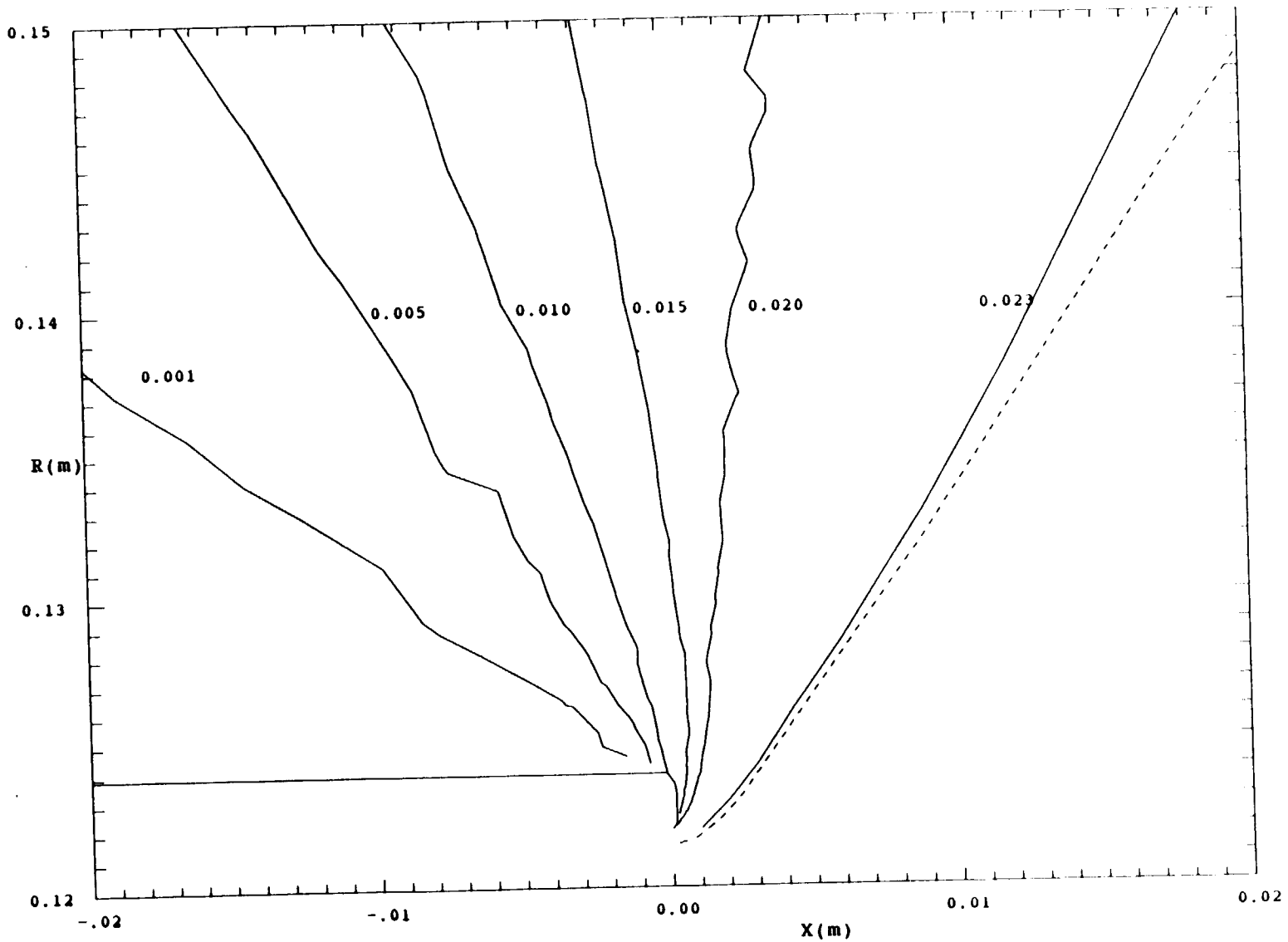

Fig(41) Carbon dioxide relative abundance distribution.

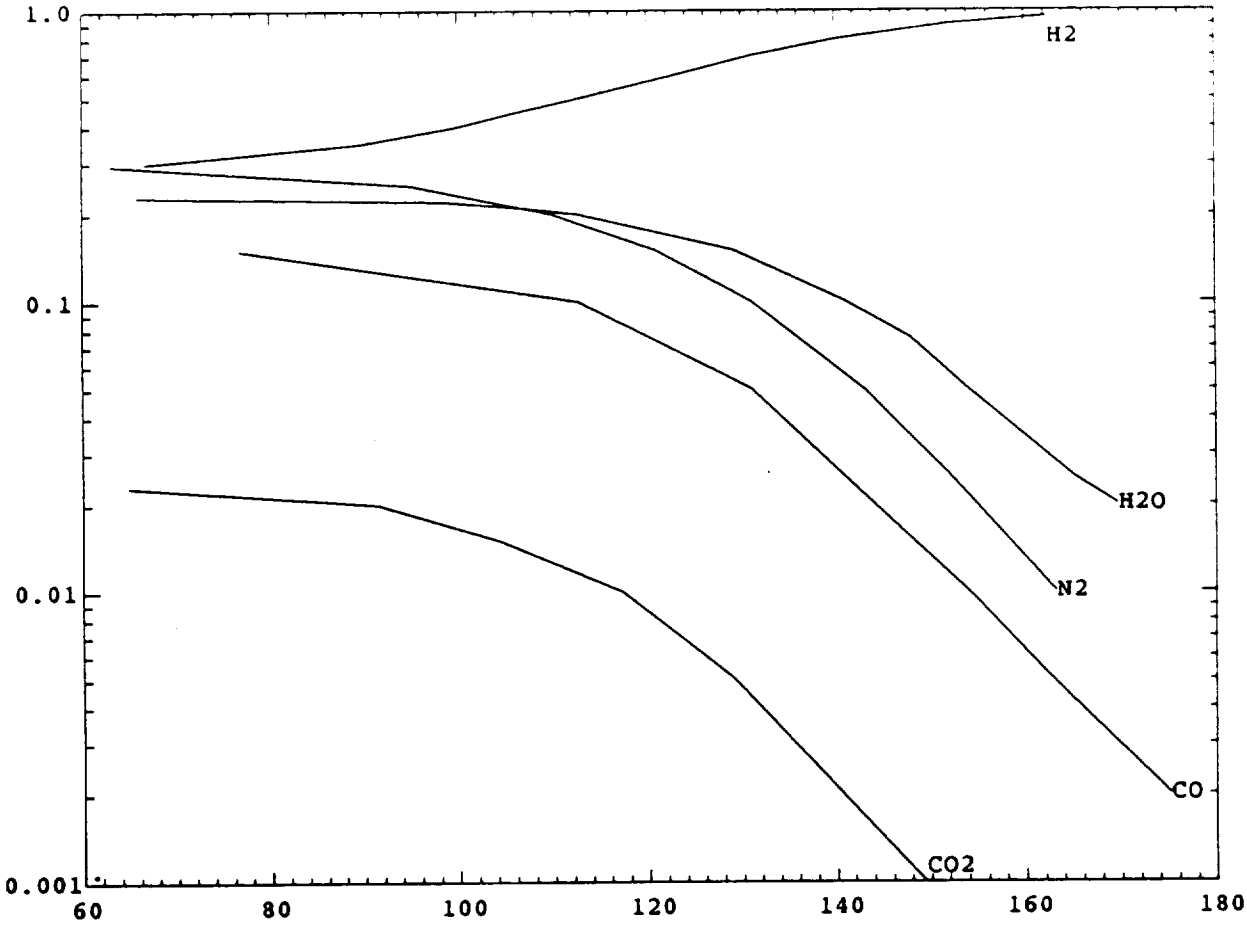

Fig(42) The relative abundance distribution by species measured along a circular arc 2 cm from the lip outer corner as a function of the mixture local mean flow angle(°).

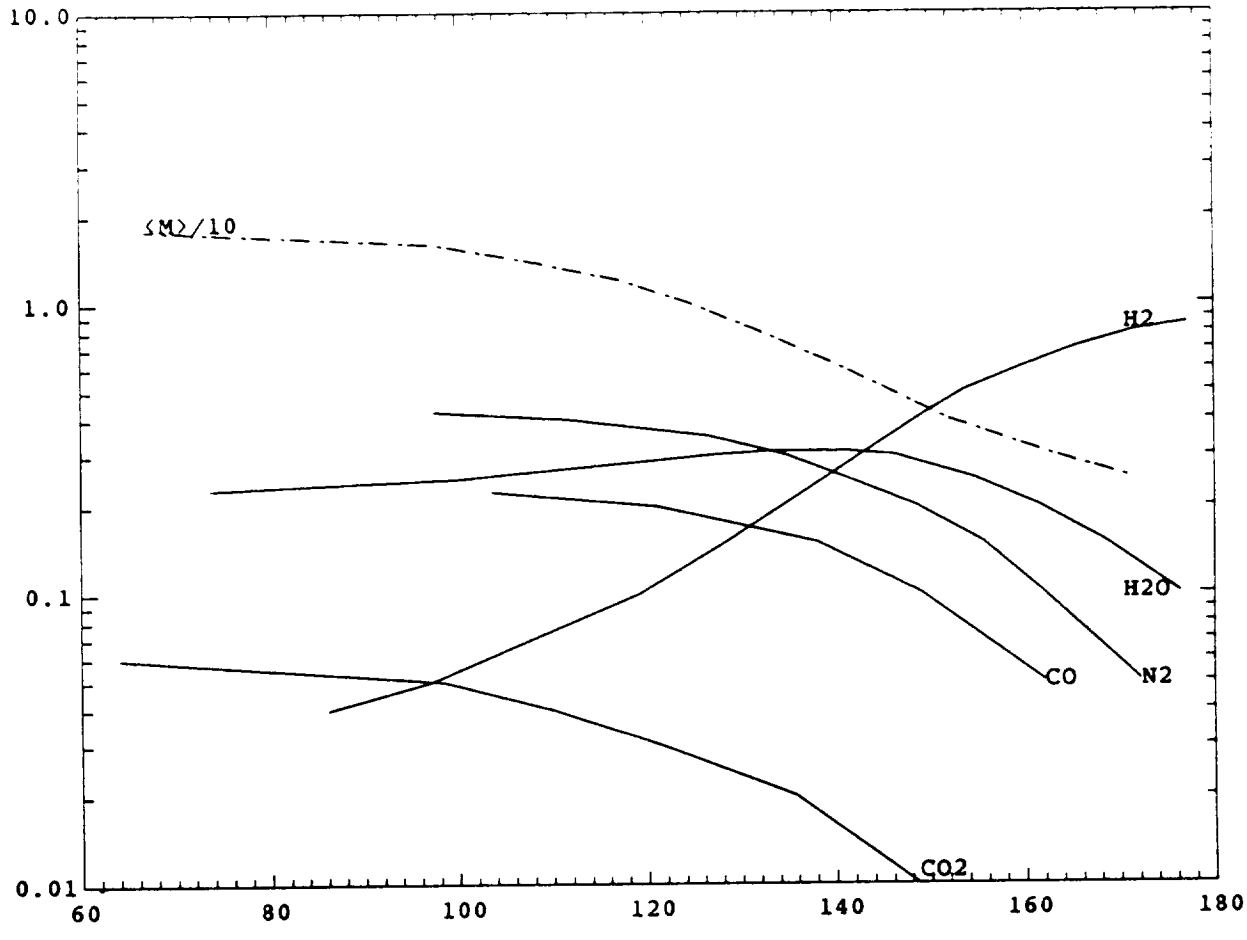

Fig(43) The mean mass fraction by species as a function of mixture local mean flow angle(°) along 2 cm circular arc.

The mass fraction of each species in the plume gas provides a different perspective of the mixture composition. Fig(43) presents the mass fraction for each species as a function of flow angle along the arc mentioned above; for reference the mean molecular weight (divided by 10) is also displayed. The H_2 mass fraction increases more rapidly than the H_2 relative abundance shown in Fig(42) and contrary to the behavior of the relative abundance in Fig(42), the H_2O mass fraction actually increases with flow angle until about 2.44(140°) before beginning to decrease.

The collision frequency distribution for the plume gas mixture in the vicinity of the lip is shown in Fig(44). At the left of the display the mean collision frequency in the mixture is about 10^5 s^{-1}, implying that the mean free time is about 10 μs. The mixture mean flow speed in this region of the flow is about 1800 m/s, see Fig(52) below. Thus molecules move (in the mean) about 1.8 cm between successive collisions (this is analogous to the conventional mean free path in an equilibrium gas which of course does not have the usual meaning in this flow since the lip flow is far from equilibrium). It is improbable that the species collision frequencies, and thus the mixture mean, can be described by an analytical statement since the mixture goes out of equilibrium just downstream of the input boundary (see selection criterion for the Monte Carlo input boundary location), since the composition is changing rapidly, since there are substantial variations in the species collision cross sections, since the species molecular masses differ substantially, etc. All collision

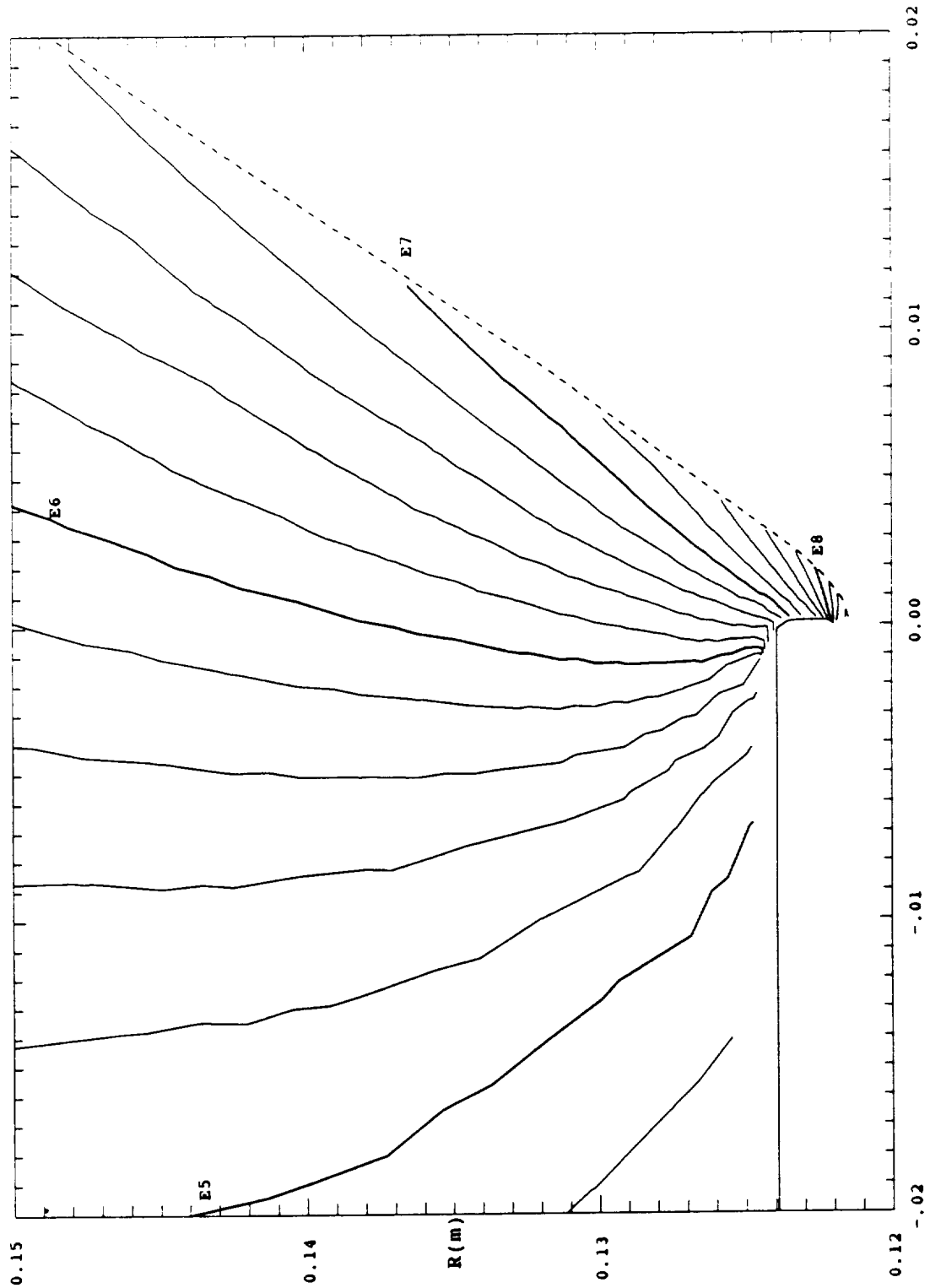

Fig(44) The mixture mean collision frequency distribution (s^{-1}).

frequencies (species as well as mixture) are probably best regarded as results from the DSMC experiment.

Even so, there are 2 species (N_2,CO) in the plume gas mixture which have equal molecular masses, nearly equal collision cross sections, the same rotational degrees of freedom, and their vibrational energies have a relative difference of only 9%. The collision frequency distribution for this pair is therefore expected to be nearly identical. These distributions are compared in Fig(45) (N_2=light and CO=dark), from which it may be observed that their collision frequency distributions are nearly equal while the collision frequencies vary thru 4 orders of magnitude.

Fig(46) and (47) compare the collision frequency distributions for the species pairs (H_2O,CO), and (H_2,CO_2). The collision frequency of H_2O (light) exceeds the collision frequency of CO (dark) by a factor of 1.4 and this ratio remains approximately constant in the geometrical domain shown, the reference molecular diameter ratio is $d(H_2O)/d(CO) = 1.25$ and the mass ratio is $m(CO)/m(H_2O) = 1.56$. A similar result for H_2 (light) and CO_2 (dark), shown in Fig(47), gives 1.3 for the ratio of collision frequencies, while $d(H_2)/d(CO_2) = 0.62$ and $m(CO_2)/m(H_2) = 22$.

The flow angle distribution for the plume gas mixture in the vicinity of the lip is given in Fig(48). On this 2.0 cm scale, there is considerable curvature in

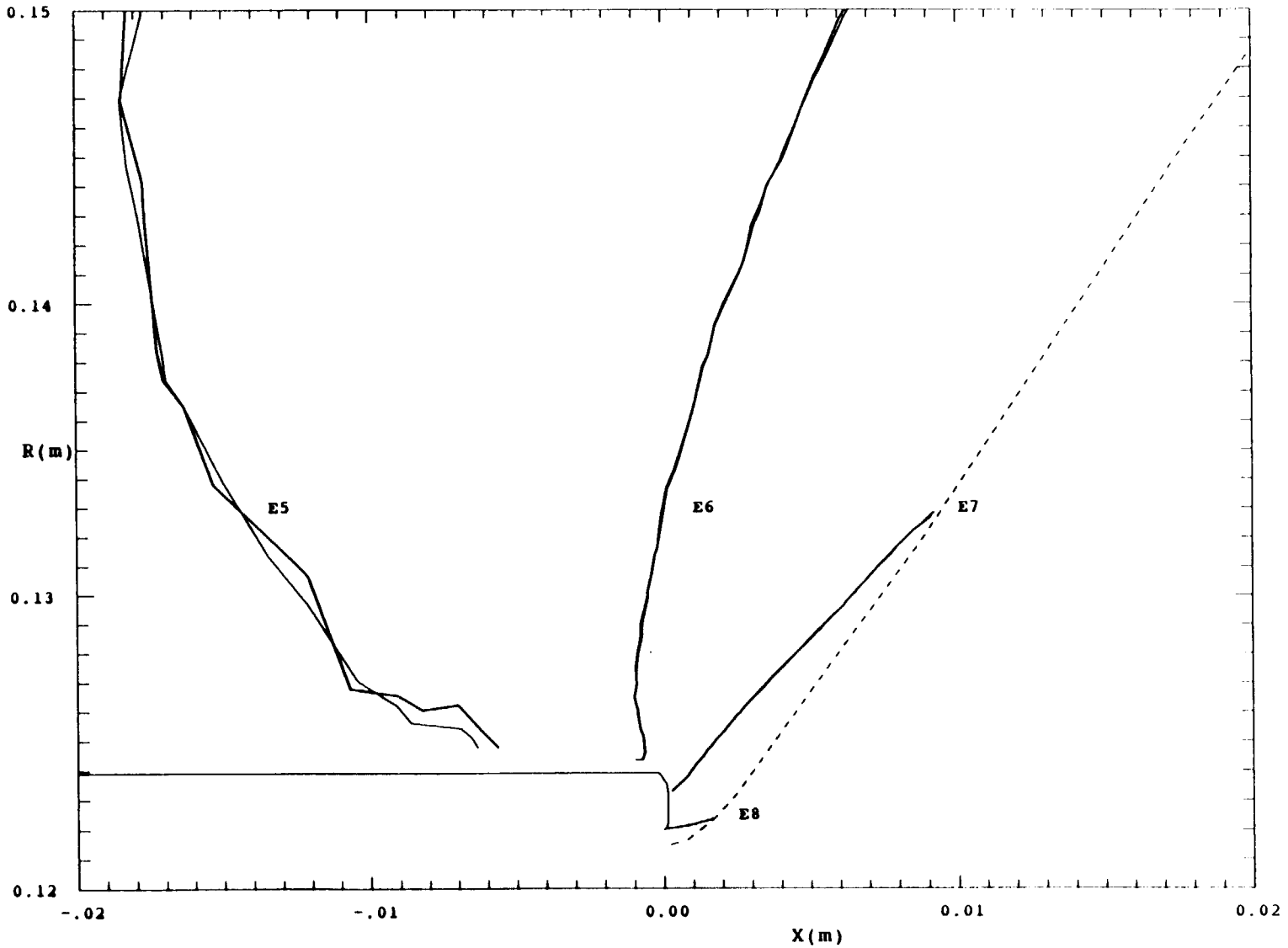

Fig(45) Overplot of N_2 and CO mean collision frequency distributions.

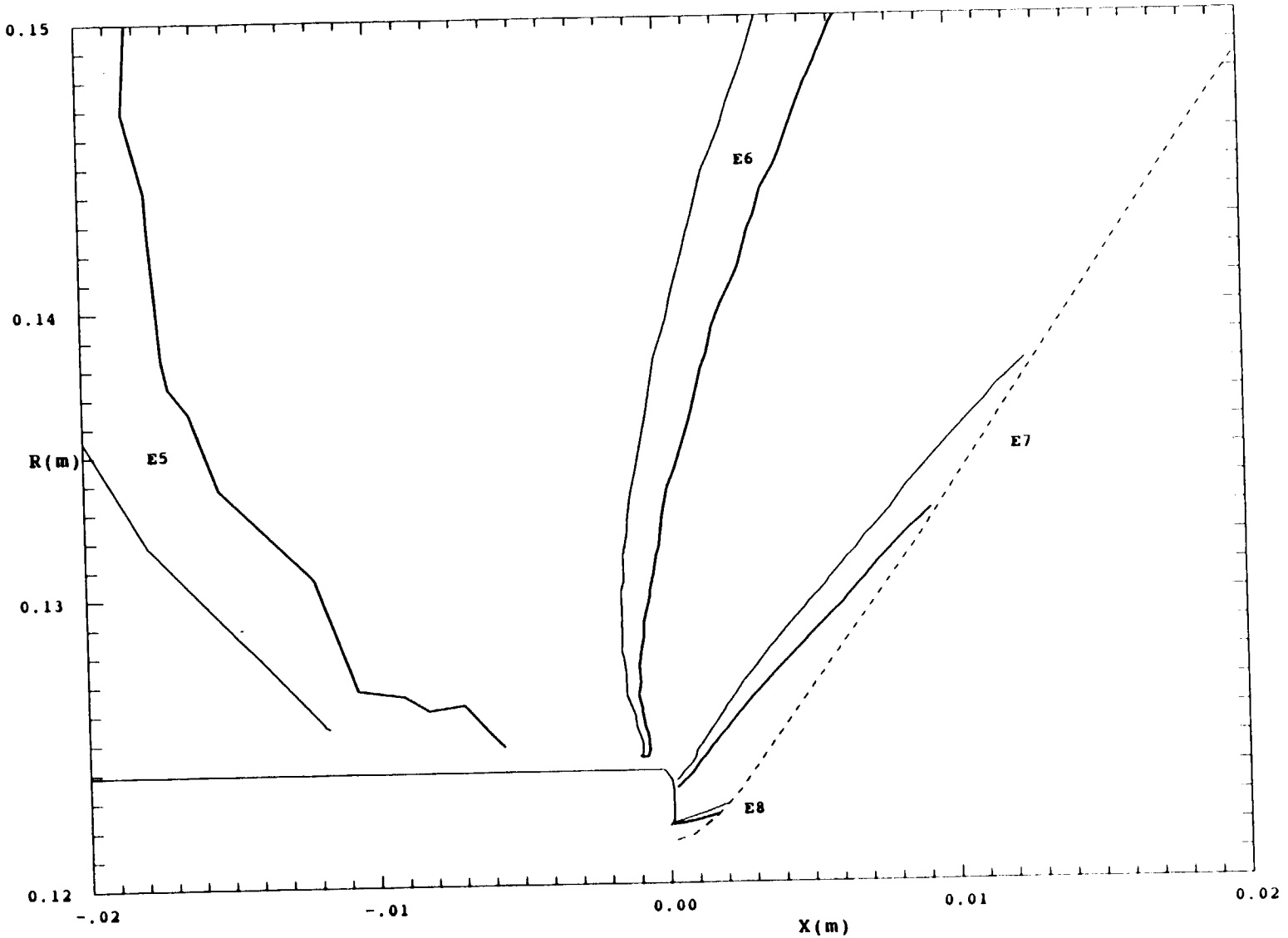

Fig(46) Overplot of H_2O (light) and CO (dark) mean collision frequency distributions.

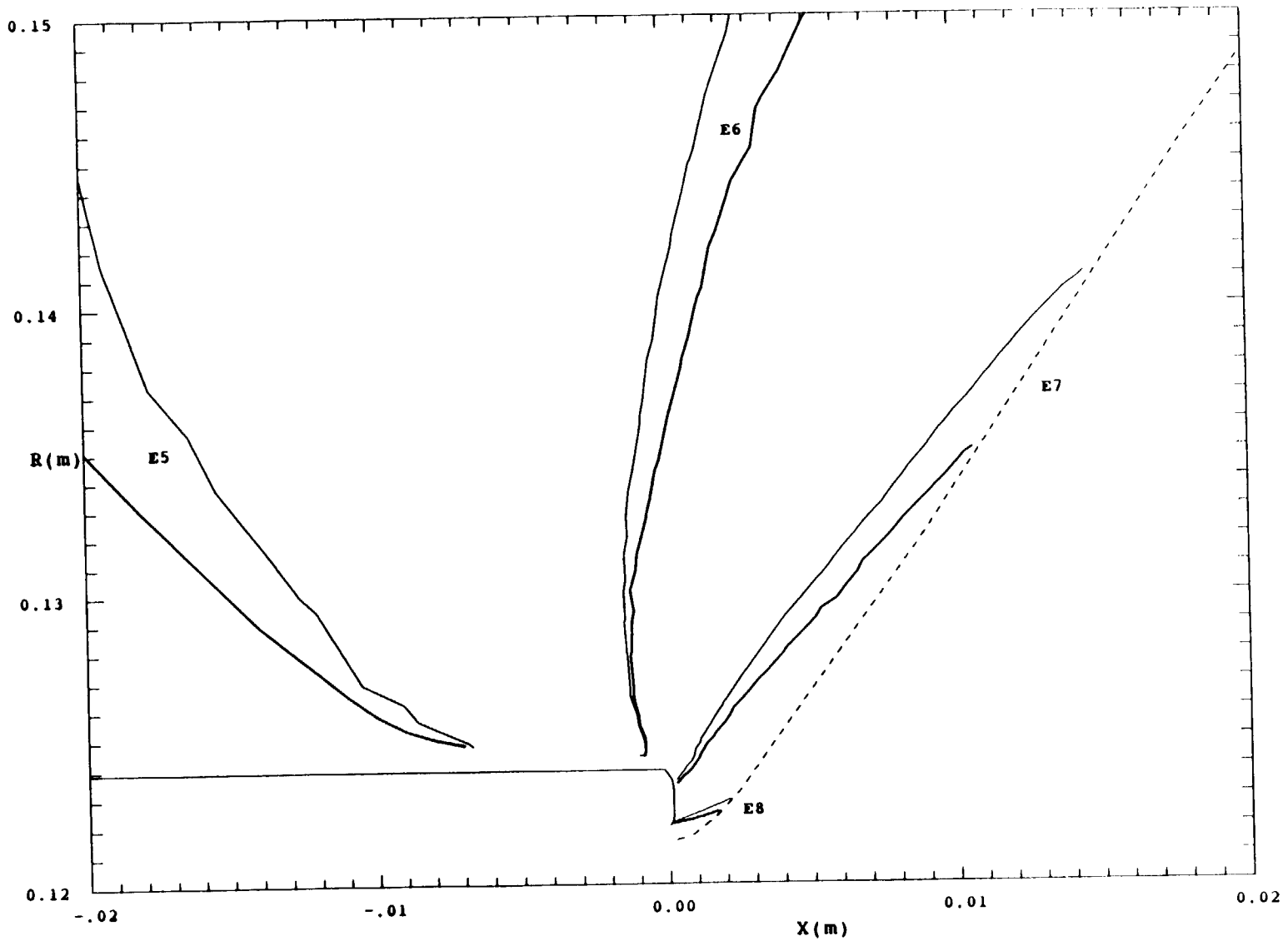

Fig(47) Overplot of H_2 (light) and CO_2 (dark) collision frequency distributions.

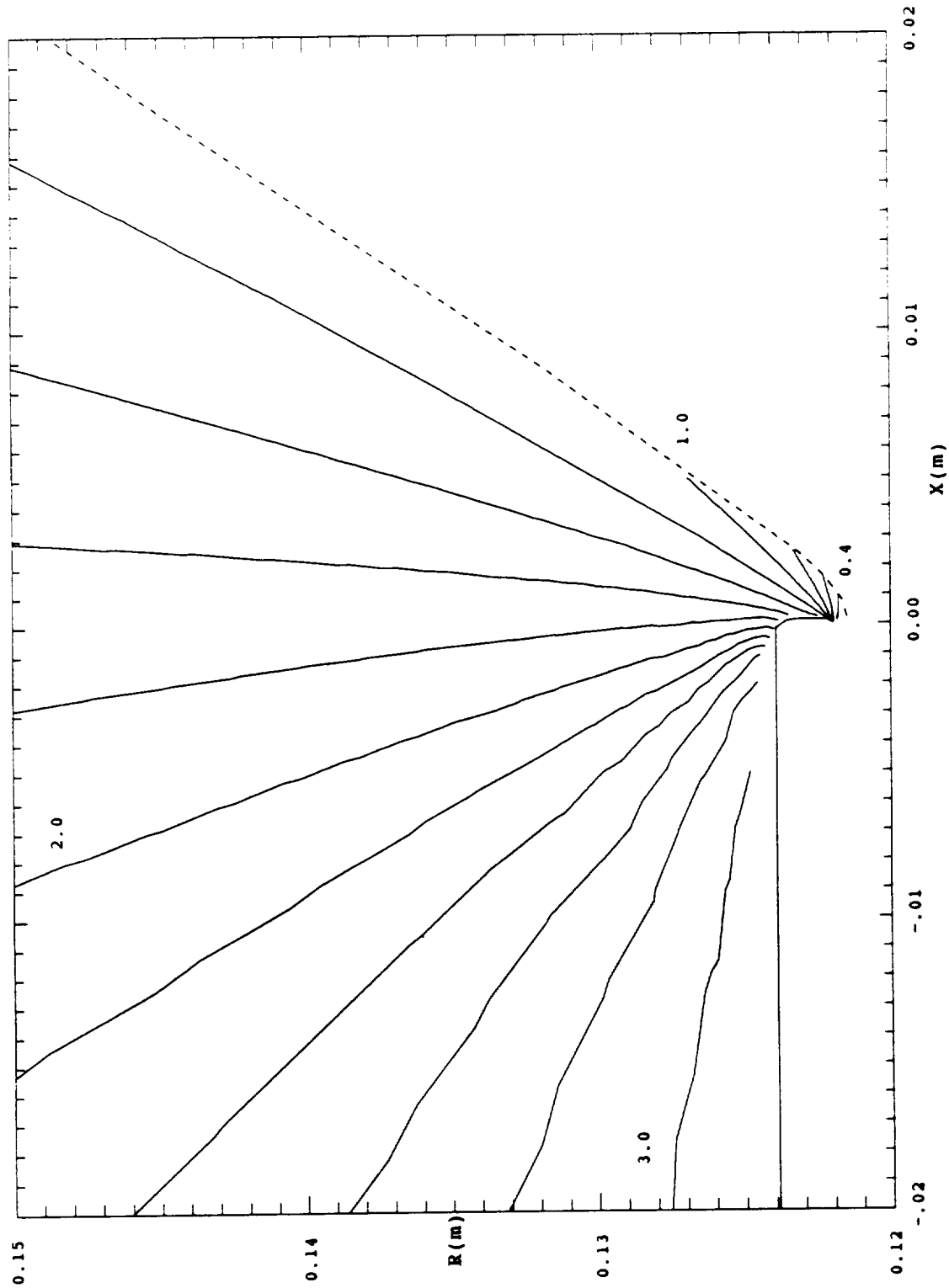

Fig(48) The plume gas mixture mean flow angle distribution (radian).

the flow angle contours at all flow angles. Fig(49) displays the flow angle distribution for the pair (N_2,CO) which have approximately equal molecular diameters and equal molecular masses and yield nearly coincident flow angle distributions. This result is consistent with the data of Fig(45) which showed that the collision frequency distributions for this species pair coincide.

Fig(50) compares the flow angle distributions for the pair (H_2O,CO), which in contrast show that the flow angle of the light species (H_2O, M=18) increases more rapidly than the heavy species (at a prescribed point in the flow the H_2O flow angle is larger than the CO flow angle, or the CO flow angle lags H_2O).

The molecular mass influence on the flow dynamics is further illustrated in Fig(51) which compares the flow angle distributions for CO_2 and H_2. Again the heavier species arrives at a prescribed flow angle later in the flow. The larger variance between the flow angle distributions for this species pair is consistent with the larger mass ratio, $m(CO_2)/m(H_2) = 22$.

The flow speed distribution for the plume gas mixture in the vicinity of the lip is given in Fig(52). These data are of course the mean values averaged over all species, but it is shown below that the speed distributions of some of the species differ substantially from these data. Thus the dynamic behavior of a particular species is more accurately described by the species data rather

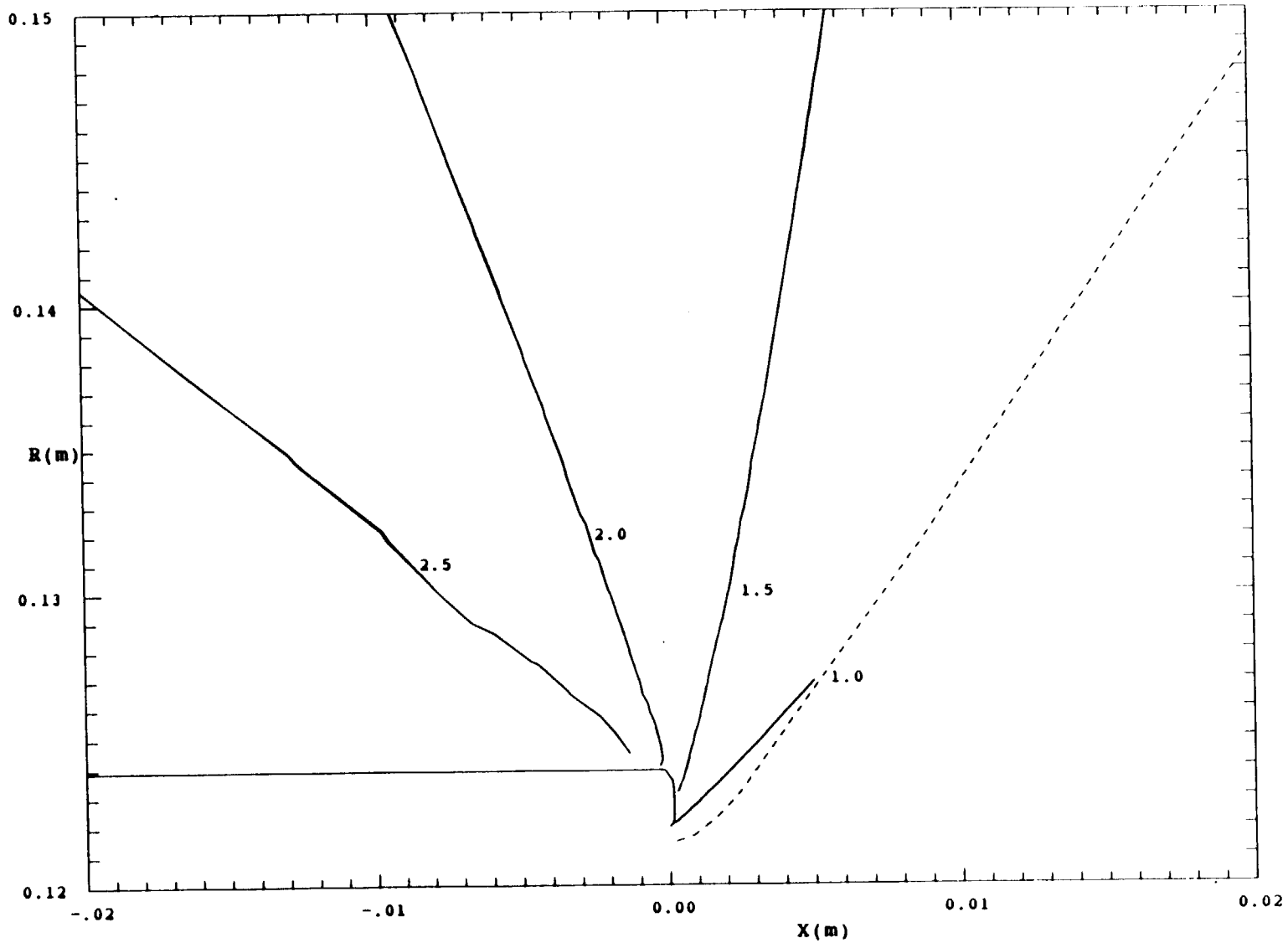

Fig(49) Overplot of N_2 and CO mean flow angle distributions.

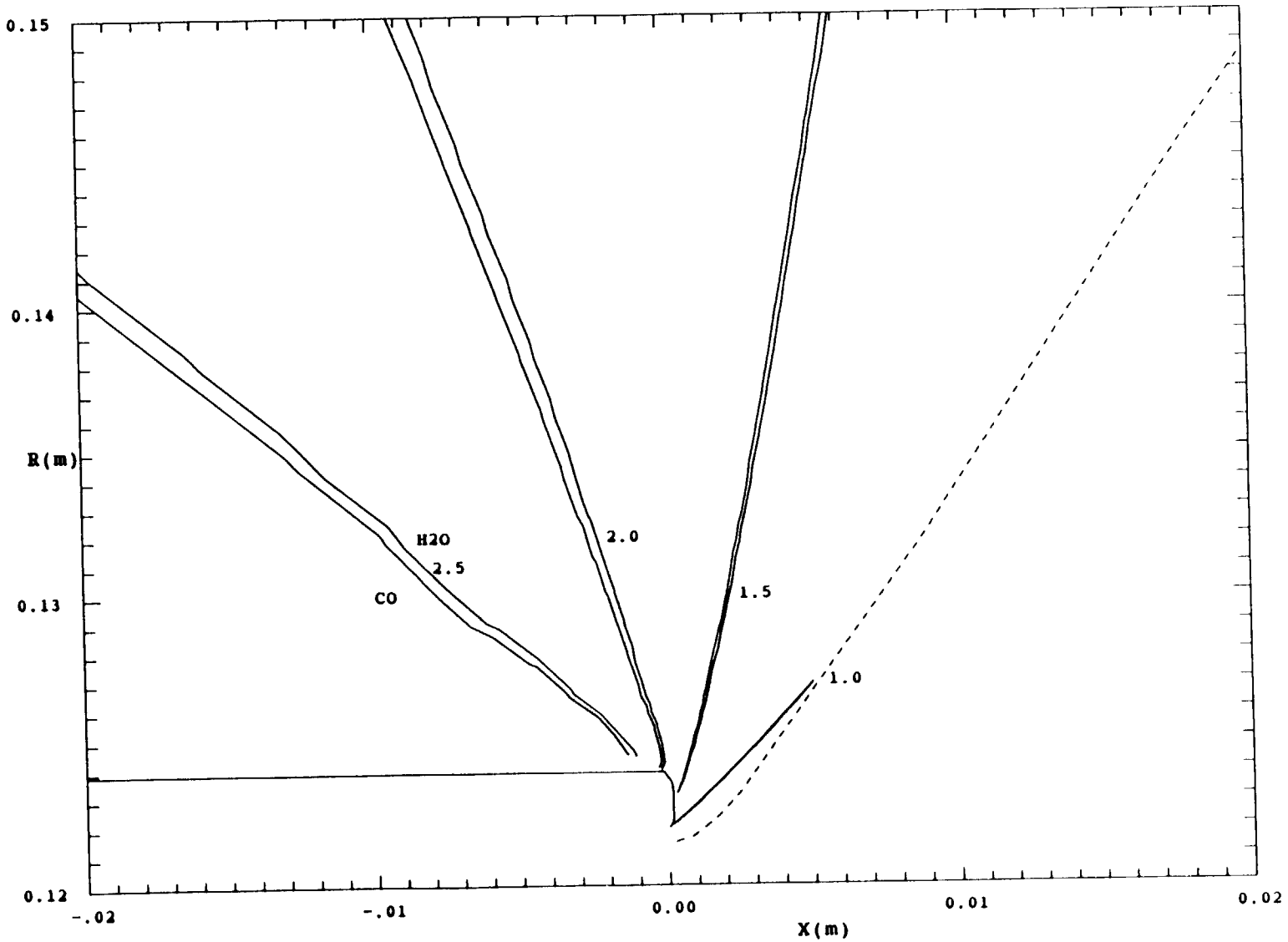

Fig(50) Overplot of H_2O and CO mean flow angle distributions.

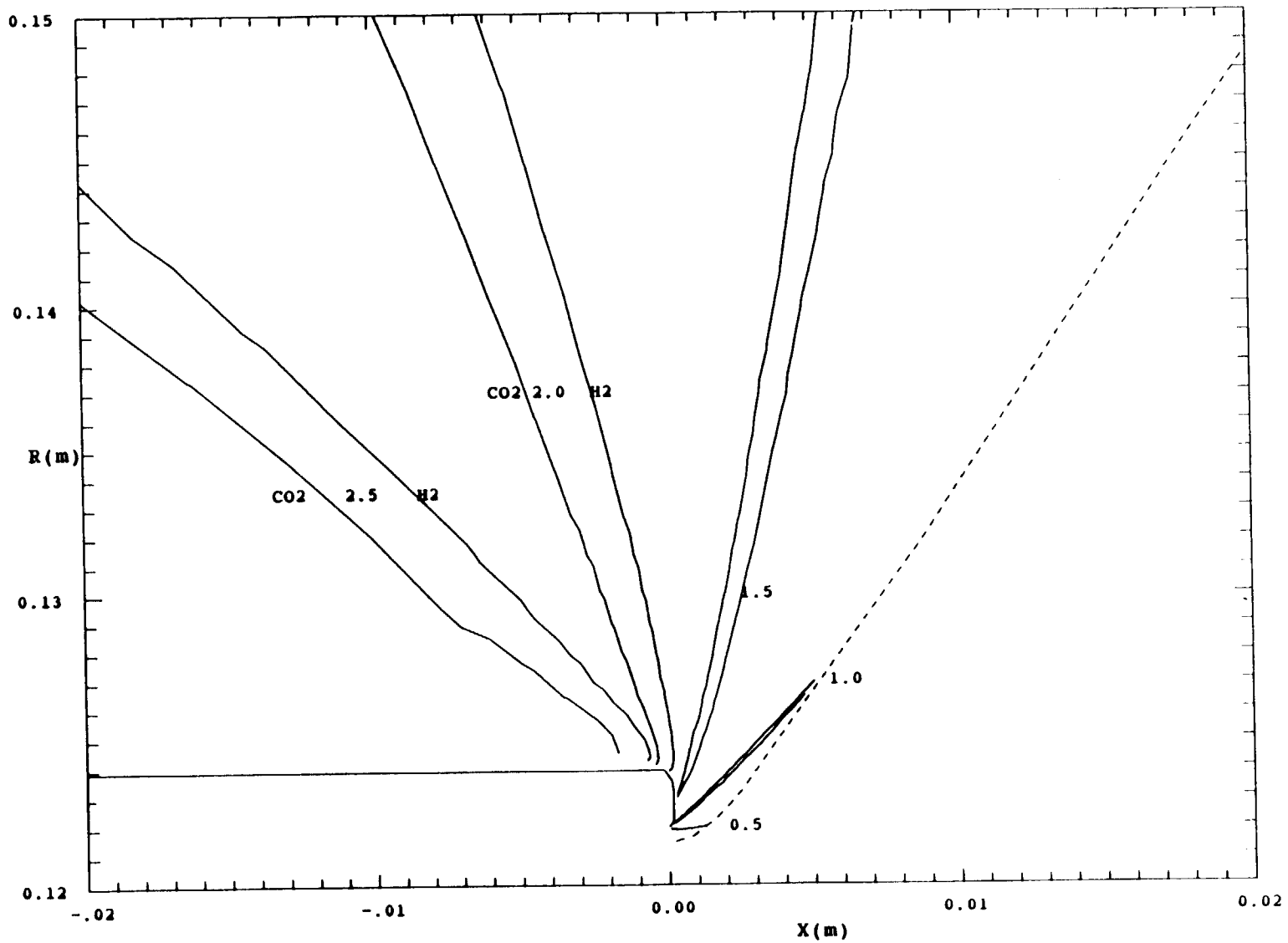

Fig(51) Overplot of H_2 and CO_2 mean flow angle distributions.

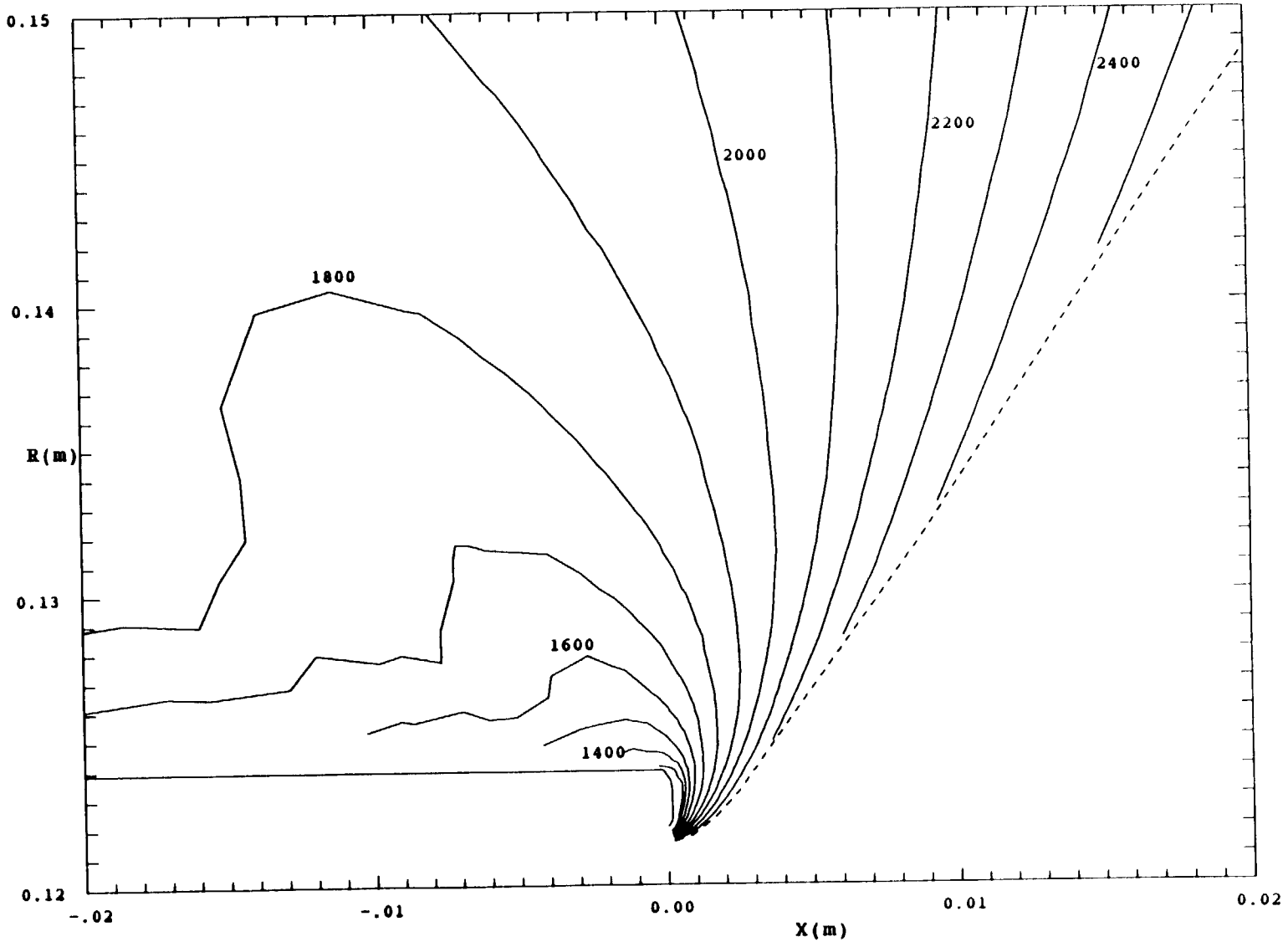

Fig(52) The plume gas mixture mean flow speed distribution.

than the mixture mean values.

The flow speed distributions for species pairs (N_2,CO), (H_2O,CO), and (H_2,CO_2) are compared in Figs(53) thru (55). The data in Fig(53) shows that the speed distribution for N_2 and CO are nearly identical (molecular mass ratio = 1).

Fig(54) shows that at the lip inner corner (equilibrium flow) the flow speed of CO and H_2O are nearly equal, but as the flow proceeds the flow speed of CO immediately begins to lag the H_2O flow speed and the divergence increases as the expansion proceeds around the lip. Fig(55) presents a similar variance between the flow speeds of CO_2 (molecular weight 44) and H_2 (molecular weight 2) but the variance increases more rapidly, in agreement with the larger mass ratio.

The results presented above imply that during the flow (expansion) around the lip the smaller mass molecules are accelerated more rapidly than the larger mass molecules such that the flow speed of the heavier species increasingly lags the flow speed of the lighter species. Therefore in the gas mixture the relative abundance of the heavier species decreases (in the flow direction) which directly yields a decreasing mean molecular weight thru the expansion. The difference in acceleration by species is quite conspicuous in Fig(55) where the flow speed of CO_2 lags H_2 (mass ratio = 22) by 20% (400

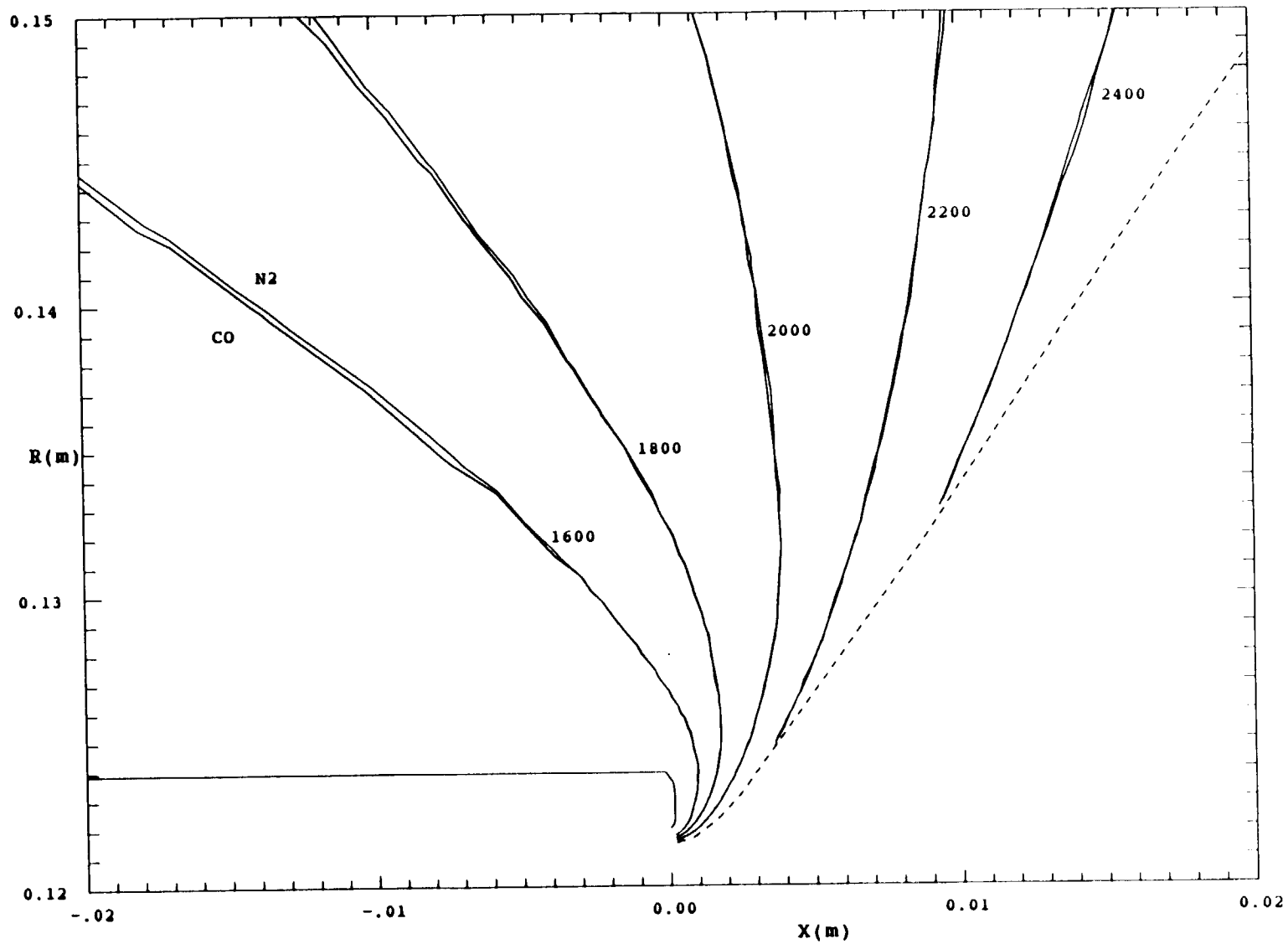

Fig(53) Overplot of N_2 and CO mean flow speed distributions.

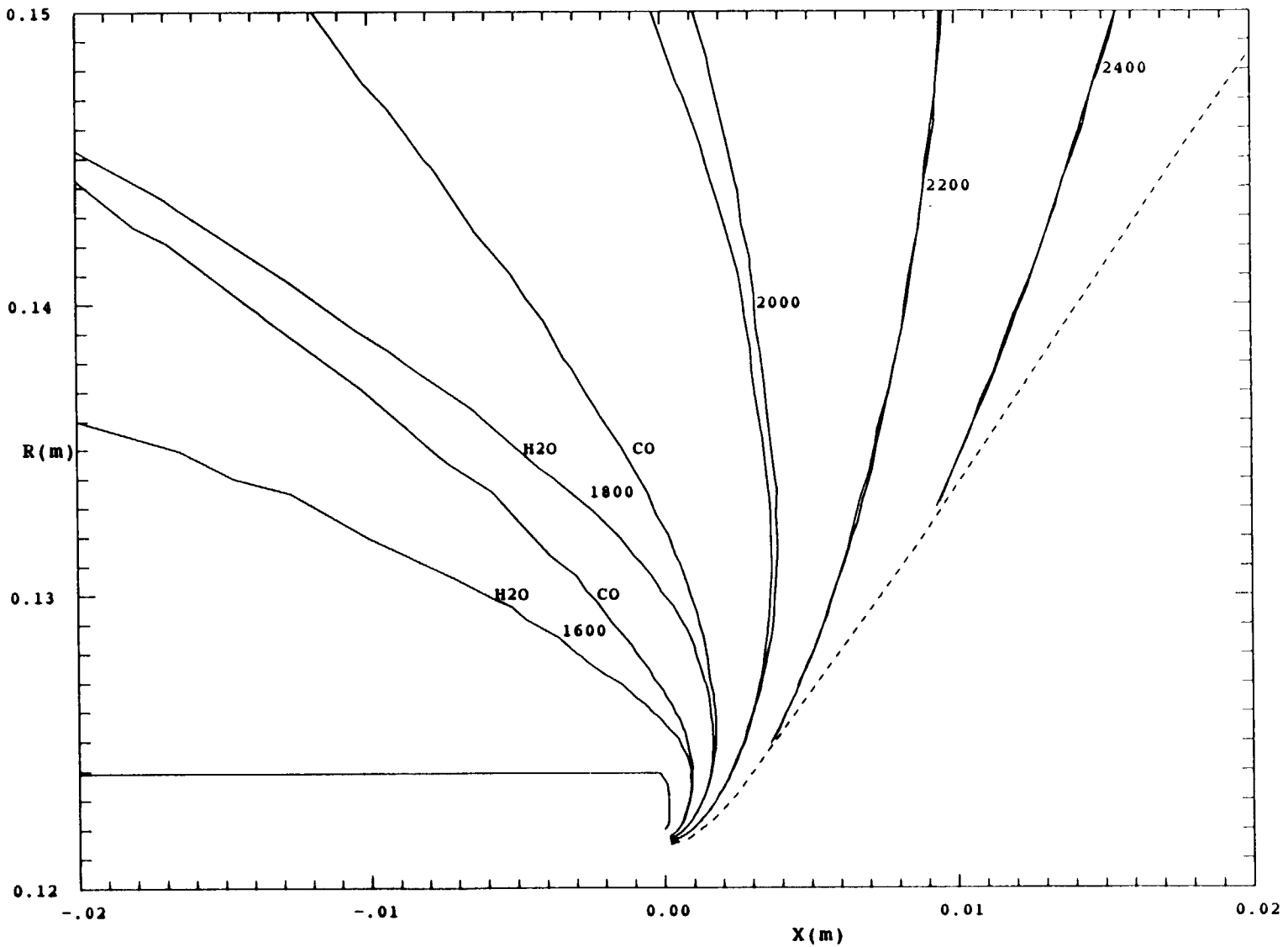

Fig(54) Overplot of H_2O and CO mean flow speed distributions.

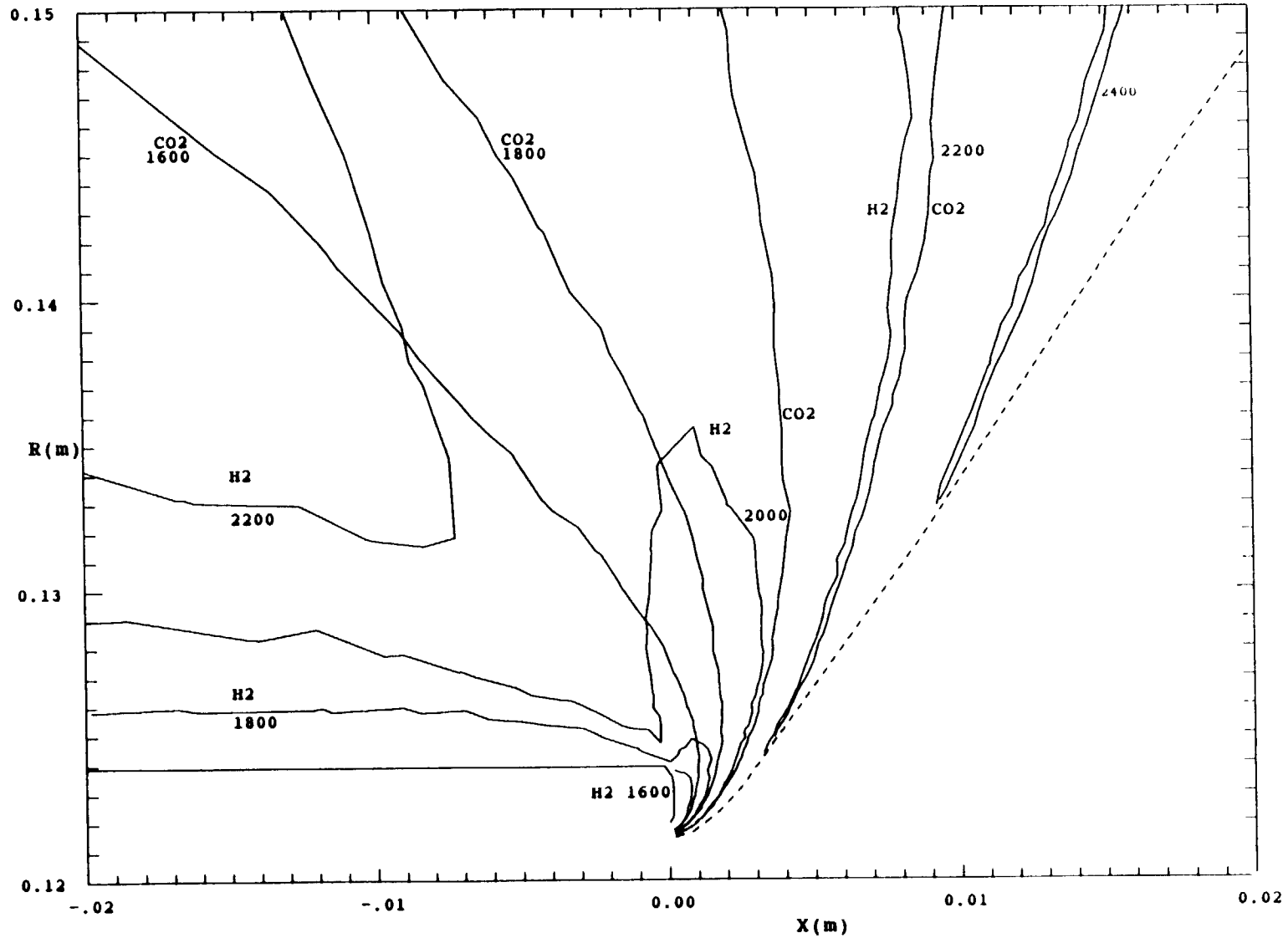

Fig(55) Overplot of H_2 and CO_2 mean flow speed distributions.

m/s, 1600 compared to 2000) while the flow is but 0.5 cm from the lip outer corner. For the pair (CO,H_2O), with the much smaller mass ratio = 1.56, the flow speed of these species is still quite divergent as displayed in Fig(54). In contrast Fig(53) shows that there is negligible difference in species acceleration for equal molecular mass species (N_2 and CO).

The plume gas mixture translational and internal 'temperature' distributions in the vicinity of the lip are given in Figs(56) and (57). In the flow direction the translational 'temperature' decreases more rapidly than the internal 'temperature', due to the very rapid decrease in collision frequency in this region of the flow, as shown in Fig(44); there are insufficient collisions (inelastic) to transfer the internal energy to translational degrees of freedom at the rate required to maintain equilibrium. In compressive flows the translational 'temperature' in contrast, increases more rapidly than the internal 'temperature', but due to the same physical process, low collision frequency. Near the Monte Carlo input boundary the translational and internal temperatures nearly coincide but rapidly diverge such that they differ by about 15% only 2 mm downstream of the input boundary (at about 0.5 cm above the lip). In the rapidly expanding plume flow the translational and internal 'temperatures' continue to diverge at least as far as the outer boundary of the flowfield as shown in Figs(8) and (9).

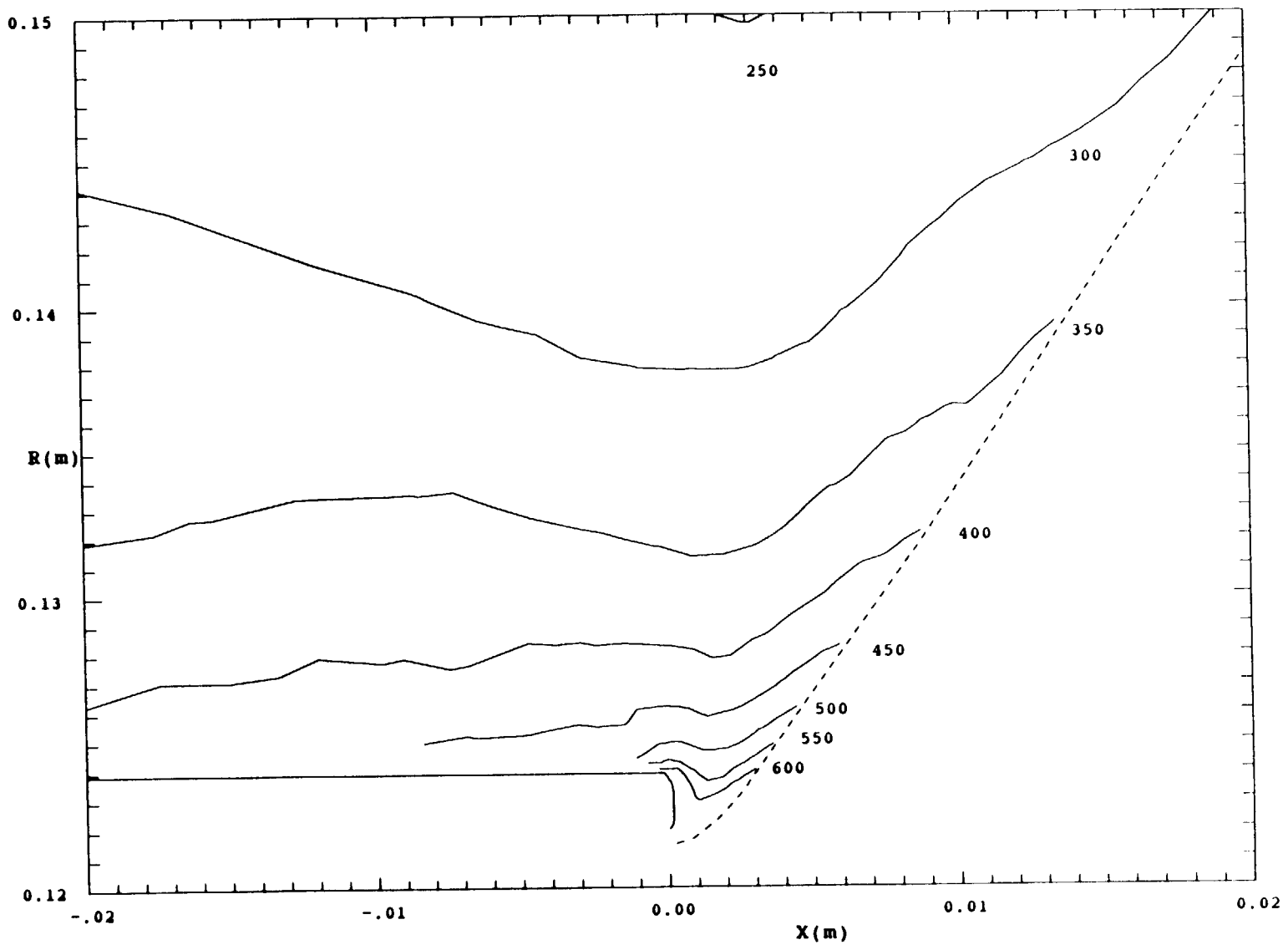

Fig(56) The plume gas mixture mean translational 'temperature' distribution (K).

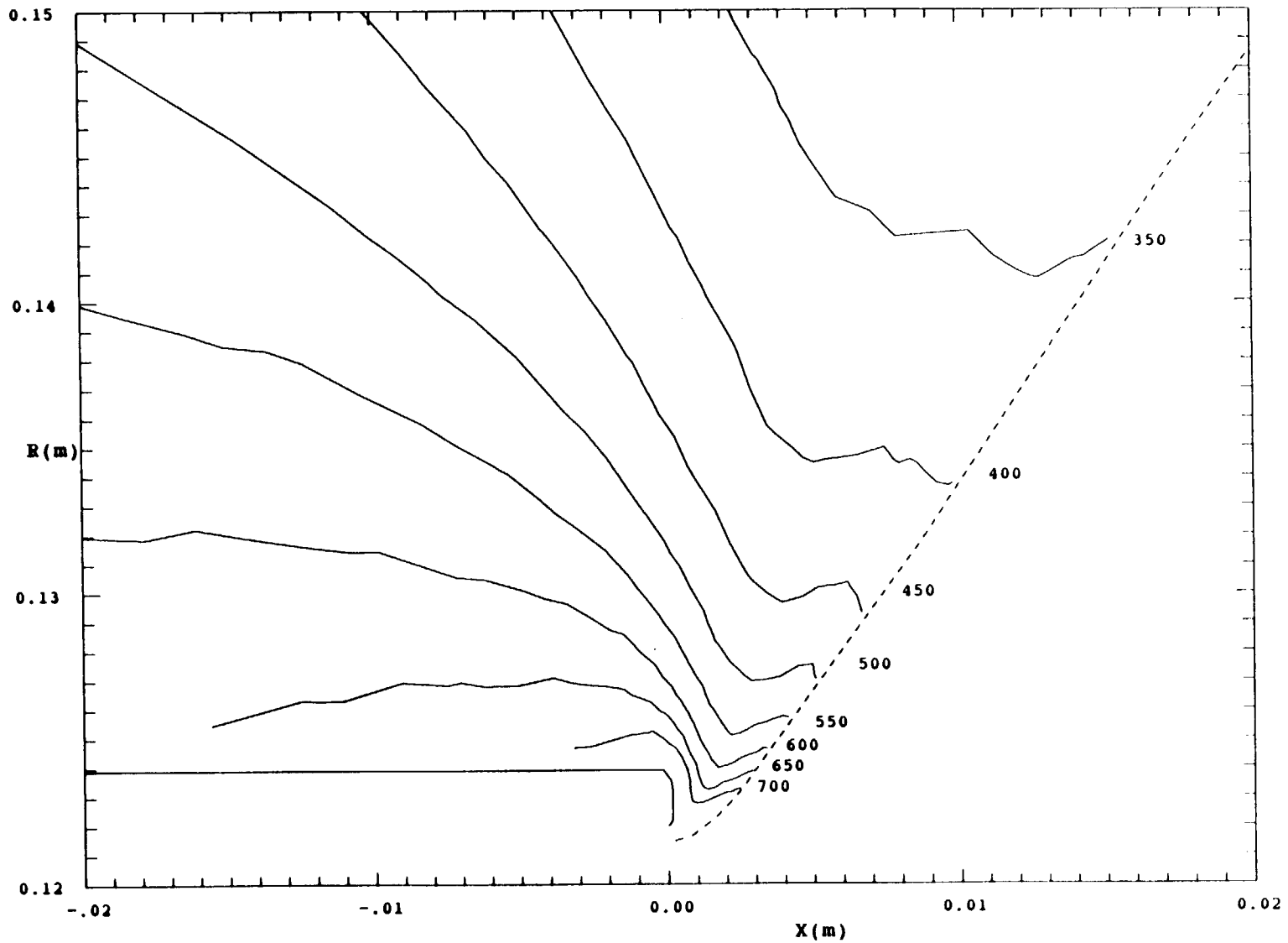

Fig(57) The plume gas mixture mean internal 'temperature' distribution (K).

The molecular hydrogen axial and radial translational 'temperature' distributions are shown in Figs(58) and (59). The data indicate that these 'temperatures' nearly coincide at the Monte Carlo input boundary (dashed curve) and for the small segment shown do not begin to diverge until about 5 mm downstream of the input boundary; thus for hydrogen the location of the input boundary is perhaps too conservative (breakdown parameter P = 0.03), however H_2 stays in equilibrium somewhat longer (in the flow direction) than the heavier species in the mixture (the CO_2 temperatures diverge more quickly). There is a deep trough in the axial mode 'temperature' distribution surface at a geometrical angle of 1.94(111°) measured from the lip outer corner, the flow angle along the bottom of this trough is about 2.07(119°). There is a corresponding cusp (ridge) in the radial mode 'temperature' distribution surface at about the same flow angle.

From the data in Figs(49) thru (55) it is clear that during the expansion around the lip, the acceleration of each species of the mixture is inversely proportional to the species molecular mass and that the species flow angle increases inversely with species mass. The larger flow angle of the lighter species may be associated with a larger ratio of axial to radial acceleration for the lighter species compared to the ratio for the heavier species. The data are consistent with an alternative interpretation of the flow dynamics: due to the higher acceleration and thus larger flow speed and flow angle of the lighter species, they advance thru the expansion more rapidly and react on

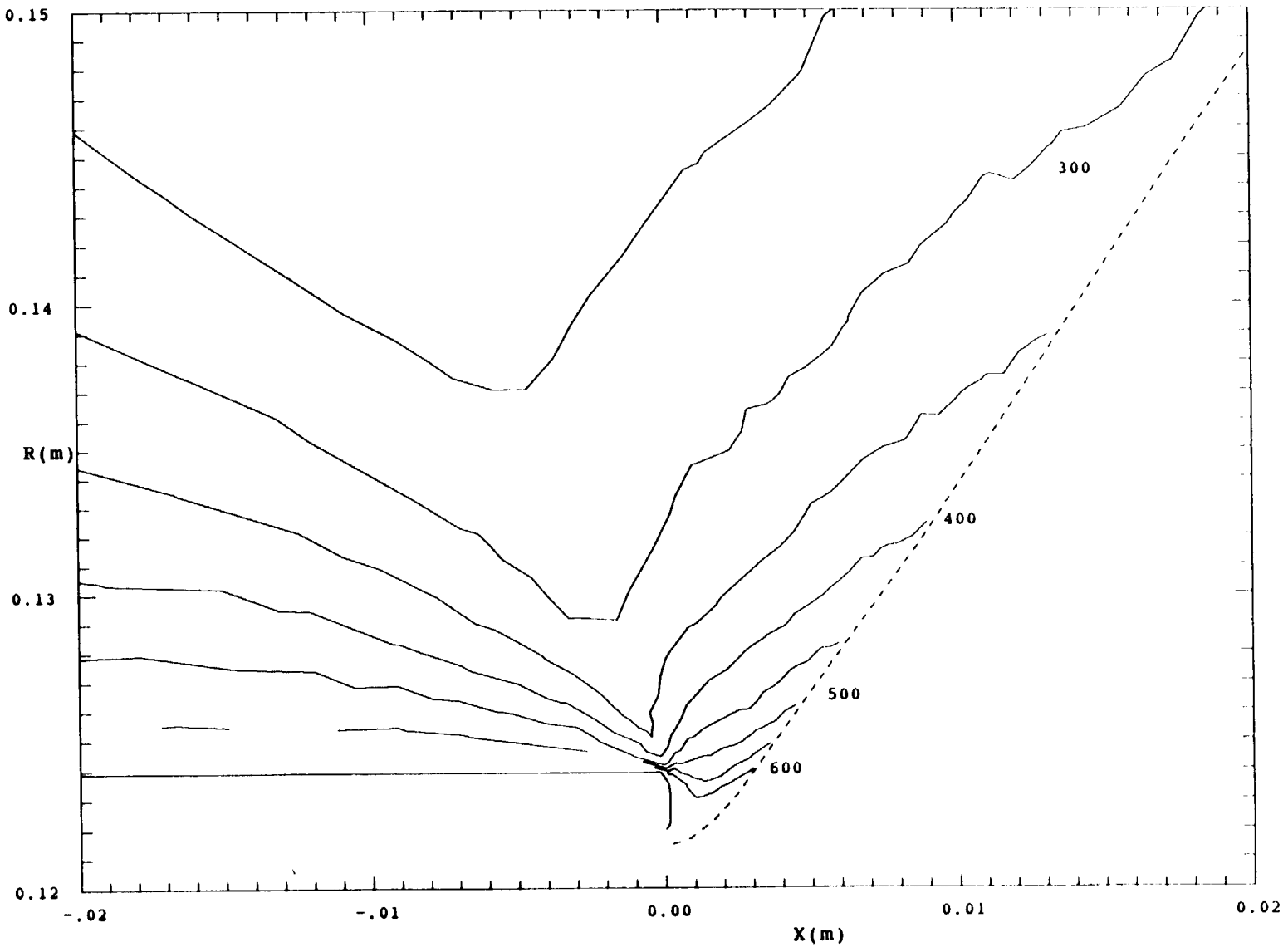

Fig(58) H_2 mean axial 'temperature' distribution (K).

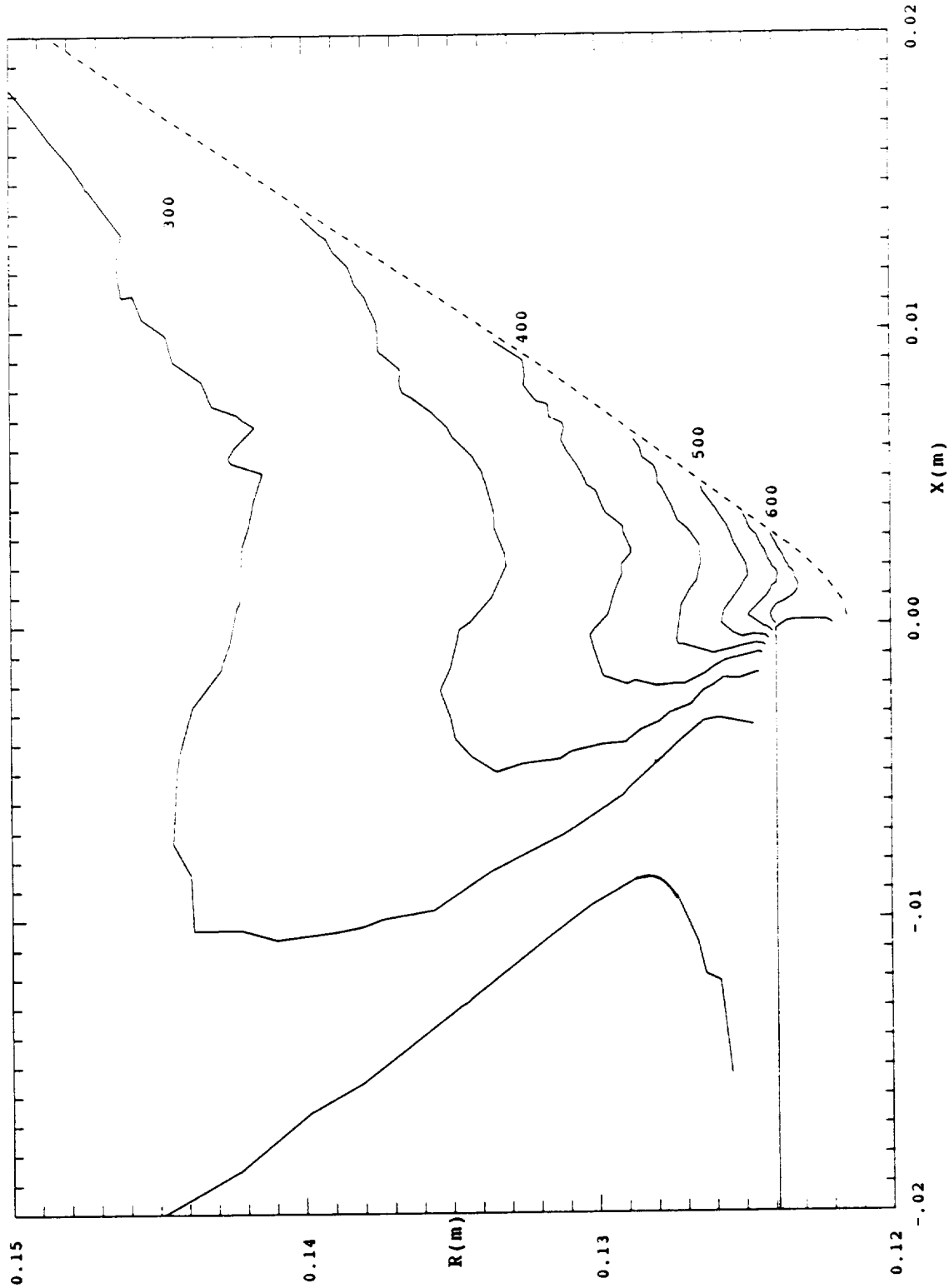

Fig(59) H_2 mean radial 'temperature' distribution (K).

the heavier species retarding the expansion of the heavier species. Referring to Figs(51) and (55) it may be seen that at large flow angles the lighter species flow rapidly into the rarefied space and then react back on the heavier species limiting their acceleration into the large flow angle space.

CONCLUSIONS

The DSMC farfield solution for the RCS plume uniquely displays heavy species enrichment of the plume gas mixture along the positive symmetry axis for flow angles $\leq 33°$; the number density of H_2 **increases** with r , $\partial n(H_2)/\partial r > 0$, while of course the CO_2 density decreases (as does the mixture), see Fig(31). These results explicitly display the effect of momentum persistence in a gas mixture consisting of species having a wide range of molecular mass. The higher collision frequency of the lighter species, see Fig(29), yields a relatively rapid collisional transfer of kinetic energy from H_2 to CO_2 thus maintaining near equality of the axial velocity components of the light and heavy species (and of course, all other species) (similarly, the radial component is nearly equal for all species); and simultaneously the higher collision frequency of the lighter species yields a larger accumulated deflection of H_2 in scattering events due to momentum persistence, since the mass ratio of H_2 with all possible collision partners has a small value. While the DSMC results clearly show the expected collective flow properties (means) for the plume gas mixture, see Figs(4) thru (11), with even greater clarity the DSMC data explicitly display the individual behavior of the seperate species in the farfield plume flow structure, see Figs(14) thru (27) and (29) thru (31). And by extension, the DSMC data reveal the internal dynamics of 'seeded' (doped) molecular beams with rare clarity.

The DSMC data support a further new interpretation of the flow dynamics at large flow angles (approaching π) : that the collision process yields a light species enrichment along the negative symmetry axis which is the inverse of the heavy species enrichment along the positive symmetry axis. The CO_2 density slope in the axial direction is much steeper than the H_2 density axial slope, $|\partial n(CO_2)/\partial x| >> |n(H_2)/\partial x|$, see Fig(31), say for $X \leq -10$. Thus in this region, the H_2 density contour surfaces approach disks, while the CO_2 contour surfaces approach cones. This yields a density cavity for the heavy species while the density of the lighter species is slightly enhanced near the axis. The distribution of the components of the plume gas mixture along the negative symmetry axis may thus be regarded as the inverse of the distribution along the positive symmetry axis. The DSMC method provides a description for the physical foundation of this flow: while the light species collision frequency are higher than the heavy species, see Figs(29) and (30), there are insufficient collisions to accelerate the heavy species; the magnitude of the axial component of the species velocity, in the high flow angle region, decreases with increasing species molecular mass, and thus the heavy species make a decreasing contribution to the total density as the flow proceeds downstream.

The flowfield solution for the RCS plume shows that all species in the exhaust gas mixture as it passes thru the nozzle exit plane are observed

The flowfield solution for the RCS plume shows that all species in the exhaust gas mixture as it passes thru the nozzle exit plane are observed everywhere in the flowfield but that the mixture composition varies continuously and smoothly over the entire solution space. The mean molecular weight decreases monatonically with increasing flow angle, see Figs(14) and (15), but depends on the molecular mass ratios and collision cross sections of the mixture constituents as well as their relative abundance at the input boundary.

The DSMC solution for the species density distribution shows that the farfield flow properties do not resemble flow from a point source, see Fig(31); and the molecular weight distribution shows that the gas composition is a fundamental, independent variable at all flow angles, see Figs(14) and (15). These results are contrary to the commonly held (but untested) assumption that the farfield flow properties of plume flows can (with adequate precision) be derived from point source flow. It is clear from the DSMC farfield plume results that this assumption is not physically realistic (and probably would not be for most exhaust mixtures, especially if the mean free path at the nozzle exit plane were relatively small).

The results show that thruout the entire DSMC flowfield, the plume flow is out of equilibrium, see Figs(8) and (9); the translational and internal 'temperatures' begin to diverge at the P = 0.03 breakdown contour and

continue to diverge thruout the farfield. This 'temperature' divergence is the direct consequence of the collision frequency droping below the value required to support eguilibration. Near the positive symmetry axis at small flow angles, the axial velocity components are nearly equal for all species (and similarly for the radial components), but the species 'temperatures' are all different, further at somewhat larger flow angles, the axial mode and radial mode 'temperatures' are unequal for each species and vary substantially from species to species. As flow angle increases the axial and radial 'temperatures' continue to diverge and the rate of divergence varies with species.

The DSMC solution in the lip flow region shows that species with equal molecular mass and nearly equal collision cross section (N_2,CO) have flow angle distributions and the flow speed distributions that are nearly identical, see Figs(49) and (53); but that for species pairs having large mass ratios and unequal collision cross sections, the pair (H_2,CO_2), both the flow angle and flow speed of the lighter species (H_2) lead the flow angle and flow speed of the heavy species (CO_2) substantially, see Figs(51) and (55). The flow angle and flow speed of these species are, of course, identical at the Monte Carlo input boundary, but they begin to diverge while the flow is only a few millimeters from the equilibrium domain (= $P \leq 0.03$). These results explicitly reveal the dynamics of the expansion around the lip; they show again, that the flow evolves partly as a mixed gas and partly as individual, seperate species, influnced by molecular mass and collision cross section. These

results support the interpretation that not only is the collision frequency insufficient to accelerate the heavy species but that the lighter species advances ahead of the heavier species and reacts back on the heavier species, retarding the expansion of the heavy species into the rarefied region.

The Direct Simulation Monte Carlo method is particularly well suited for exploring the structure of flowfields extending across all flow domains and for investigating the internal gas dynamics of complex flows (say, rocket plumes). Since the DSMC method does not use temperature as an internal variable, very complex flows can be investigated without reference to the thermodynamic state of the gas (which is generaly unknown, and frequently unknowable). The method is particularly suitable for large flows since the solution space can conveniently be divided into subspaces each of which can be scaled to satisfy local constraints. The flowfield properties displayed in many of the figures in this paper are simply inaccessible to continuum methods, such as the variation in flow behavior by individual species as explicitly displayed in Figs(31) and (55) for H_2 and CO_2 which can only be detected by molecular dynamic methods such as the DSMC. The information content in the RCS plume solution, such as in Figs(14), (31), (51) and (55), graphically illustrate the value of doing gas dynamics at the molecular level.

ACKNOWLEDGEMENTS

The DSMC solution for the RCS plume flowfield was generated with codes which are directly traceable to G. A. Bird, and which were, of course, essential to this work. We, among many researchers, are profoundly indebted to Graeme Austin Bird for having created a whole new way of thinking about physics and doing gas dynamics with his Direct Simulation Monte Carlo method. We are further indebted and ever greatful to Graeme for having generously served with immeasurable grace and patience, as our mentor over the years.

We thank S. D. (Bud) Smith for his valuable contributions in many discussions about continuum methods and their application, and for providing a set of continuum solutions for the RCS engine internal flow.

We thank M. P. Schuler for valuable data analysis work on the substantial data base produced by the RCS plume flow solution, and for extensive algorithm and program development and testing, yielding numerous powerful graphics programs which were essential for analysis, interpretation, and presentation of the results of the DSMC computer experiment on the RCS engine.

REFERENCES

1) Hueser, J. E., Melfi, L. T. jr., Bird, G. A., and Brock, F. J., Analysis of Large Solid Rocket Engine Exhaust Plumes Using the Direct Simulation Monte Carlo Method, AIAA Paper 84–0496, AIAA 22nd Aerospace Science Meeting, 9–12 Jan 1984, Reno, Nevada

2) Hueser, J. E., Melfi, L. T. jr., Bird, G. A., and Brock, F. J., Rocket Nozzle Lip Flow by Direct Simulation Monte Carlo Method, Journal of Spacecraft and Rockets, V 23, pp. 363, 1986

3) Bird, G. A., Molecular Gas Dynamics, Clarendon Press, Oxford, 1976

4) Bird, G. A., Breakdown of Continuum Flow in Free Jets and Rocket Plumes, Rarefied Gas Dynamics, Progress in Astronautics and Aeronautics, V 74 II, edited by Sam S Fisher, AIAA, New York, 1981, pp. 681–694.

5) For plume flow the breakdown parameter $P = (C_0/\nu\rho)(d\rho/ds)$, where C_0 = stream speed, ρ = mass density, ν = collision frequency, and s = distance along the local streamline.

6) Bird, G. A., Monte Carlo Simulation in an Engineering Context, Rarefied Gas Dynamics, Progress in Astronautics and Aeronautics, V 74 I, edited by Sam S. Fisher, AIAA, New York, 1981, pp. 239–255.

7) Borgnakke, C. and Larsen, P. S., Statistical Collision Model for Monte Carlo Simulation of Polyatomic Gas Mixtures, Journal of Computational Physics, V 18, 1975, pp. 405–420.

8) Bird, G. A., Simulation of Multi–Dimensional and Chemically Reacting Flows, Rarefied Gas Dynamics, 11th Symposium, Paris, 1979.

9) Chapman, S. and Cowling, T. G., The Mathematical Theory of Nonuniform Gases, University Press, Cambridge, 1961

10) Results similar to those presented in Fig(33) were used (along with the data in Fig(14)) to estimate the total force applied to a single spacestation solar panel during an RCS(L1L) steady firing (about 40 ms after start), assuming the Shuttle was docked in 'baseline' position: The normal force on the panel (incident momentum flux density integrated over the area of the panel) was approximately 159.1 N (35.8 lb); This plume flux incident on the solar panel also produced a torque (moment) about the long axis of the spacestation of approximately 3020 Nm (117.4 ft lb).